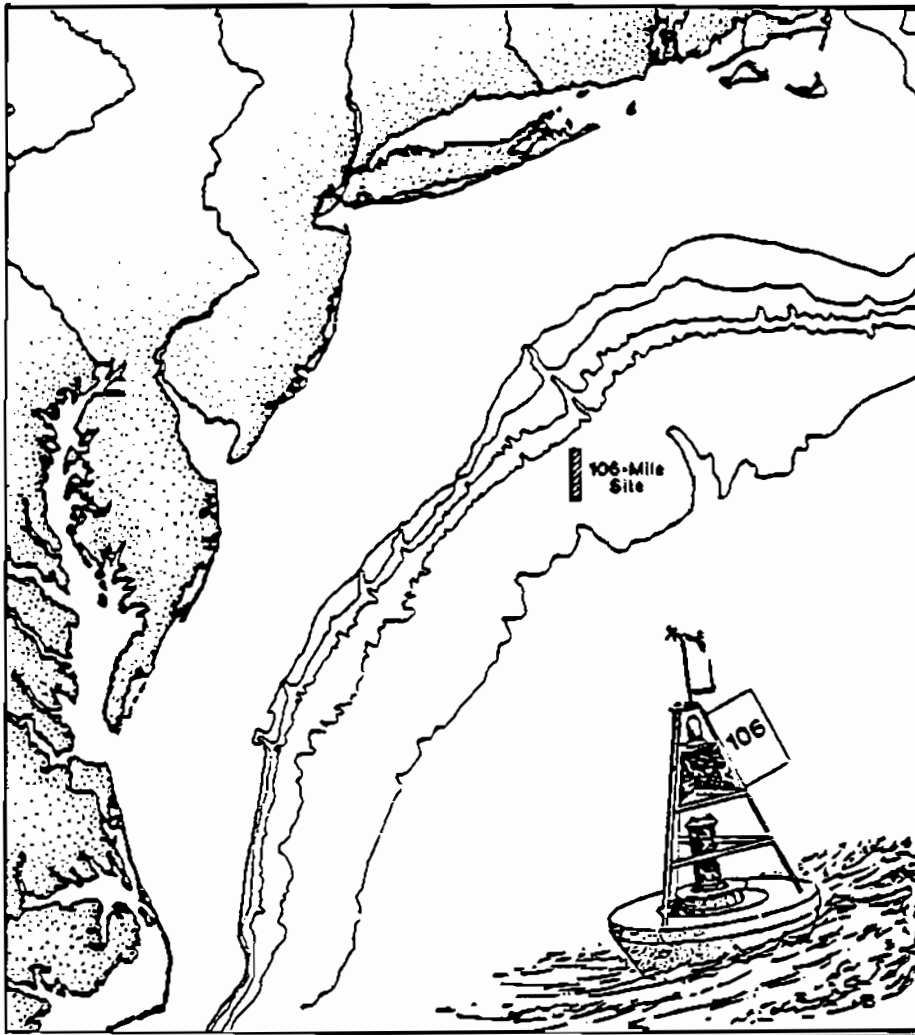




Final Report on Current Meter Measurements at the 106-Mile Site in Support of Municipal Waste Disposal



FINAL REPORT

**CURRENT METER MEASUREMENTS
AT THE 106-MILE SITE
IN SUPPORT OF
MUNICIPAL WASTE DISPOSAL**

April 25, 1988

**U.S. ENVIRONMENTAL PROTECTION AGENCY
Office of Marine and Estuarine Protection
Washington, DC**

Prepared Under Contract No. 68-03-3319

TABLE OF CONTENTS

EXECUTIVE SUMMARY.....	i
1. INTRODUCTION.....	1
1.1 Background.....	1
1.2 Physical Oceanography of the 106-Mile Site.....	1
1.2.1 Overview.....	1
1.2.2 Field Programs Applicable to 106-Mile Site.....	6
1.2.3 Summary of Findings.....	8
1.3 Objectives.....	23
2. FIELD PROGRAM.....	24
2.1 Moorings.....	24
2.2 Data Processing.....	28
3. DATA INTERPRETATION AND ANALYSIS.....	29
3.1 Introduction.....	29
3.2 Time Series.....	30
3.3 Basic Statistics.....	48
3.4 Inertial and Tidal Motions.....	52
3.5 Spectra and Coherence.....	63
4. SUMMARY.....	67
5. REFERENCES.....	71

LIST OF TABLES

Table 2-1	EPA 106-Mile Site Moorings.....	26
Table 3-1	Events Occurring at the 106-Mile Site, September 1986 to April 1987.....	35
Table 3-2	Basic Statistics for 3-HLP and 40-HLP records from moorings X and Y.....	49
Table 3-3	Basic statistics for 3-HLP and 40-HLP records from MASAR moorings C and D for two six-months periods in 1984 and 1985.....	51
Table 3-4	Frequency distribution of speeds and directions and summary statistics for the 3-HLP current records from (a) X1061, (b) X1063, (c) X1067, (d) X1068, and (e) Y1061.....	53

LIST OF FIGURES

Figure 1-1	Locations of slopewater between the edge of the continental shelf and the Gulf Stream, from Cape Hatteras to the Grand Banks.....	3
Figure 1-2	Mid-Atlantic Slope and Continental Rise showing moorings in place during 1984-1985.....	7
Figure 1-3	Empirical scheme of slopewater circulation containing Coastal Labrador Sea Water (CLSW) inflow from the Grand Banks partly retro-reflecting, partly flowing southwestward along the continental margin; a western Slope Sea gyre; and inflow from the Gulf Stream thermocline.....	9
Figure 1-4	Upper-level currents averaged over the period of displaced Gulf Stream position, 10 October 1984-January 1986.....	11
Figure 1-5a	MASAR hydrographic section for the northern transect on February 21, 1985.....	14
Figure 1-5b	MASAR hydrographic section for the northern transect on May 14, 1985.....	15
Figure 1-5c	MASAR hydrographic section for the northern transect for September 9, 1985.....	16
Figure 1-6	The mean position, standard deviation and extreme positions of the GS front taken from all available digitized, satellite derived sea-surface temperature maps for the month of October 1985.....	19
Figure 1-7a	Temperature, salinity, and density distributions in a vertical section across the continental shelf on 19 July 1975 for a section off the eastern shores of Virginia.....	21
Figure 1-7b	Temperature, salinity, and density distributions in a vertical section across the continental shelf on 21 July 1975 for the same transect as Figure 1-7a.....	22
Figure 2-1	A chart of the 106-Mile Site with EPA mooring positions X and Y, and MASAR mooring positions C and D, indicated.....	25
Figure 2-2	The configurations of EPA moorings X and Y deployed southwest and northeast of the 106-Mile Site, respectively.....	27
Figure 3-1	40-HLP stick plot of the first three months of deployment.....	31
Figure 3-2	40-HLP stick plot of the second three months of deployment.....	32
Figure 3-3	3-HLP temperature records of the first three months of deployment.....	33
Figure 3-4	3-HLP temperature records of the second three months of the deployment.....	34

LIST OF FIGURES Cont'd

Figure 3-5a	Oceanographic Analyses of AVHRR Satellite Imagery, September 15, 1986.....	37
Figure 3-5b	Oceanographic Analyses of AVHRR Satellite Imagery, October 6, 1986.....	38
Figure 3-5c	Oceanographic Analyses of AVHRR Satellite Imagery, November 19, 1986.....	39
Figure 3-5d	Oceanographic Analyses of AVHRR Satellite Imagery, November 24, 1986.....	40
Figure 3-5e	Oceanographic Analyses of AVHRR Satellite Imagery, December 29, 1986.....	41
Figure 3-5f	Oceanographic Analyses of AVHRR Satellite Imagery, February 18, 1987.....	42
Figure 3-5g	Oceanographic Analyses of AVHRR Satellite Imagery, March 23, 1987.....	43
Figure 3-5h	Oceanographic Analyses of AVHRR Satellite Imagery, April 13, 1987.....	44
Figure 3-6	Depth-time isotherm contours from mooring X.....	46
Figure 3-7a	3-HLP velocity records of the first three months of deployment.....	59
Figure 3-7b	3-HLP velocity records of the first three months of deployment.....	60
Figure 3-8a	3-HLP velocity records of the second three months of deployment.....	61
Figure 3-8b	3-HLP velocity records of the second three months deployment.....	62
Figure 3-9a	Variance preserving rotary spectra of currents at 48m on mooring X.....	64
Figure 3-9b	Variance preserving rotary spectra of currents at 248m on mooring X.....	65
Figure 3-9c	Variance preserving rotary spectra of currents at 249m on mooring Y.....	66
Figure 3-10a	Coherence squared and phase differences between current records from depths of 48m and 248m on mooring X.....	68
Figure 3-10b	Coherence squared and phase differences between current records from depths of 248m and 1000m on mooring X.....	69
Figure 3-10c	Coherence squared and phase differences between current records from 248m on mooring X and 249m on mooring Y.....	70

EXECUTIVE SUMMARY

In September 1986, two current meter moorings were deployed for a period of seven months on the 2500-m isobath, respectively, northeast and southwest of the 106-Mile Deepwater Municipal Sludge Disposal Site. The moorings were designed to monitor the current and temperature structure of the upper layers of the ocean in the vicinity of the 106-Mile Site in order to assess the effects of various current regimes on the disposal of sludge. The southwest mooring was instrumented with current meters at 50-, 100-, 250-, and 1000-m nominal water depths, and with temperature recorders at approximately 25-m spacing from the current meters from 50m to 250m. The northeast mooring had data from the 250- and 1000-m levels.

The 106-Mile Site is situated, with water depths ranging from approximately 1000m to 2700m, in a distinct part of the coastal ocean between the Gulf Stream and the shelf break known as the Slope Sea. Mean flow, for the deployment period, was 6-7 cm s⁻¹ southwest along the isobaths and was uniform with depth over the upper 250m of the water column. This characteristic southwest flow at the 106-Mile Site is considered to be the northern part of the anticlockwise western Slope Sea gyre. During the seven-month deployment, an energetic warm-core ring (86-E) moved through the site in November followed by a smaller, clockwise rotating, warm eddy that was apparently a remnant of warm-core ring (86-F). Another small warm eddy, mostly confined to the continental slope, was observed in October trailing a large warm-core ring (86-A) that had passed through the 106-Mile Site in early September. This small, energetic, October warm eddy drew out a 75- to 100-m thick filament of cool shelf water into the Slope Sea.

The January to March period was not affected by eddies and was characterized by strong surface cooling that produced a homogeneous 250-m deep layer of 12°C water by convective overturning in early February. After the formation of the 12°C water, known as the slopewater pycnostad, the upper 50 to 100m of the water column experienced a number of warm outbreaks. One was due to a large Gulf Stream filament trailing a meander crest, and one was due to the interaction of the Gulf Stream and a ring (86-I) that was stalled near the Hudson Canyon in March and April.

In February, at the 1000-m level, a cool, small (~12 km long) Labrador Sea Water (LSW) anomaly was observed advecting along the 2500-m isobath with the mean flow. Many of the observed phenomena in these data, including shelfwater intrusions, small warm eddies, warm outbreaks, and LSW anomalies, have rarely or never been observed in time series records. Major features such as warm-core rings, the mean southwest flow, and the formation of the 12°C slope water have been previously studied in recent Slope Sea observational programs; however, the databases from these studies are limited.

1. INTRODUCTION

1.1 BACKGROUND

The 106-Mile Deepwater Municipal Sludge Site was designated in 1986 for the disposal of municipal sludges. As part of a monitoring program for the disposal of sludge at the site, two current meter moorings were deployed to monitor the temperature and current structure of the upper ocean over a seven-month period from September 1986 to April 1987. Background material on the dumping of sludge at the 106-Mile Site is given in EPA (1987).

Both the near- and farfield fate of sludge dumped in the deep ocean should be evaluated, including the analysis of the transport and mixing processes at the site and in adjacent waters, for a wide range of space and time scales. The physical disposal processes involved in the dispersal of sludge are advection by the current field, mixing by turbulence and large-scale shear flows, and sinking of sludge particles through the water column. Transport and mixing are profoundly affected by the types of circulations encountered by the sludge particles on their way to the seafloor. The Slope Sea, the region between the Gulf Stream and the shelf break in the Mid-Atlantic Bight where the 106-Mile Site is situated, is a very complex region of the coastal ocean. Circulation features affecting the 106-Mile Site include the Gulf Stream, warm-core anticyclonic rings, the Slope Sea gyre, and shelf-slope front exchange processes. These processes are briefly discussed in terms of the transport and mixing of sludge waste in the Monitoring Plan (EPA, 1987). The physical oceanography of the southern part of the Mid-Atlantic Bight slope is summarized in the following section.

1.2 PHYSICAL OCEANOGRAPHY OF THE 106-MILE SITE

1.2.1 Overview

The physical environment of the 106-Mile Site determines how dumped waste will be transported away from the site and mixed with the surrounding waters, and eventually determines its fate. A thorough knowledge of the

physical environment is needed in order to assess where waste goes, what the rates and mechanisms of mixing with the receiving waters are, and where on the seabed it ends up. Because sewage sludge has essentially the same density as sea water and the majority of particles are silt sized, the sludge constituents will take several weeks to several months to reach the seabed in water depths, typical of the site, of 200 to 2700m. Because the current flows are fairly strong ($\sim 0-50 \text{ cm s}^{-1}$), the particles may be transported a considerable distance in that time. Therefore, a large scale view of the circulation (i.e., patterns of water movement) is required to assess the fate of the sludge due to currents and mixing. The physical environment needs to be characterized on time scales ranging from days to years and length scales of a few km to ~ 1000 km. The circulation at the 106-Mile Site should be viewed in the context of the circulation of the Mid-Atlantic Bight encompassing the continental shelf, slope, and rise, and the Gulf Stream (GS) from New England to Cape Hatteras. The oceanographic regime occurring at the time and place of a release is, of course, important for initial mixing and dispersion; however long-term farfield transport and fate are a more complex issue because of the variability of the receiving waters over a wide range of length and time scales, and the close proximity of radically different current systems in the Mid-Atlantic Bight.

The 106-Mile Site is situated within a distinct part of the ocean known as the Slope Sea (Csanady and Hamilton, 1987). It is probably one of the most complex bodies of water in the world, and though the Slope Sea and the Gulf Stream have been studied since the 1930s (Rossby, 1936), it is only recently that a modern synthesis of the circulation has been put together (Csanady and Hamilton, 1987; SAIC, 1987) and some of its features confirmed by the recent Mid-Atlantic Slope and Rise (MASAR) and Shelf Edge Exchange Program (SEEP-I) experiments. Figure 1-1 shows a sketch of the Slope Sea bounded by the Gulf Stream in the south and shelf water in the north. The upper 50 to 75m of the water column in the Slope Sea is often a mixture of shelf water, slopewater and Gulf-Stream-derived water, producing complex salinity and temperature structures. The shelf break region between Cape Hatteras and Georges Bank has a complex salinity and temperature front separating the cooler, fresher shelf waters from the warmer, more saline slopewaters. The mixing processes along this shelf-slope front, producing

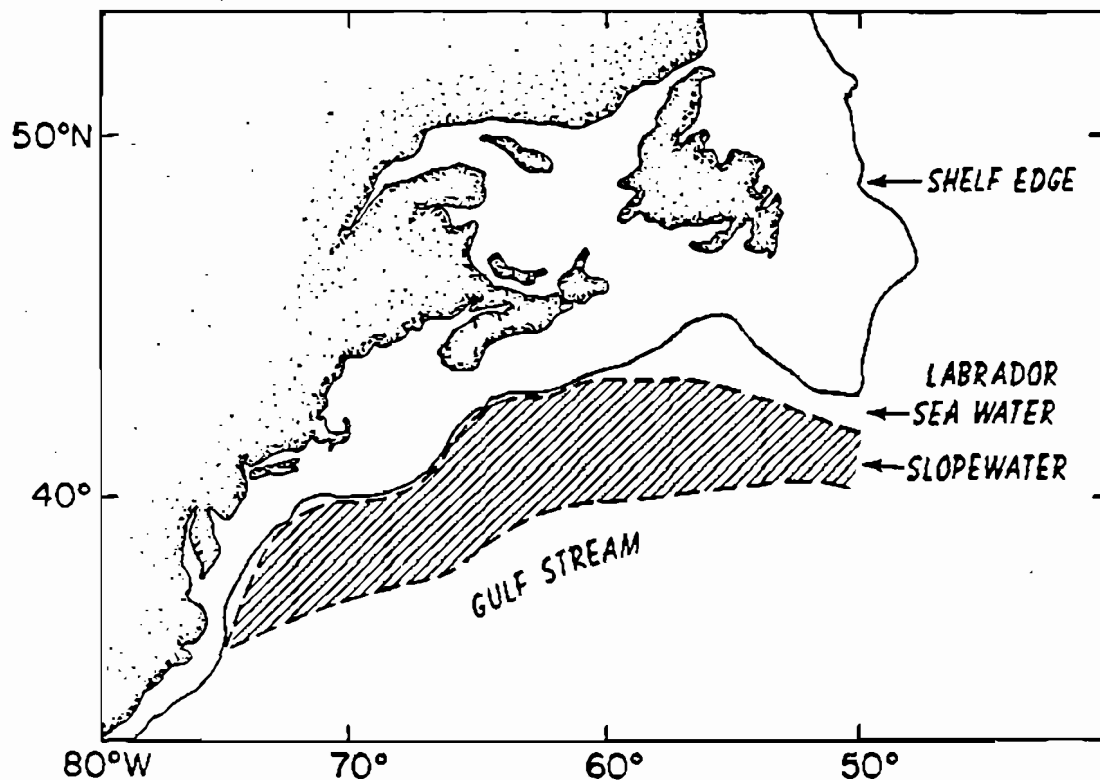


Figure 1-1. Location of slopewater between the edge of the continental shelf and the Gulf Stream, from Cape Hatteras to the Grand Banks. Most of the area is occupied by slopewater except in the northeast corner where coastal Labrador Sea water intrudes.

cross-front exchanges possibly important of introducing sludge onto the shelf, are extremely complex and not well understood or comprehensively measured.

The recent MASAR experiment has shown that the Gulf Stream has profound influences on the circulation over the slope. The Gulf Stream, part of the western boundary current system of the North Atlantic Ocean, leaves the continental margin at Cape Hatteras and behaves like a free-meandering jet, flowing into progressively deeper water. It is warmer than surrounding waters and separates the Sargasso Sea on the south side from the much cooler slopewater on the north. There is a sharp temperature front, easily observed from satellites, between the shoreward side of the jet and the slopewater, that is often referred to as the "north wall" of the Gulf Stream (GS). The high speed currents of the GS are generally restricted to the upper 1000m of the water column. Maximum surface speeds may exceed 200 cm/s. Gulf Stream meanders are large shoreward (north) and seaward (south) sinuous displacements of the GS front that move east along the path of the jet. The meanders have wavelengths ranging from 100 km to 1000 km, periods of 4 to 100 days, and downstream propagation speeds dependent upon wave periods such that 4- to 5-day period waves, with wavelengths of about 180 km, propagate at about 40 km/day and 40-day period waves, with wavelengths of 600 km, propagate at about 20 km/day (Tracey and Watts, 1986). The meander displacements are constrained near Cape Hatteras, but show an almost linear increase in amplitude as they move east. Near the New England Seamounts, the path of the GS has an envelope that is about 500 km wide (Cornillon, 1986).

The larger meanders can pinch off to the north or south of the GS to produce detached clockwise rotating warm-core rings or anticlockwise rotating cold-core rings, respectively. A warm-core ring is essentially a rotating, bowl-shaped parcel of Gulf Stream and Sargasso Sea water about 100 to 150 km in diameter, 1000-m deep in the center, with maximum speeds of about 150 cm/s. Once it has formed in the Slope Sea, it moves west at approximately 6 km/day (Joyce, 1984). These rings have complex life histories before they coalesce with the Gulf Stream, often near Cape Hatteras. Warm-core rings can interact with the GS and shelf waters, extruding warm and cold streamers from these waters that can wrap around the outer edges of the ring. The passage of a ring along the slope can

apparently trigger instabilities and waves on the shelf-slope front that may also form smaller warm- and cold-core eddies, about 20 to 50 km in diameter, in the upper slope aiding the exchange of shelf and slopewaters. About five to eight rings per year move into the western Slope Sea (Fitzgerald and Chamberlin, 1983; Brown et al., 1986). Thus, sludge dumped into the strongly sheared currents of a ring will be transported and mixed in a different physical and biological environment than when a warm-core ring is not present over the dumpsite.

The previous discussion has concentrated on the upper-layer circulation processes of the Slope Sea. Because sludge particles settle through the water column, the deep circulation over the slope and rise also needs to be considered. Strong fluctuating currents (20 to 60 cm/s) are found near the bottom on the continental rise of the Mid-Atlantic Bight. They are due to planetary wave motions, having periods of 10 to 100 days, thought to be generated by the meandering Gulf Stream. These currents are known as topographic Rossby waves (TRWs) (Rhines, 1971; Luyten, 1977; Hamilton, 1984) and are characterized by fluctuating currents that increase in magnitude from about 1000-m depth towards the seabed. These TRWs propagate away from the deep GS region towards the slope in a generally west or southwest direction. The near-bottom TRW currents may be strong enough to move fine sludge particles that reach the bottom, thus helping to disperse them.

The near-bottom mean flow in water depths shallower than about 4000m on the continental rise and lower part of the slope is part of the Western Boundary Undercurrent (WBUC). The WBUC is formed by the sinking of cold arctic water in the region of the Denmark Strait and has been traced as far south as the Grand Bahama Bank (27 N). On the Mid-Atlantic Bight slope and rise, this mean current (~2 to 3 cm/s) follows the general trend of the isobaths and passes under the Gulf Stream at Cape Hatteras. Thus, sludge particles in the lower water column tend to be transported southwest by this deep current system. Over the deeper part of the steep slope (1000- to 2000-m depth), fluctuating and mean currents seem to be weaker with a different vertical structure than on the rise. This lower slope region may be a sink for suspended sediment derived from land and the continental shelf.

The few deep measurements, made by the SEEP-I and MASAR programs, over the lower slope tend to confirm the existence of this low energy region.

This brief review of the various regimes and phenomena that affect the farfield fate of sludge material dumped at the 106-Mile Site is followed by a discussion of recent measurement programs (primarily MASAR and SEEP-I) and their implications for transport and mixing. The discussion will concentrate on the upper-layer circulation of the Slope Sea, including the effects of warm-core rings and Gulf Stream incursions, and the possibilities of exchanges with the outer shelf across the shelf-slope front.

1.2.2 Field Programs Applicable to 106-Mile Site

The most useful data on currents and hydrography of the western Slope Sea and the Gulf Stream were taken during two extensive moored array studies funded by the Department of Energy (DoE): the Shelf Edge Exchange Program (SEEP-I, Aikman et al., 1987); and the Minerals Management Service (MMS): the Mid-Atlantic Slope and Rise (MASAR) study (SAIC, 1987); and associated studies. A sketch map of the arrays is given in Figure 1-2. The complete array (SEEP, MASAR, the Gulf Stream current meter moorings off Cape Hatteras, and the Inverse Echo Sounder Array under the GS (funded by the Office of Naval Research (ONR) and the National Science Foundation (NSF)) was in place during 1984. The MASAR arrays were maintained from March 1984 to March 1986. Both the MASAR and SEEP programs had extensive hydrographic components. The MASAR study conducted eight seasonal hydrographic surveys over the two years, using closely spaced stations along the two mooring transects. This study produced the first documentation of the seasonal cycle of formation and erosion of the slopewater pycnocline, a well-mixed layer of water found between about 50m and 200m throughout the Slope Sea with a temperature of 12°C, salinity 35.5‰, and hence a density of 27.0 sigma-t. Because the MASAR northern mooring transect off New Jersey is just to the south of the 106-Mile Site, it provides the best long-term set of current meter measurements appropriate to the site. The U.S. Environmental Protection Agency (EPA) measurement program, discussed in this report, was designed to extend and complement to the MASAR study.

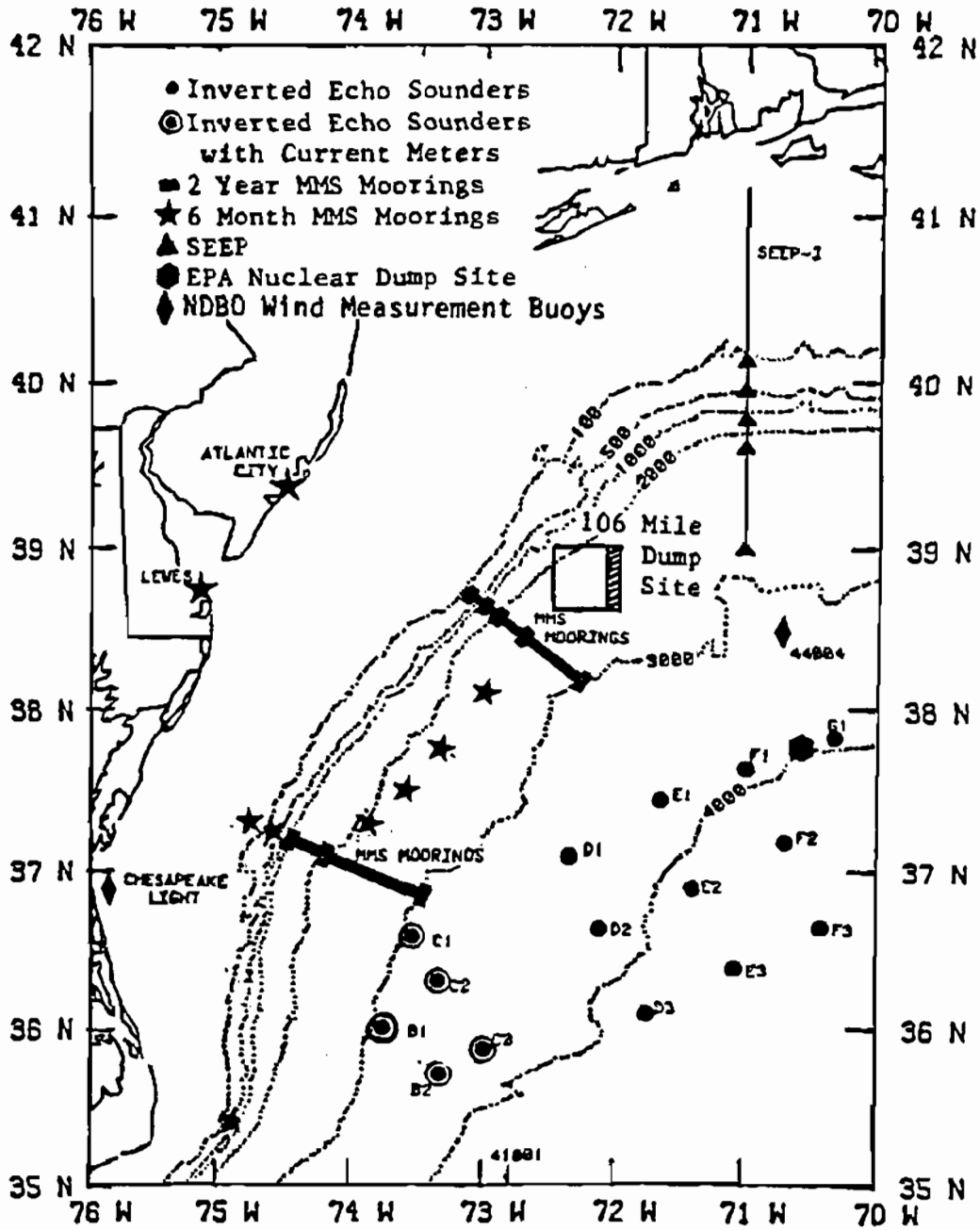


Figure 1-2. Mid-Atlantic Slope and Continental Rise showing moorings in place during 1984-1985. The 106-Mile Site is marked.

Site-specific studies at the 106-Mile Site were conducted by the National Oceanic and Atmospheric Administration (NOAA) between 1974 and 1978 (Ingham et al., 1977) concentrating on warm-core ring tracking (Bisagni, 1976) and hydrography. There is also extensive historical hydrography, mainly in the eastern part of the Slope Sea, including Gulf Stream '60 (Fuglister, 1963) and McLellan's extensive surveys (McLellan et al., 1953; McLellan, 1956, 1957). Prior to MASAR and SEEP, Woods Hole maintained a mooring at "Site D" in 2600m of water south of Nantucket Island (Thompson, 1977). However, because of the use of surface floatation on the moorings, the upper-layer measurements were contaminated by mooring motions due to surface waves and the later (1972 to 1973) subsurface moorings concentrated on deep currents. Near bottom currents have been measured at a number of sites on the continental rise, including the 2800-m low-level radioactive waste site which is adjacent and southeast of the 106-Mile Site (Hamilton, 1982; 1984).

1.2.3 Summary of Findings

1.2.3.1 Slope Sea Circulation

The underlying circulation pattern of the Slope Sea has been derived from historical hydrography (Csanady and Hamilton, 1987) and is shown in Figure 1-3. The prominent western gyre is probably variable in size and strength depending on the configuration of the Gulf Stream, the strength of the inflow from the Labrador Sea, and the strength of the large scale wind forcing. The detailed dynamics are not established, and the evidence for the gyre and its variability is largely empirical. Large perturbations such as warm-core rings and upper-slope eddies are essentially superimposed on this basic circulation. The 106-Mile Site and the northern MASAR mooring transect are approximately situated in the strongest part of the southwest flowing arm of the anticlockwise gyre. This fact provides an explanation for the predominantly southwest mean currents (~10 cm/s) that have been measured at the 106-Mile Site (Bisagni, 1983) and the MASAR northern transect (SAIC, 1987). Evidence for a distinct northeast return flow along the north wall of the GS comes primarily from sea surface temperature maps derived from the

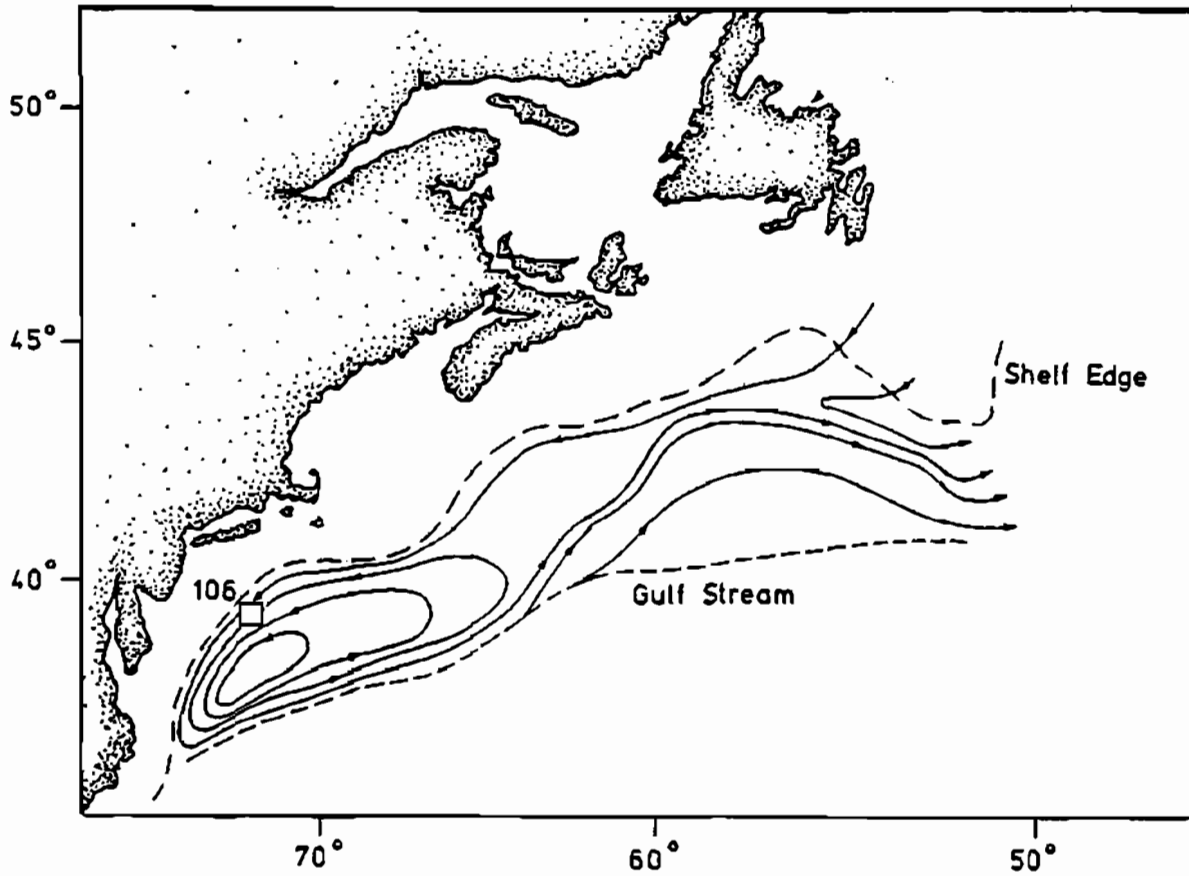


FIGURE 1-3. CONCEPTUAL MODEL OF THE CIRCULATION IN THE UPPER LAYERS OF THE SLOPE WATER FROM CSANADY AND HAMILTON (1987). THE 106-MILE SITE IS SHOWN IN THE INSHORE ARM OF THE SLOPE SEA GYRE. THE DASHED LINES INDICATE THE EDGE OF THE CONTINENTAL SHELF AND THE HISTORIC MEAN POSITION OF THE NORTHERN EDGE OF THE GULF STREAM.

Advanced Very High Resolution Radiometer (AVHRR) on polar orbiting satellites. Cooler, fresher water is often observed stretching from the outer shelf and upper slope regions off Chesapeake Bay and extending in a narrow band for several hundred kilometers along the north wall of the GS. The position of this shelf and slope outflow can vary from the eastern shores of Virginia to just north of Cape Hatteras, depending on the configuration of the GS. The MASAR study measured coherent, upper-slope, along-isobath currents between the north and south transects for a period of about 150 days beginning in September 1984. There were comparable periods when there was no observable correlation between the along-isobath current fluctuations of the two transects, indicating that there were substantial periods when the western Slope Sea gyre did not extend to the Chesapeake Bay transect (SAIC, 1987).

The position of the GS also has an indirect effect on the strength of the upper-layer flow at 106-Mile Site. During most of the MASAR study (March 1984 to March 1986), the GS was, on average, about 100 km closer to the New Jersey shelf break than in a normal year. Only in the period between May and September 1984 did the GS follow a path approximating its historical or normal position. The mean upper-layer currents (at approximately 100-m to 200-m depths) for May to September 1984 (GS normal) and October 1984 to January 1986 (GS displaced north of its historical mean position) are shown in Figure 1-4. In the latter case, mean southwesterly flows are seen over the New Jersey Slope (moorings B and C), but mean easterly flow is at the 3000-m isobath (mooring E). Thus, flow at mooring E appears to be in the southern limb of the anticlockwise rotating gyre. In the normal GS period, flows over the slope (200- to 2000-m isobaths) are weaker at both transects than in the displaced GS period. The most substantial southwest flow is observed at E1; mooring H is in the GS most of the time. The implication is that the gyre has more room when the GS follows its normal path and the upper-layer of circulation is more diffused, with maximum southwesterly flow occurring seaward of the 2000-m isobath. With the GS displaced, the surface area of the western Slope Sea is reduced and the gyre appears stronger with maximum speeds occurring closer to or over the slope. Monthly mean along-isobath currents at B5 were found to be highly correlated (correlation coefficient, $R, \sim 0.79$) with a monthly mean distance of the GS front from the

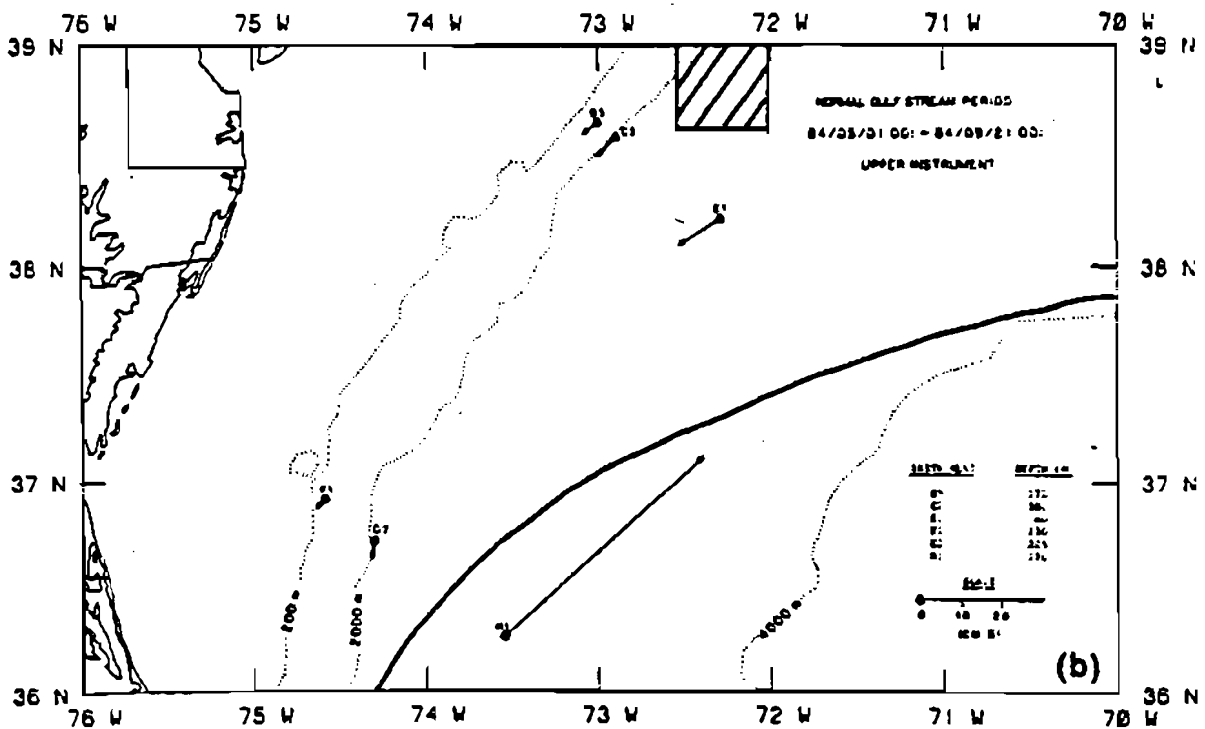
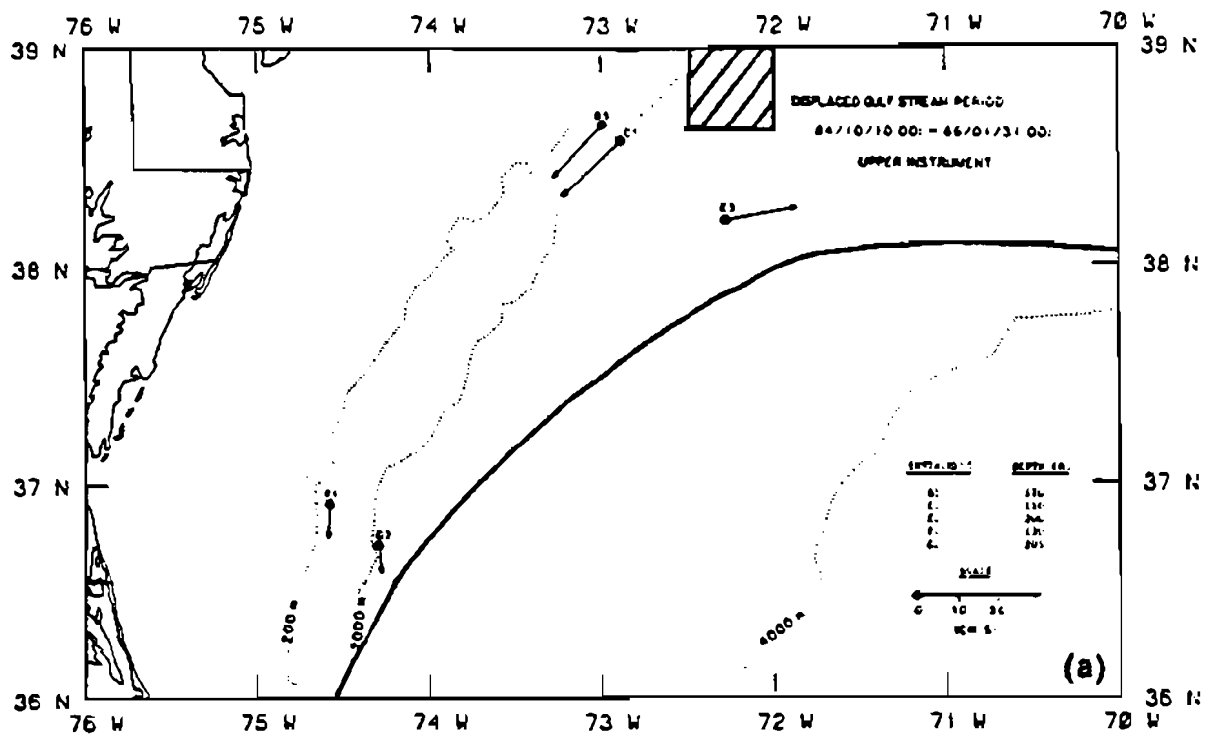


Figure 1-4. (a) Upper-level currents averaged over the period of displaced Gulf Stream position, 10 October 1984 - 31 January 1986. (b) Upper-level currents averaged over the period of normal Gulf Stream path, 1 May - 21 September, 1984. The mean position of the GS front for the indicated periods, taken from daily AVHRR imagery, is shown by the solid line. The position of the 106-Mile Site is shown.

shelf break measured along the northern MASAR transect. This direct relationship between the strength of the southwest flow over the New Jersey slope and the position of the GS front is an important result of the MASAR field study (SAIC, 1987). The dynamics of such a "teleconnection" are not yet understood.

The transition of the GS from normal to displaced state and vice versa was documented, with satellite imagery and current meters, three times in the MASAR study. The transitions took about a week and seem to be caused by the coalescence of cold-core rings (twice) or warm-core rings (once) with the GS in the vicinity of Cape Hatteras (SAIC, 1987). The long time scales of GS variability indicate that dispersion studies for farfield fate at the 106-Mile Site should obtain time series of several years duration in order to obtain reasonable statistics on the variability of the circulation in the western Slope Sea.

1.2.3.2 Slope Sea Hydrography

The depth of mixing and the salinity, temperature, and density structure of the upper layers are important environmental constraints on the mixing and dispersion of sludge. The surface mixed layer depth is an important parameter for model calculations of farfield dispersion (Walker et al., 1987). Typically, the upper layers of the Slope Sea in spring and summer consist of a characteristic well-mixed layer above the main thermocline between about 50- and 150-m depth. This layer is known as the slopewater pycnostad and has a characteristic temperature and salinity of about 12°C and 35.5‰, respectively. Above the pycnostad, 0 to 50m in depth, there are complex mixtures of shelf, GS, and slopewater. GS water can overrun the surface waters of Slope Sea through filaments, warm outbreaks and extrusions. The latter are usually due to the interaction of the GS with warm-core rings. Filaments are shallow (20 to 50m deep) elongated fingers of GS water that trail from the crests of some meanders. They are generated by the circulation in the trough of a GS meander and are thought to be fairly passive (Bane et al., 1981). Warm outbreaks are similar to but larger than filaments and persist for several weeks (Cornillon, 1986). In the fall and winter, more frequent storms and atmospheric cooling tend to mix the surface

layers and reduce the vertical gradients of salinity and temperature for both shelf and slope water.

Exchange events can also occur with shelf water due to rings, upper-slope eddies, and wind-driven flows. Hydrographic sections that transect across the Slope Sea often show large subsurface elliptical shaped masses of cooler, fresher water of shelf origin, apparently detached from shelf. The recent SEEP studies have shown that these apparently isolated water masses in the slope water are probably attached to the shelf-slope front through complex three-dimensional structures (R.W. Houghton, Lamont-Doherty Geological Observatory, 1986, personal communication). The complexity and heterogeneity of the upper 50- to 75-m of the water column at the 106-Mile Site indicate that a single conductivity-temperature-depth (CTD) cast, particularly in summer, at the dumpsite may not be representative of the hydrographic structure over the length scales of the dispersion processes and may also be difficult to interpret in terms of salinity and temperature of different water masses. Examples of the variability of the hydrography are shown in selected salinity, temperature, and sigma-t (density) sections from the northern MASAR transect (Figures 1-5a through 1-5c).

An important result of the MASAR study was the documentation of the formation and erosion of the slope water pycnocline over the annual seasonal cycle. Part of this cycle is illustrated by the sections in Figures 1-5a through 1-5c. The slope water pycnocline is formed by convective overturning in the late winter (February) due to the cumulative effect of winter storms and intense winter atmospheric cooling. The result is shown in Figure 1-5a where the upper 200m of the water column is perfectly mixed (temperature 12°C, salinity 35.4‰, 26.9 sigma-t). Time series of temperature from the MASAR moorings and the southern transect hydrographic section for February 1985 showed that the formation of this deep mixed layer occurred throughout the western Slope Sea at about the same time. Thus, the overturning of the upper layers in late winter is not a local phenomenon. By the middle of May (Figure 1-5b), this mixed layer has been overrun by shelf and GS water, which provide a stratified cap to the pycnocline (50 to 150-m), isolating it from atmospheric exchanges. The fall section (Figure 1-5c) shows no trace of the pycnocline. There is now an intense seasonal thermocline at about 30-m depth formed by atmospheric heating through the summer. Note in this figure the

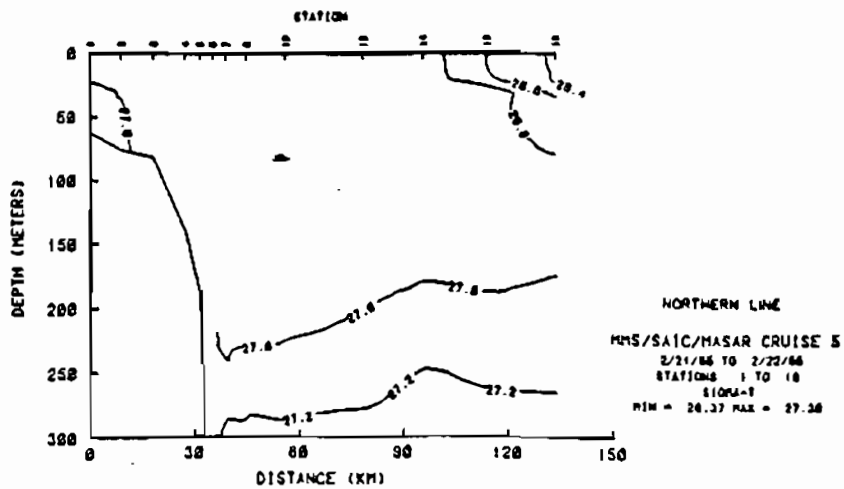
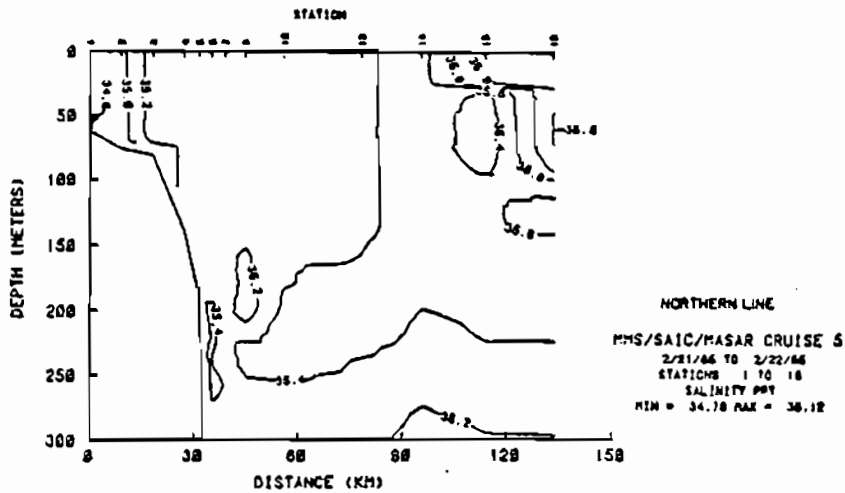
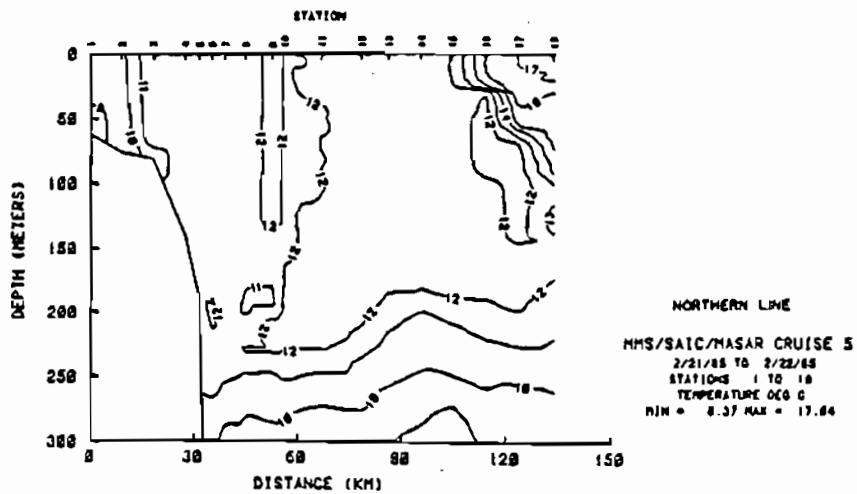


Figure 1-5a. MASAR hydrographic section for the northern transect on February 21, 1985.

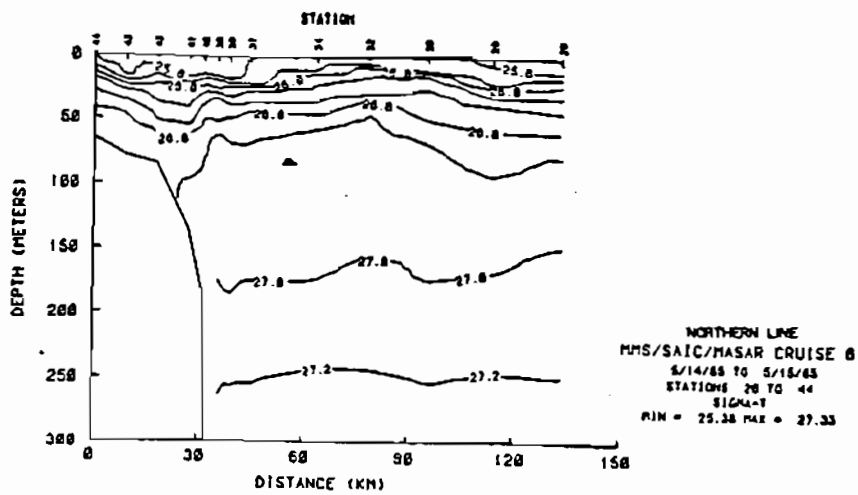
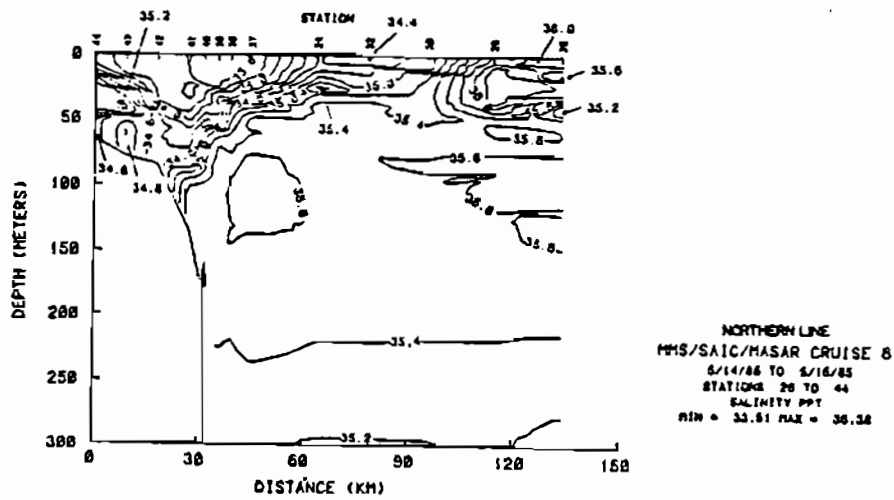
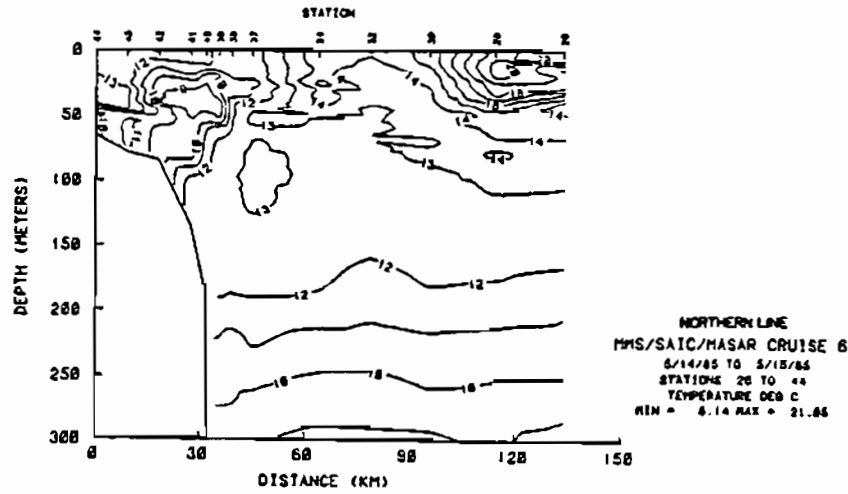
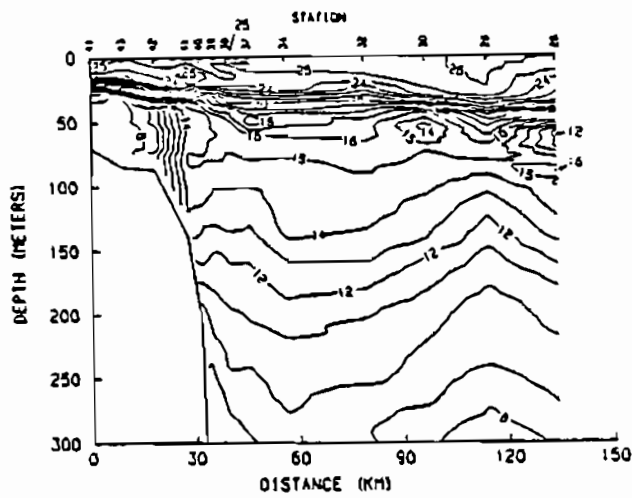
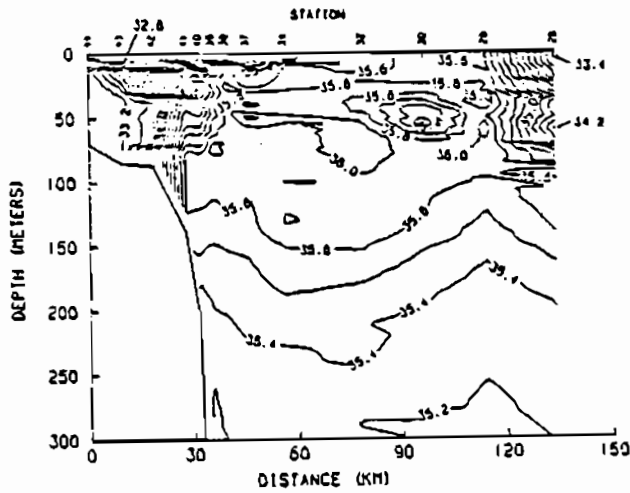


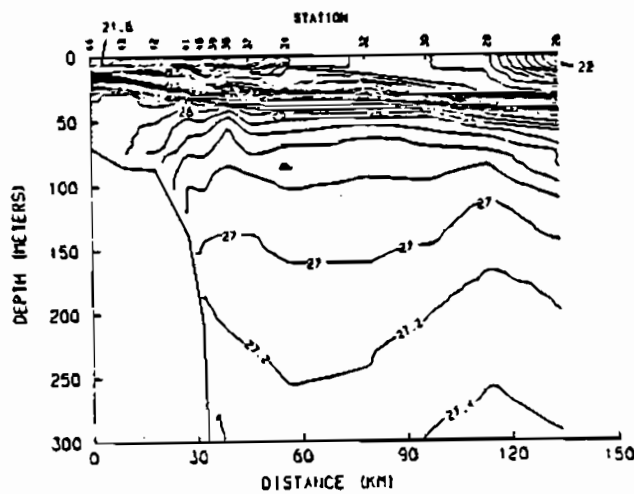
Figure 1-5b. MASAR hydrographic section for the northern transect on May 14, 1985.



NORTHERN LINE
 MMS/SAIC/MASAR CRUISE 7
 9/ 9/85 TO 9/ 9/85
 STATIONS 26 TO 44
 TEMPERATURE DEG C
 MIN = 7.23 MAX = 26.26



NORTHERN LINE
 MMS/SAIC/MASAR CRUISE 7
 9/ 9/85 TO 9/ 9/85
 STATIONS 26 TO 44
 SALINITY PPT
 MIN = 32.58 MAX = 36.26



NORTHERN LINE
 MMS/SAIC/MASAR CRUISE 7
 9/ 9/85 TO 9/ 9/85
 STATIONS 26 TO 44
 SIGMA-T
 MIN = 21.38 MAX = 27.53

Figure 1-5c. MASAR hydrographic section for the northern transect for September 9, 1985.

intense salinity and temperature front in the lower part of the water column at the shelf break and the occurrence of cool, fresh water of shelf origin (Stations 30 and 26) at about 50-m depth at distances of more than 100 km from the slope.

The erosion of the pycnostad between April and September is caused by the upwelling of water from the GS thermocline (800m deep in the Sargasso Sea), which is oxygen depleted and nitrate rich (Rossby, 1936; McLellan et al., 1953). Convective overturning in the late winter increases the oxygen content (~ 5 ml/L), and the high biological productivity in the spring decreases the nitrate levels ($\sim 7 \mu\text{g at/L}$) of the pycnostad, from the values found in the thermocline east of the GS.

Thus, sludge dumped in slopewater during the late winter convective overturning could be readily mixed over the upper 200m of the water column. In the late fall, however, an intense seasonal thermocline may limit vertical mixing, due to winds, to the upper 20m of the water column. The frequent occurrence of complex water mass structures and fronts in the upper 50 to 75m of the Slope Sea may also mean that horizontal mixing is inhibited, with the sludge possibly being confined to a distinct water mass, thus slowing the processes that lead to dilution and dispersion.

1.2.3.3 Warm-Core Rings and the Gulf Stream

Warm-core rings are spawned from GS meanders, and are reabsorbed by the GS after a lifetime of anywhere from 2 to 12 months. A ring in the Slope Sea is a visitor, and although it can cause motions and exchanges of the surrounding waters, it may be regarded as a temporarily detached part of the GS which is, biologically, relatively unproductive compared to the surrounding slopewater. Thus, sludge that is dumped into the center part of ring may experience high currents ($\sim 150 \text{ cm s}^{-1}$) in a variety of directions depending on the position of the release relative to the ring center. Over the slope, the characteristic signals from moored upper-layer instruments of the passage of a ring are strong clockwise rotating northward currents accompanied by a sharp increase in temperature. However, the mass transport of the sludge as it is dispersed within the rotating mass of water is southwest at about 5 cm/s^{-1} as the center of the ring moves towards Cape

Hatteras. A ring in the region between the 106-Mile Site and Cape Hatteras may be reabsorbed into the Gulf Stream or lose mass to the GS in ring-GS interaction at any position. Therefore, sludge particles within a ring are most likely to be introduced into the swiftly flowing jet of the GS proper. However, rings on occasion show evidence of spiral-shaped filaments of shelf or slope water within the center part of the rotating mass. Thus, there is a possibility of exchange with the shelf and slope water even for sludge dumped in the center of a ring, as further discussed in the next section.

The Gulf Stream itself may on occasion flow over the 106-Mile Site. Figure 1-6 shows the mean, standard deviation and extreme positions of the GS north wall taken from all available (two per day) AVHRR images for the month of October 1985. Thus, the shoreward extreme position shows the GS flowing across the majority of the dumpsite. This situation is probably fairly rare depending on the average path of the GS during the year. In 1985, due to the displaced GS path as previously discussed, the monthly statistical position diagrams (like Figure 1-6) show that the 106-Mile Site had direct GS current events three to four months of the year. If a GS meander crest moves through the site, it may affect the flow regime for several days at a time. Sludge released into the GS is probably the most favorable situation for rapid dispersion of the waste because of high velocities ($\sim 200 \text{ cm s}^{-1}$) and strong vertical and horizontal velocity shears. However, GS flows through the 106-Mile Site are likely to be east or northeast and thus, in terms of LPCs at the eastern site boundary, it will probably cause violations due to the speed at which the sludge waste would be advected eastward. A similar situation of strong east currents would occur if waste is dumped on the northern edge of a warm-core ring.

1.2.3.4 Shelf-Slope Exchanges

The most complex and difficult issues in determining the fate of sludge waste are the transport and mixing processes across the shelf-slope front and the possibility of introducing sludge particles onto the highly productive, important fisheries of the outer continental shelf. A number of mechanisms have been proposed for the exchange of shelf and slope water across the front, such as the generation of intrusions due to the passage of rings

North-Wall Location Envelope for October, 1985

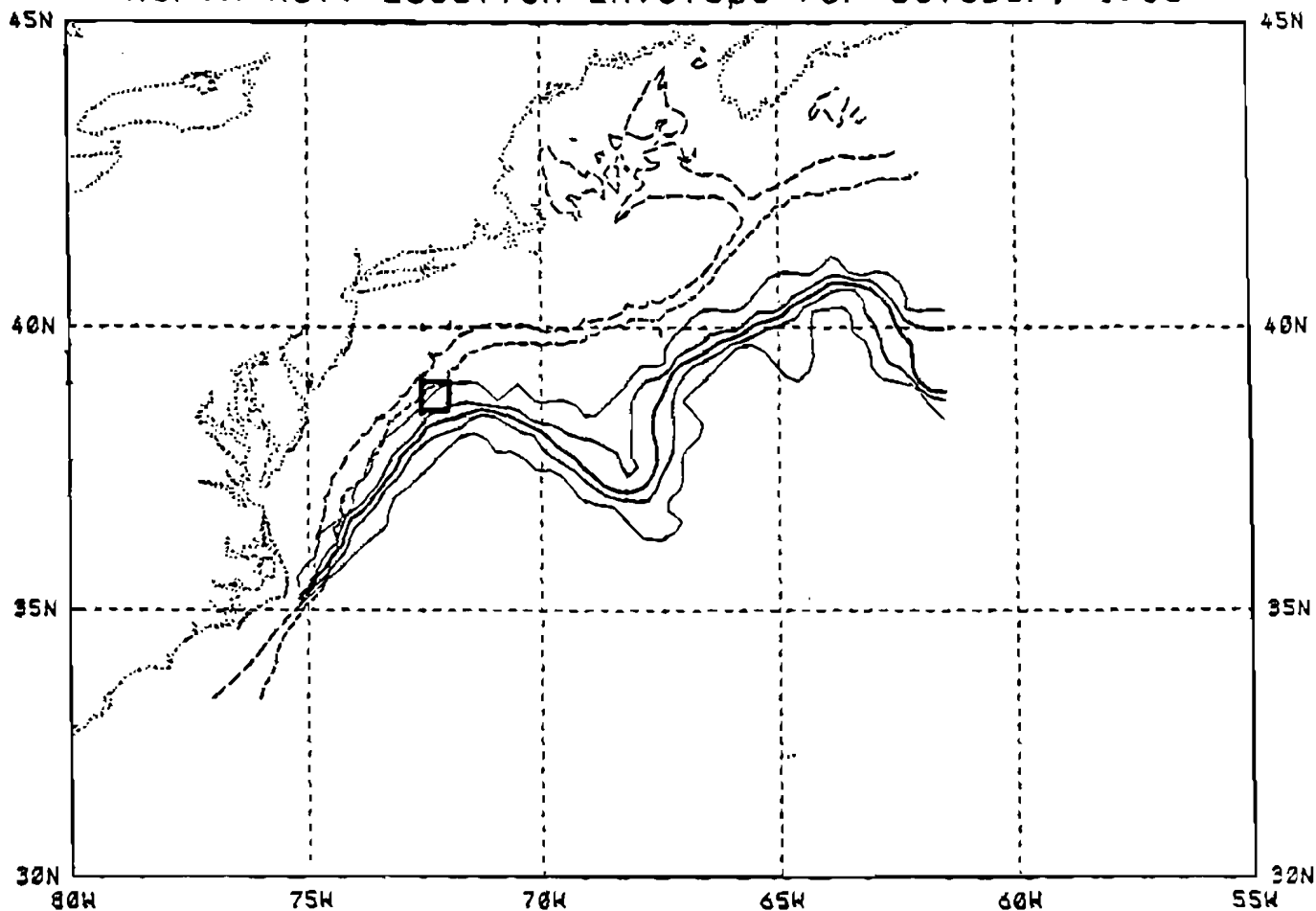


Figure i-6. The mean position (heavy line), standard deviation and extreme positions (thin line) of the GS front (north wall) taken from all available digitized, satellite-derived (AVHRR) sea-surface temperature maps for the month of October 1985. The position of the 106-Mile Site is shown.

along the slope, frontal instabilities, the effects of small clockwise and anticlockwise eddies on the upper slope, wind-forced and density-driven intrusions, and mixing mechanisms such as caballing and double diffusion (Garrett and Horne, 1978). Caballing is the process where two water masses of similar density but different temperature and salinity (i.e., cooler and fresher versus warmer and salty) mix to produce denser water (due to the non-linear nature of the equation of state for sea water), which then sinks. Double diffusion is the process where water masses separated by a temperature and salinity front become interleaved along isopycnal surfaces. This usually occurs at the shelf-slope front (see Figure 1-5c). It is likely that these mechanisms produce episodic events of limited spatial extent, though intrusions seem to be relatively long lived (days to weeks), and the onshore-offshore fluxes are estimated to be comparable to the average onshore-directed cross-shelf flux of salt required for a salt balance on the Mid-Atlantic Bight shelf (Ketchum and Keen, 1955). These mechanisms produce movements of water from the slope to the shelf and vice versa which have not been quantified or experimentally studied. Most of the evidence is from satellite imagery and hydrographic sections across the shelf and slope. However, intrusions of slopewater do occur episodically on the shelf, and these provide pathways for sludge particles to be injected onto the shelf and then transported by density- and wind-driven upwelling flows towards the shore.

An example of wind, and possibly density-driven intrusion at thermocline depth on the shelf, during summer, is given in Figures 1-7a and 1-7b. The transects were taken across the shelf off the eastern shore of Virginia at about 38°N. The salinity intrusion at about 20-m depth extends about halfway across the shelf on July 19, 1975, just above the cold pool of 8°C water. A sharp front separates the cold pool from slopewater (temperature > 12C) in the lower half of the water column similar to the May 1985 MASAR transect (Figure 1-5b). In two days, under strong upwelling favorable southerly winds, the salinity intrusion has grown by about 40 km, to reach the shallow inner shelf (Figure 1-7b). This example of a rapidly developing intrusion of slopewater provides a pathway for sludge particles trapped in the seasonal thermocline to reach the inner shelf. In winter, the evidence from hydrography and current meters is that onshore directed, wind-

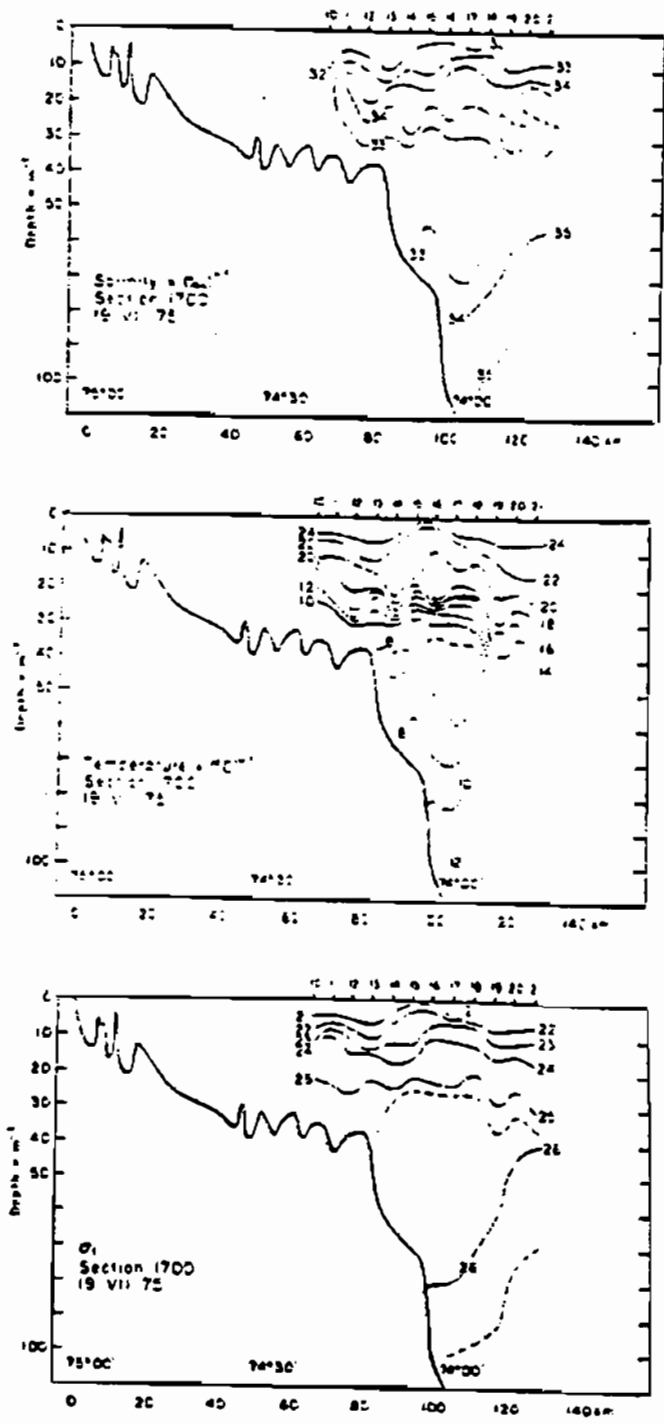


Figure 1-7a. Temperature, salinity, and density distributions in a vertical section across the continental shelf on 19 July 1975 for a section off the eastern shores of Virginia ($\sim 38^\circ\text{N}$).

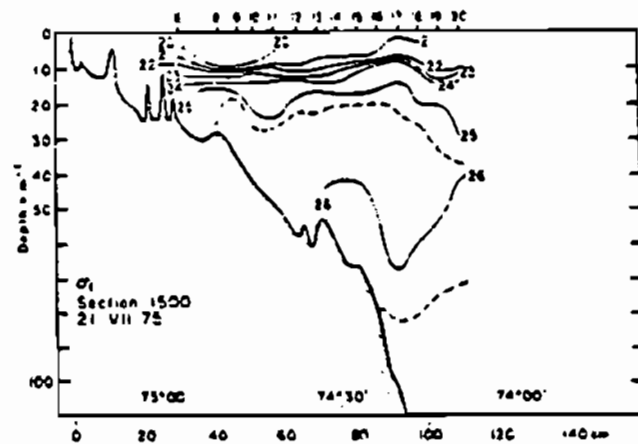
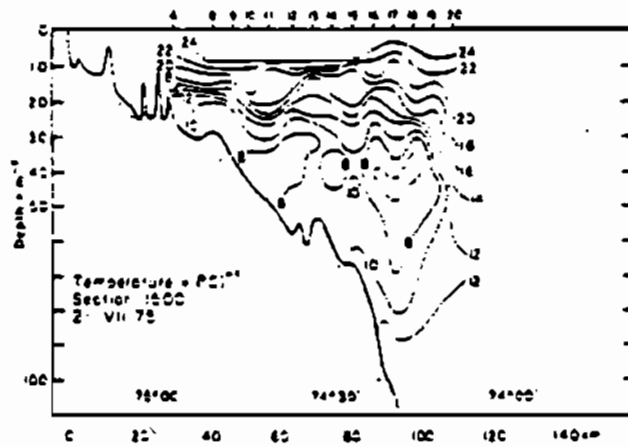
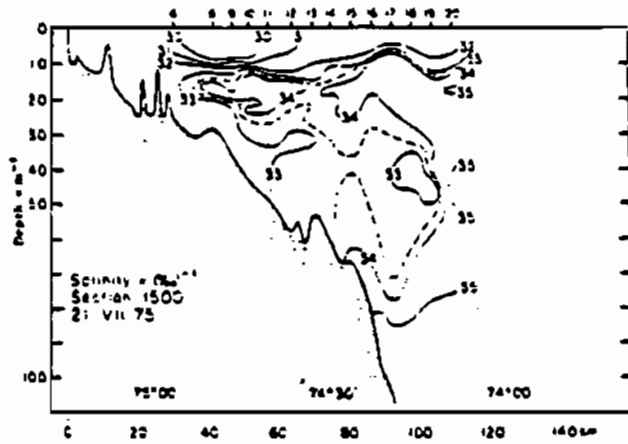


Figure 1-7b. Temperature, salinity, and density distributions in a vertical section across the continental shelf on 21 July 1975 for the same transect as Figure 1-7a.

driven flows are more likely to occur near the shelf bottom than at thermocline depth (Boicourt and Hacker, 1976). The presence of canyons, shelf valleys and other topographic features may locally enhance wind- and density-driven shoreward flows.

The SEEP experiment and recent examination of historical hydrography (Churchill et al., 1986) have shown that warm-core rings may be responsible for substantial intrusions of slopewater onto the shelf. Thus, waste dumped just south of a ring can be moved onto the shelf by shoreward ring currents. Similarly, the occurrence of smaller clockwise and anticlockwise rotating eddies in the wake of a ring or an anticlockwise cold-core eddy preceding a ring (Churchill et al., 1986) can inject near surface slopewater onto the shelf. There is some evidence that these events are more likely in summer, when the shelf-slope front is confined to the lower water column, than in winter, when the front extends from surface to bottom. Once injected onto the shelf by an intrusion or exchange process, sludge particles would be transported and mixed by shelf circulations, including wind-forced and density-driven flows associated with major river outflows.

1.3 OBJECTIVES

The main objective of the current meter program was to monitor the current and temperature structure of the upper ocean near the 106-Mile Site in order to assess the physical processes affecting the transport and mixing of sludge. This study extends previous measurement programs by monitoring currents and temperatures closer to the surface (50m) and by extending the time series available for use with dispersion models (Walker et al., 1987) for statistical characterization of the current and temperature fields.

The MASAR program, funded by MMS, maintained a transect across the slope and rise of four to five moorings just to the south of the 106-Mile Site between March 1984 and March 1986 (SAIC, 1987). The instruments nearest the surface were deployed at 100m or deeper in MASAR. The deeper instruments on the EPA moorings (100-m, 250-m and 1000-m nominal depths) correspond to the depths of meters deployed on the MASAR deepwater moorings (SAIC, 1987).

The statistical characterization of the EPA current measurements includes evaluating the along-isobath coherence of the current fields at

moderate (75 km) separation (i.e., approximately the north-south extent of the site). This evaluation allows some estimation of the along-isobath spatial scales over which current measurements at a single position have some validity. This estimation is important for dispersion modeling using current meter data. The MASAR data showed that current fluctuations in the upper layer on the slope were intermittently coherent, depending on the configuration of the Gulf Stream, between the New Jersey and Virginia Beach transects--a distance of about 250 km (SAIC, 1987). This coherence is a reflection of the large scales inherent in the gyre circulation of the western Slope Sea, when large perturbations such as rings are not present.

2. FIELD PROGRAM

2.1 MOORINGS

Two moorings, X and Y, were deployed on the 2500-m isobath, northeast and southwest of the 106-Mile Site on September 19, 1986, and recovered on April 23, 1987. The positions are given in Figure 2-1, and details of the instrumentation and mooring designs are given in Table 2-1 and Figure 2-2, respectively.

Table 2-1 shows the data variables returned from each instrument. Mooring Y, as deployed, had Aanderaa current meters at 48m and 97m (Figure 2-2); however, these top two instruments were lost because the spindle failed on the 97-m Aanderaa (see cruise reports for Work Assignment No. 31 for details). All the instruments experienced a 95 to 100% tape transport, but the majority ran out of tape before retrieval because of various delays in scheduling the recovery cruise. The instrument problems are as follows: the General Oceanics MK II Niskin Winged Current Meter (X1062) had a faulty tiltmeter and thus, a good temperature, but no current record was obtained. The Sea Data temperature recorder (X1066) at 199m had missing data at the beginning of the tape; and the rotor of the deepest Aanderaa in Mooring Y (Y1062) apparently fouled about 10 days after deployment, producing unrealistically low speeds ($<2 \text{ cm s}^{-1}$).

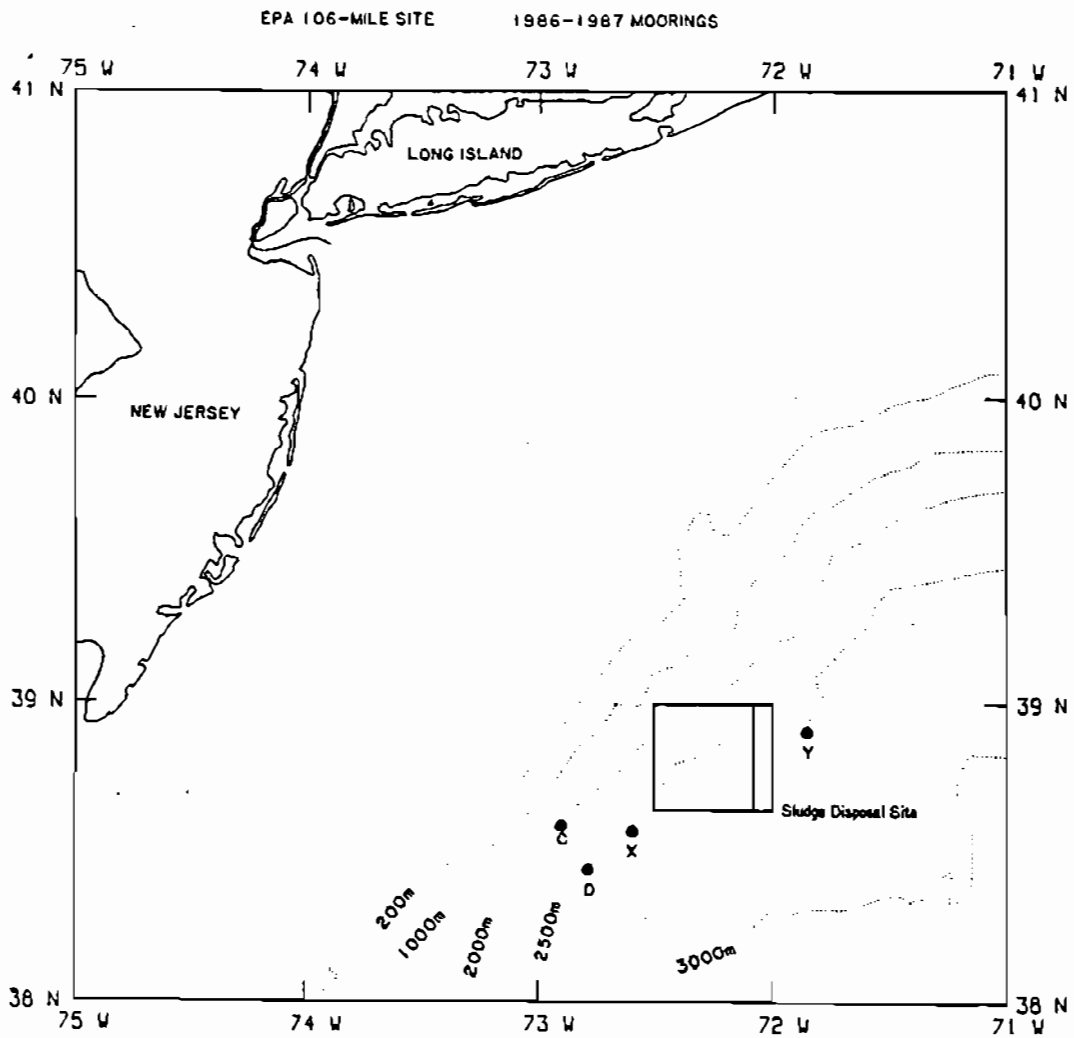


Figure 2-1. A chart of the 106-Mile Site with EPA mooring positions X and Y, and MASAR mooring positions C and D, indicated.

Table 2-1. EPA 106-Mile Site Moorings.

Mooring X: Southwest of Dumpsite
 Position: 38°34.5'N 72°36.6'W
 Water Depth: 2500-m

Instrument ID	Instrument Type	Depth from Surface (m)	Variables	Data Return
X1061	Aanderaa RCM-4	48 m	Spd, Dir, Temp.	Good 100%
X1062	General Oceanics	72 m	Temp.	Tilt meter failed
X1063	Aanderaa RCM-4	95 m	Spd, Dir, Temp.	Good 100%
X1064	Sea Data TR-2	124 m	Temp.	Good 100%
X1065	Sea Data TR-2	150 m	Temp.	Good 100%
X1066	Sea Data TR-2	199 m	Temp.	Short 88%
X1067	Aanderaa RCM-4	248 m	Spd, Dir, Temp.	Good 100%
X1068	Aanderaa RCM-5	1000 m	Spd, Dir, Temp.	Good 100%

Mooring Y: Northeast of Dumpsite
 Position: 38°54.4'N 71°51.7'W
 Water Depth: 2500-m

Instrument ID	Instrument Type	Depth from Surface (m)	Variables	Data Return
Y1061	Aanderaa RCM-4	249 m	Spd, Dir, Temp.	Good 100%
Y1062	Aanderaa RCM-5	1005 m	Temp.	Rotor fouled soon after deployment

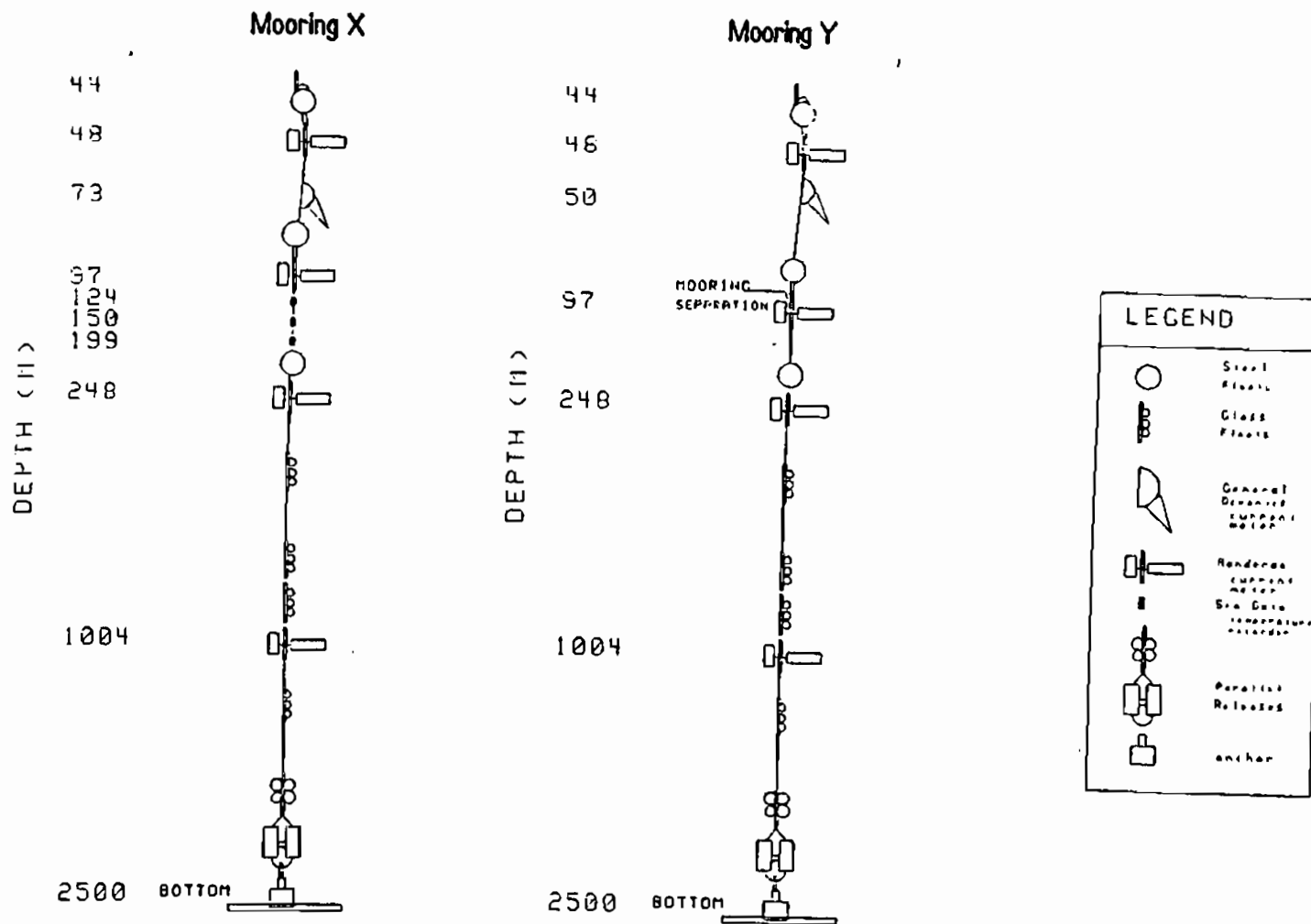


Figure 2-2. The configurations of EPA moorings X and Y deployed southwest and northeast of the 106-Mile Site, respectively.

2.2 DATA PROCESSING

The Aanderaa tapes and Sea Data Microcassettes were transcribed to computer files using Aanderaa and Sea Data tape readers by SAIC in Raleigh, NC, whereas the General Oceanic cassettes were transcribed to 9-track computer tape by General Oceanics. The digital data were converted to engineering units using the manufacturer's calibration information and then edited to remove out-of-range values and sharp spikes. The resulting small gaps were filled by linear interpolation. After the start and end times of each raw data time series were precisely established and the magnetic variation applied to current direction data, the data were filtered with a 3-hour low pass (3-HLP) Lanczos kernel decimating to intervals of one hour. This filter removes high frequency noise from the time series and establishes a common time interval of one hour between data points. To further display low frequency data, the 3-HLP data were filtered with a 40-HLP Lanczos kernel and decimated to 6-hour intervals. This filter effectively removes tidal and inertial signals from the time series.

The current vector time series were resolved into U- and V-components such that the positive V-component is directed approximately along the trend of the local isobaths at 060°T . Thus, the positive U-component is directed away from the slope at 150°T . (Such rotated vector time series are denoted by "R60" after the meter identification (ID) in the plot labels--refer to Figure 3-1 in Section 3.2).

The five-character time series IDs are constructed from the mooring designation X or Y, 106 denoting the 106-Mile Site, and the number of the instrument from the top of the mooring. Thus X1067 represents the Sea Data record from the seventh instrument down from the top of mooring X (see Table 2-1). This designation is often shortened to X7, for example, in the following discussion.

3. DATA INTERPRETATION AND ANALYSIS

3.1 INTRODUCTION

The current and temperature records are best described in a phenomenological manner: the records illustrate the effects on the current and temperature field of a sequence of events passing the moorings. These major events are primarily the passage of warm-core rings, but could include smaller eddies, extrusions or filaments of shelf water, and Gulf Stream phenomena. These events are superimposed on the basic southwesterly flow of upper slope water through the site, which is part of the northern limb of the western Slope Sea gyre. A brief description of the physical processes affecting the circulation at the 106-Mile Site is given in Section 1.2. Refer to Csanady and Hamilton (1987) and SAIC (1987) for a review of circulation in the region; Joyce (1984) for a description of the current and hydrographic fields in a warm-core ring; to Brown et al. (1986) for a statistical description using satellite imagery of the life history of rings from birth by the pinching of a northward Gulf Stream meander, to death by absorption, often near Cape Hatteras, with the Gulf Stream; and to Beardsley and Boicourt (1982) for a review of shelf circulation in the Mid-Atlantic Bight.

In the interpretation of mooring data events, it is necessary to use AVHRR imagery where possible to obtain a spatial view of the features passing the mooring and thus confirm the analyses. Because the satellite imagery provides a detailed picture of the sea surface temperature field, which is sometimes obscured by clouds, and the mooring provides subsurface time series, the interpretation of the events is not always clear. Warm-core rings are named by the Marine Climatology Investigation, National Marine Fisheries Service (NMFS), Narragansett, Rhode Island, according to the year of formation and a sequence letter. Thus, the prominent November warm-core ring seen in the EPA current records and AVHRR imagery (see Figure 3-5c in Section 3.2) is named 86-E.

3.2 TIME SERIES

The 40-HLP current meter records from both moorings are given in Figures 3-1 and 3-2. The corresponding 3-HLP temperature records are shown in Figures 3-3 and 3-4. A compilation of the features present in these records is provided in Table 3-1 and the satellite images (NOAA/NESS oceanographic analyses) are given in Figures 3-5a through 3-5h. The strongest fluctuations result from warm-core rings and are characterized by increases in temperature at depths up to 1000-m accompanied by strong (50 cm s^{-1}) upper-layer currents. If the mooring is on the offshore side of the ring center as the eddy moves southwest along the slope, the current vectors will have a southwest component and rotate cyclonically (anticlockwise) as the ring passes the mooring. If the current meters are on the shoreward side of the ring center, the current vectors have a northeast component and rotate anticyclonically (clockwise).

The seven-month deployment measured one major ring in November (86-E) followed by a smaller, weaker warm eddy in December which seems to be situated inshore of the 2500-m isobath and is apparently a remnant of ring 6-F (Figures 3-5c, d and e). A similar sequence occurs in September and October (Figures 3-5a, b). However, the current measurements in September only caught the northern edge of the September warm-core ring (86-A), but the trailing warm upper-slope eddy (not named by NMFS) showed substantial flows to 1000m and was effective in extruding a tongue of shelf water into the Slope Sea. The temperature signal indicated that the shelf water was coming from the total shelf depth of about 100-m. This kind of event was rarely measured by the MASAR current meters because the uppermost slope and rise meters were at 100-m depth. It is possible that smaller warm eddies are remnants of large warm-core rings (i.e., 86-F), or generated by rings, or that smaller upper-slope eddies are more ubiquitous than previously thought; such eddies have very weak surface temperature signatures and are thus not readily detected in satellite SST observations. However, such eddies may be detected from satellite imagery by their effects on surrounding water masses (i.e., cold filaments wrapping around the center - Figure 3-5d).

The November warm-core ring (86-E) translated from mooring Y to X in about 10 days. This translation speed of 8.7 cm s^{-1} (7.5 km/day) is



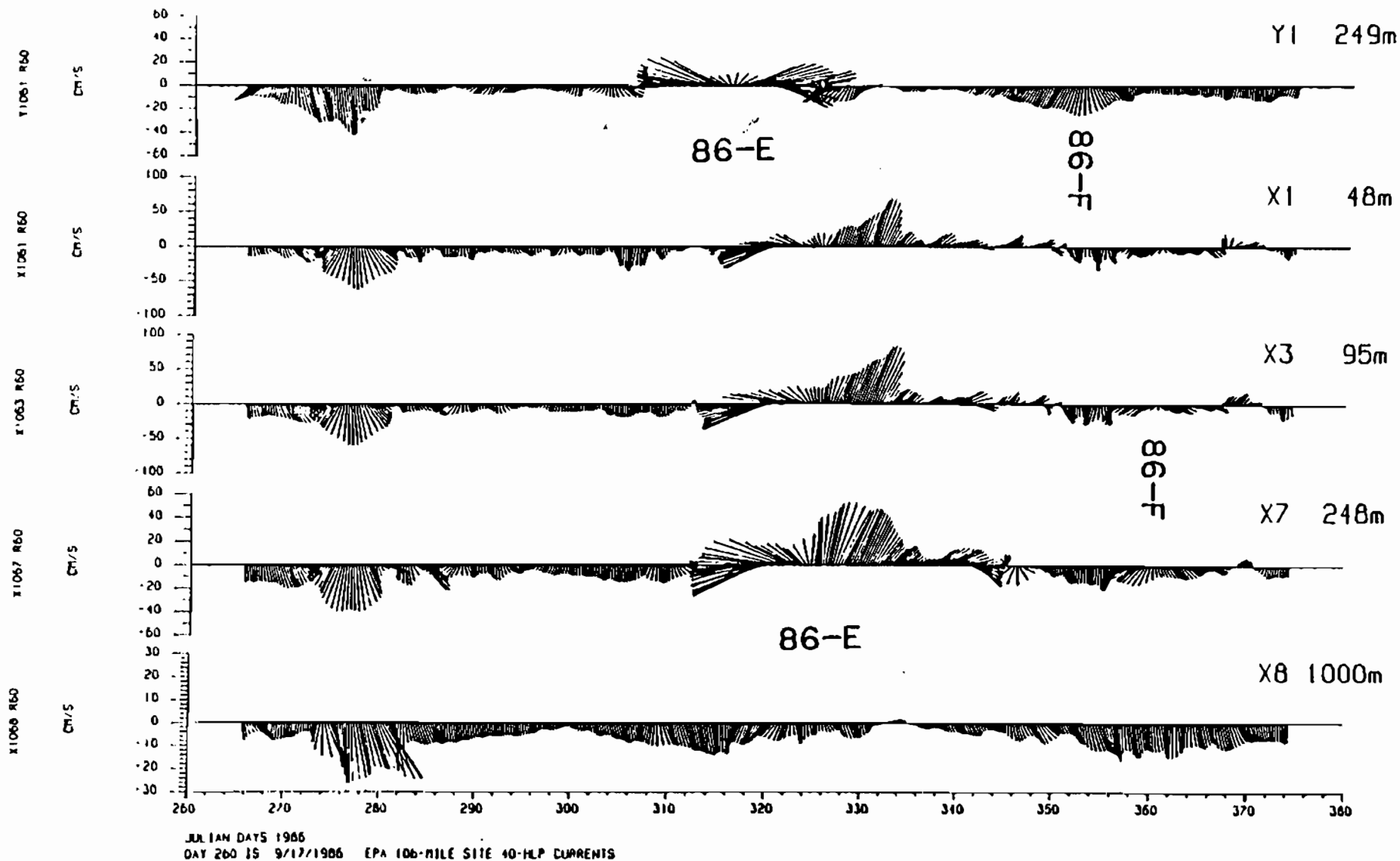


Figure 3-1. 40-HLP stick plot of the first three months of deployment. Stick vectors oriented upward represent along-isobath currents directed toward 060°T. Cross-isobath currents directed toward 150°T are represented by horizontal sticks pointing to the

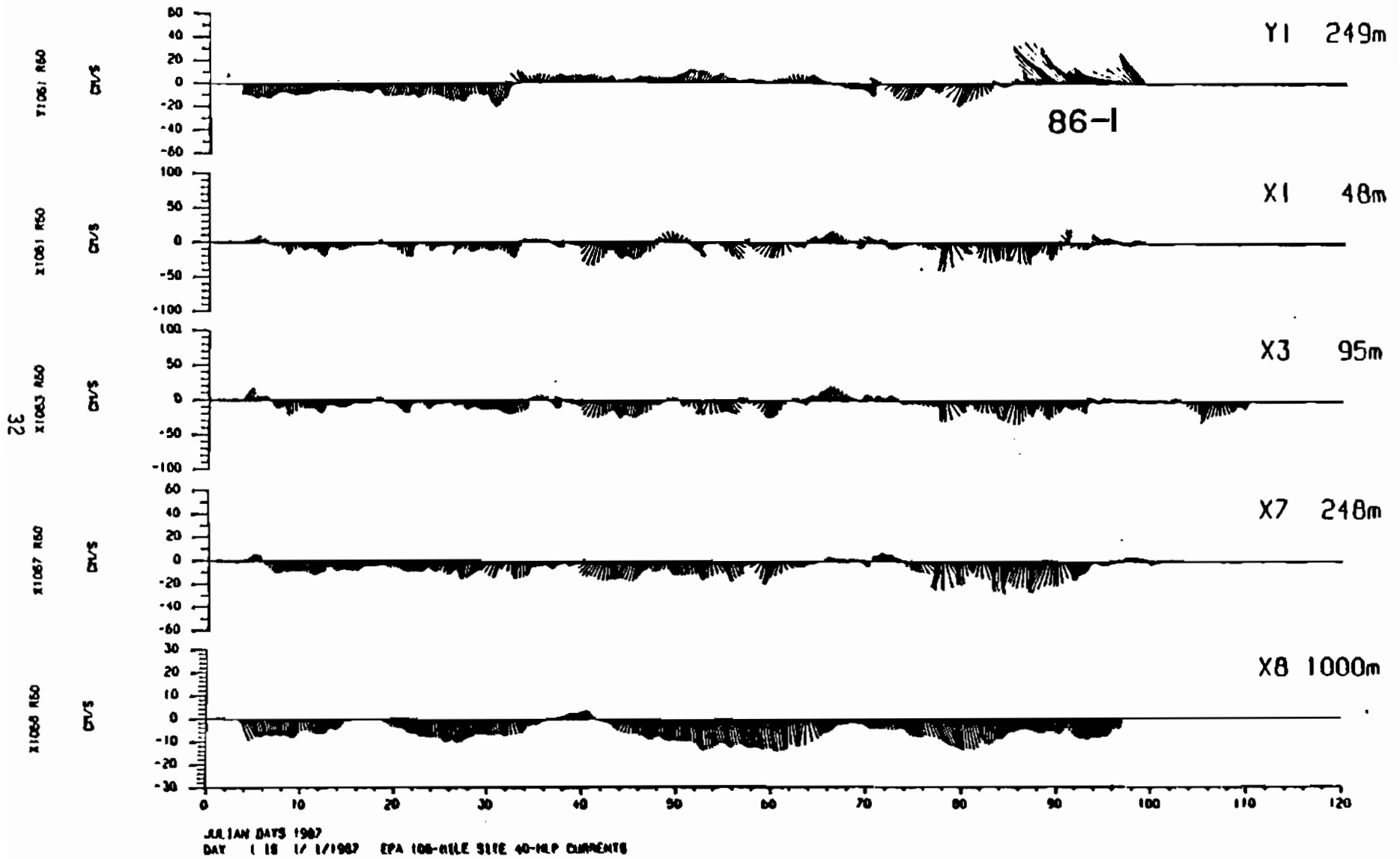


Figure 3-2. 40-HLP stick plot of the second three months of deployment.

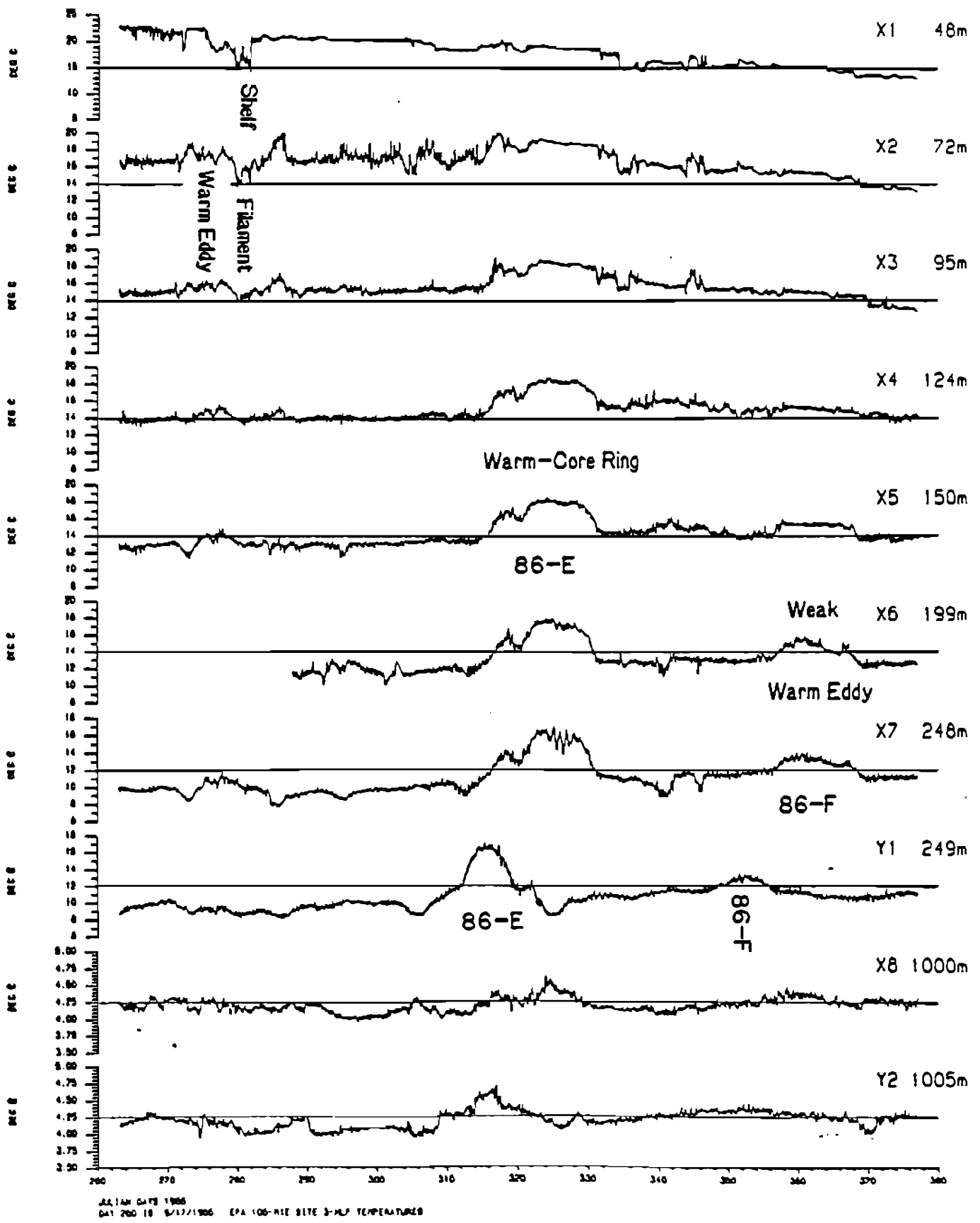


Figure 3-3. 3-HLP temperature records of the first three months of the deployment.

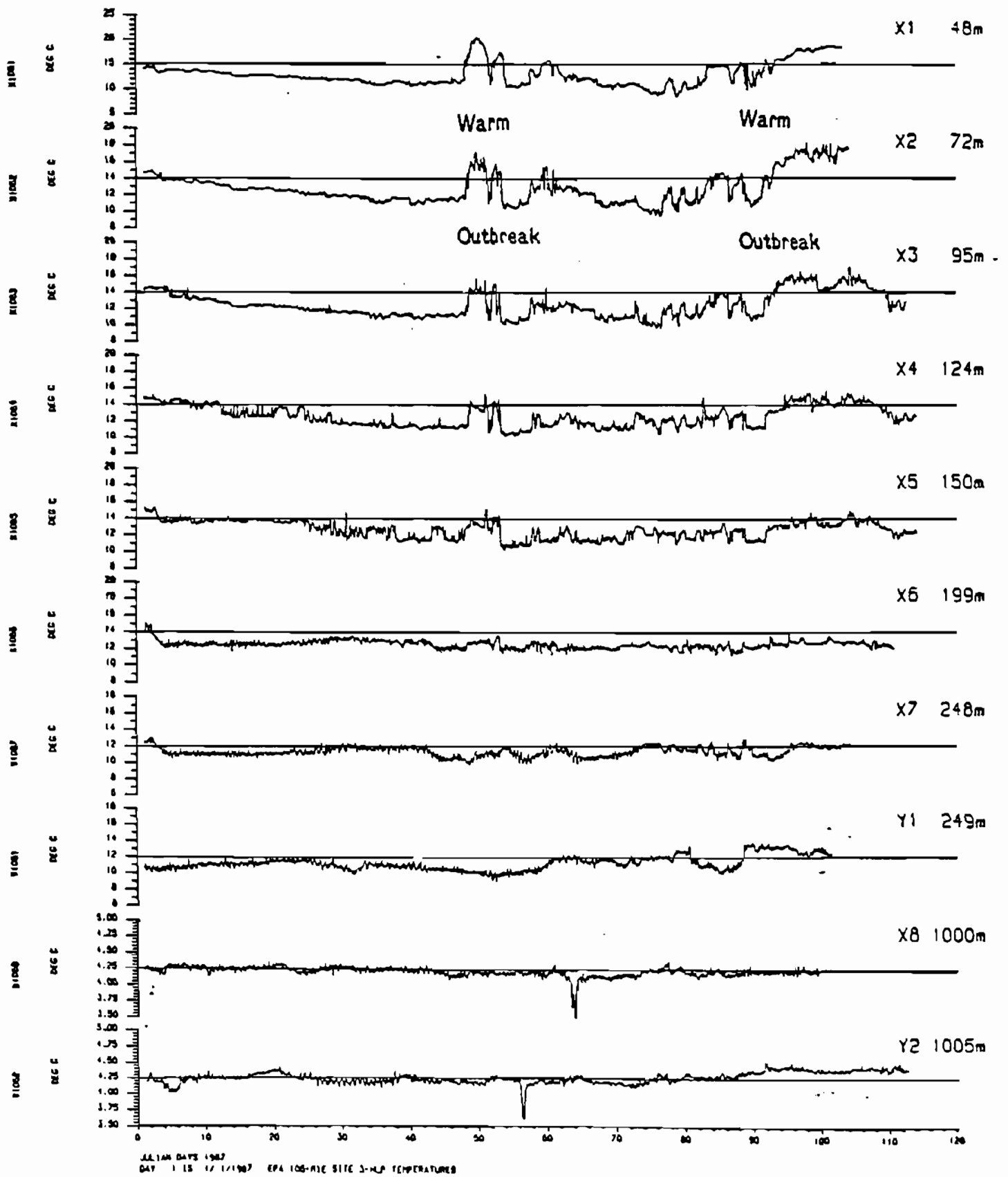


Figure 3-4. 3-HLP temperature records of the second three months of the deployment.

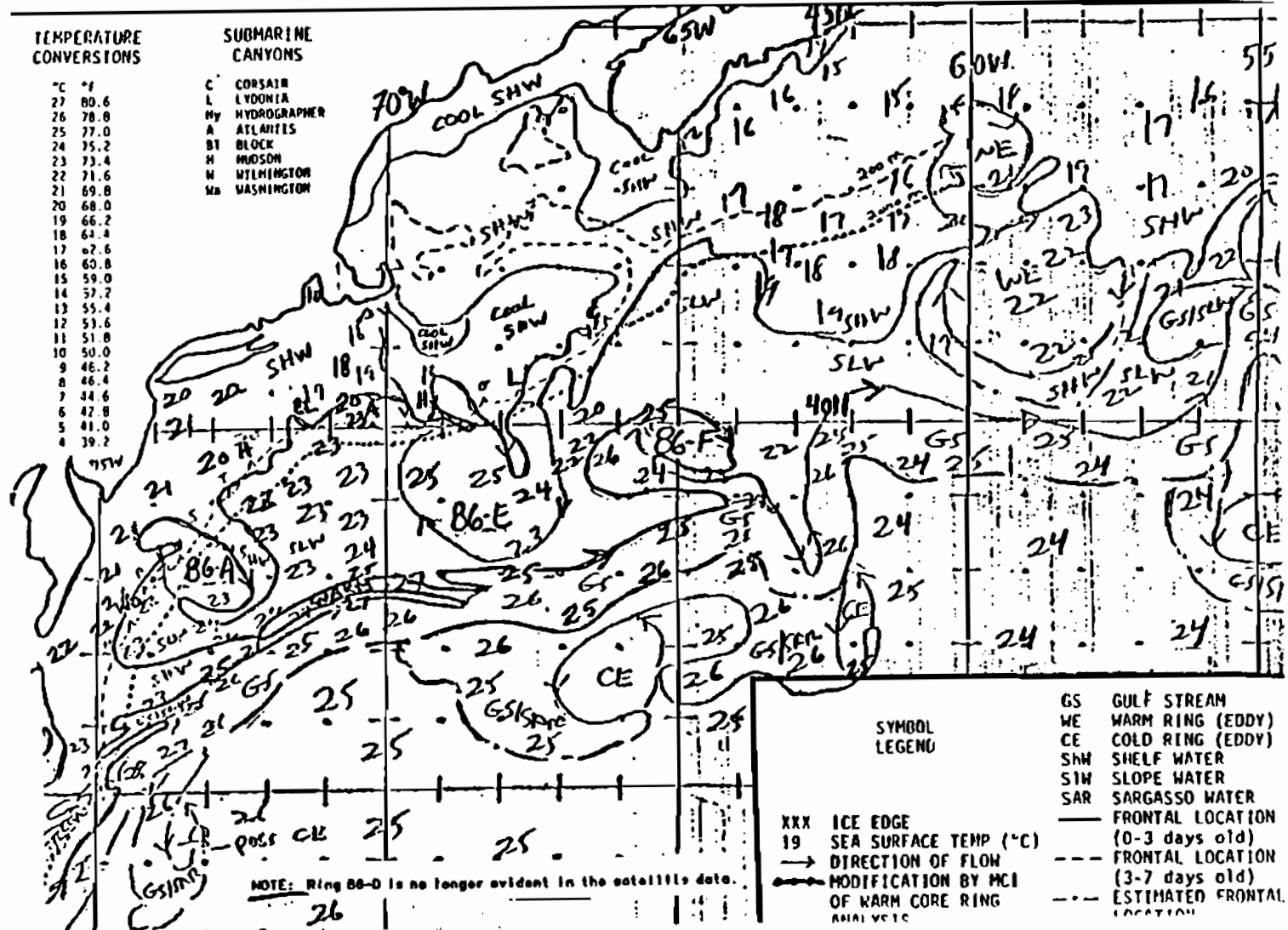
Table 3-1. Events Occuring at the 106-Mile Site, September 1986 to April 1987.

Dates	Julian Day	Satellite Imagery	Description
9/22-10/1	265-274	09/15	S-SW flow of trailing edge of large ring [86-A] that was over the site at the beginning of September.
10/2-10/9	275-282	10/06	The ring [86-A] undergoes a strong interaction with GS off the mouth of the Chesapeake. A small anticyclone, trailing this ring, appears on the upper slope that pulls a filament of cooler shelf water southward over mooring X. Eddy produces cyclonically rotating currents at X at depths to 1000m.
10/8-10/9	281-282	10/06	Cool filament shows strong temperature signals at 48m and 72m at mooring X.
11/1-11/21	305-325	11/19	An energetic warm-core ring [86-E] moves through mooring X. Initial behavior of the current vectors similar to that of Y. After day 326, strong NE flow indicates ring center has moved further offshore and ring translation speed along the slope seems to have decreased. Note that no clear ring signal is seen at 1000m in the currents.
11/10-12/10	314-344	11/24	The ring [86E] moves through mooring X. Initial behavior of the current vectors similar to that of Y. After day 326, strong NE flow indicates ring center has moved further offshore and ring translation speed along the slope seems to have decreased. Note that no clear ring signal is seen at 1000m in the currents.
12/2-12/10	336-344	11/24	Moderate offshore flow (~20 cm/s). The filament of cooler shelf water wrapped clockwise round the ring [86-E] is observed as approx. 2°C step-like temperature drop at 48, 72, 95m at X on days 334-336.
12/24-1/4	358-369	12/29	Imagery shows a very weak eddy onshore of mooring X. This is apparently a remnant of ring 86-F. A deep warm eddy temperature signal is observed at 150, 199, and 248m, but not at the surface. Only weak cyclonically rotating southerly flow is observed at X1, X3, and X7 consistent with the mooring being on the outer edge of the ring.

Table 3-1 Cont'd

Dates	Julian Day	Satellite Imagery	Description
12/12-12/24	346-358	12/29	This weak eddy [86-F] passed Y1 centered around day 352. Stronger southerly currents are observed at this time indicating that Y was closer to the center than when the eddy passed X.
1/1-2/17	1-58	None	January is characterized by slow cooling of the surface layers and generally weak southwestward flows.
2/17-2/23	48-54	2/18	A massive warm event occurs at the surface with decreasing amplitude with depth. It is not observed below 150m (X5). Clockwise rotating currents northeasterly (~20 cm/s) are observed at X1 and very weakly at X3. Imagery shows that this surface warm event is due to a large GS filament overlying the lower slope.
2/25, 3-5	56,64	None	A cool temperature spike is observed first at Y2 and then at X8 (1000m depth) implying a small lens of cooler fresher water as moving along the isobath consistent with the southwesterly currents observed at X8.
3/29-4/12	88-102	3/23	A large ring [86-I] approaching the site shows strong onshore northerly currents at Y1. The center is east of the mooring.
4/4-4/2	94-112	4/13	The eddy [86-I] remains fairly stationary near the Hudson Canyon and appears to be advecting warm water, from a GS warm outbreak, south of the ring into the region of mooring X. X1 and X3 show weak onshore flow with high temperature. No warming is observed below 150m.

15 Sept 1986
 16 Sept 1986



37

Figure 3-5a. Oceanographic Analyses of AVHRR Satellite Imagery, September 15, 1986.

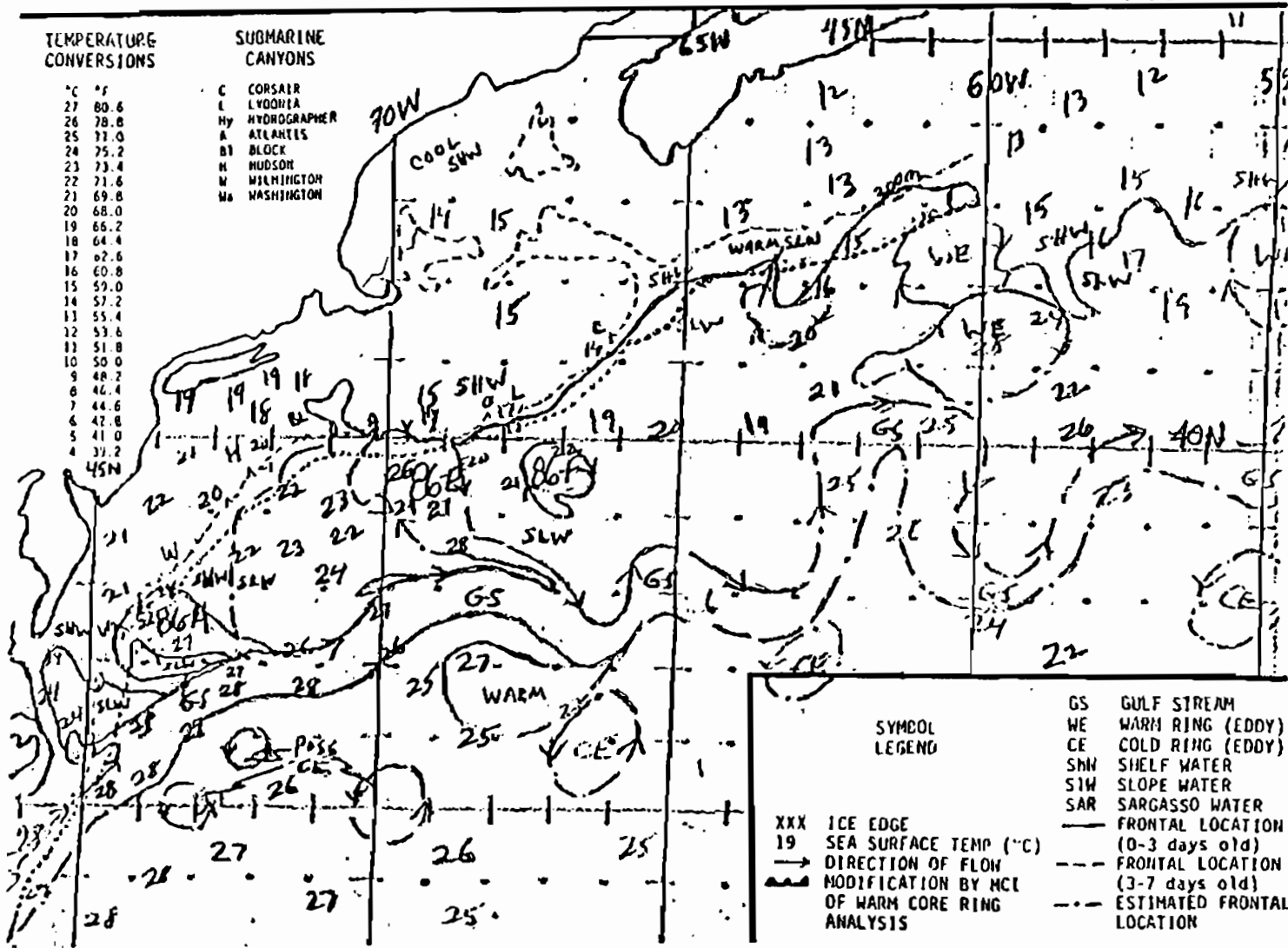
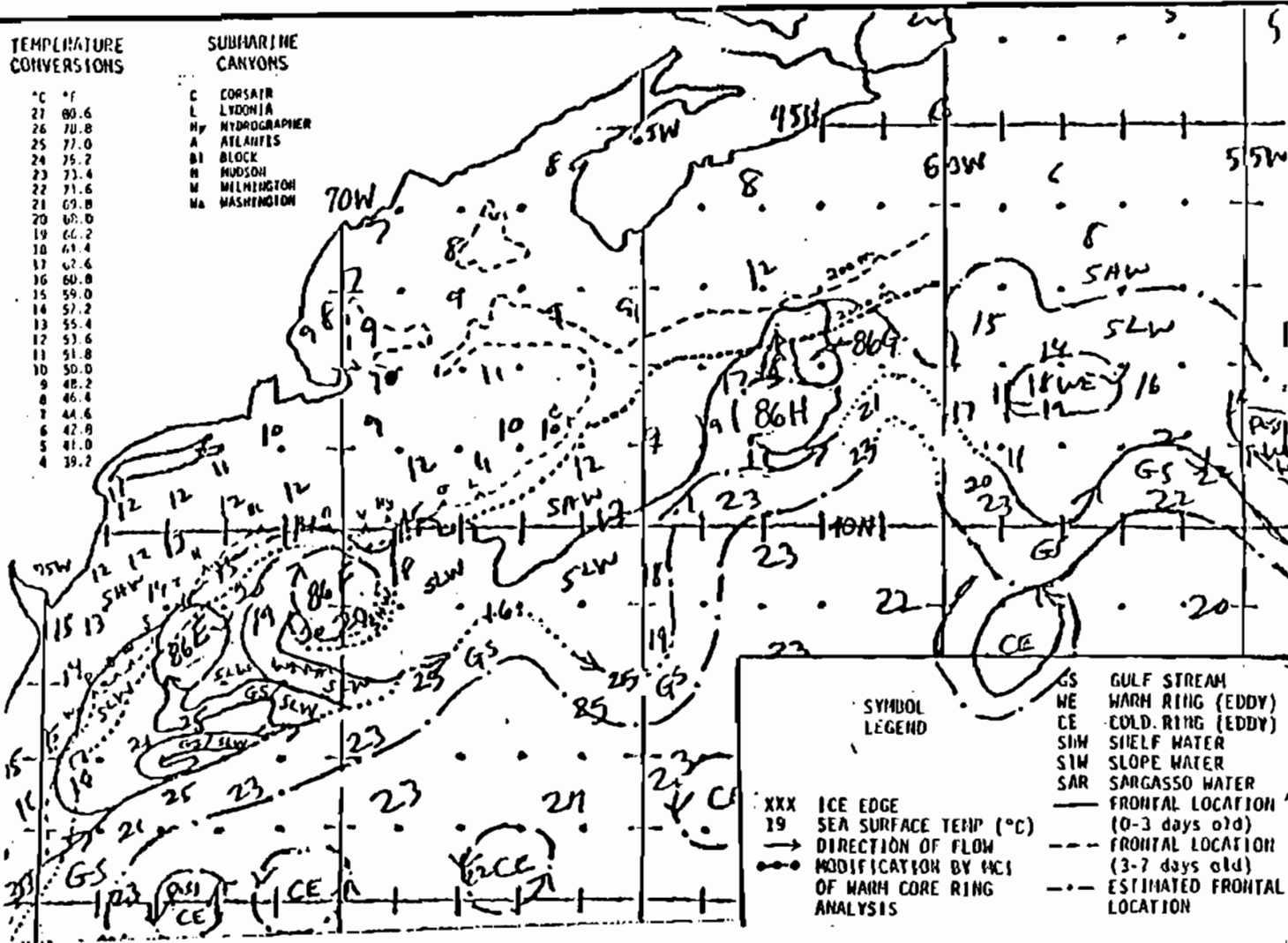


Figure 3-5b. Oceanographic Analyses of AVHRR Satellite Imagery, October 6, 1986.



39

Figure 3-5c. Oceanographic Analyses of AVHRR Satellite Imagery, November 19, 1986.

TEMPERATURE
 CONVERSIONS

°C	°F
27	80.6
26	78.8
25	77.0
24	75.2
23	73.4
22	71.6
21	69.8
20	68.0
19	66.2
18	64.4
17	62.6
16	60.8
15	59.0
14	57.2
13	55.4
12	53.6
11	51.8
10	50.0
9	48.2
8	46.4
7	44.6
6	42.8
5	41.0
4	39.2

SUBMARINE
 CANYONS

C	CORSAIR
L	LYDONIA
Hy	HYDROGRAPHER
A	ATLANTIS
BT	BLOCK
H	HUDSON
M	MILINGTON
Wa	WASHINGTON

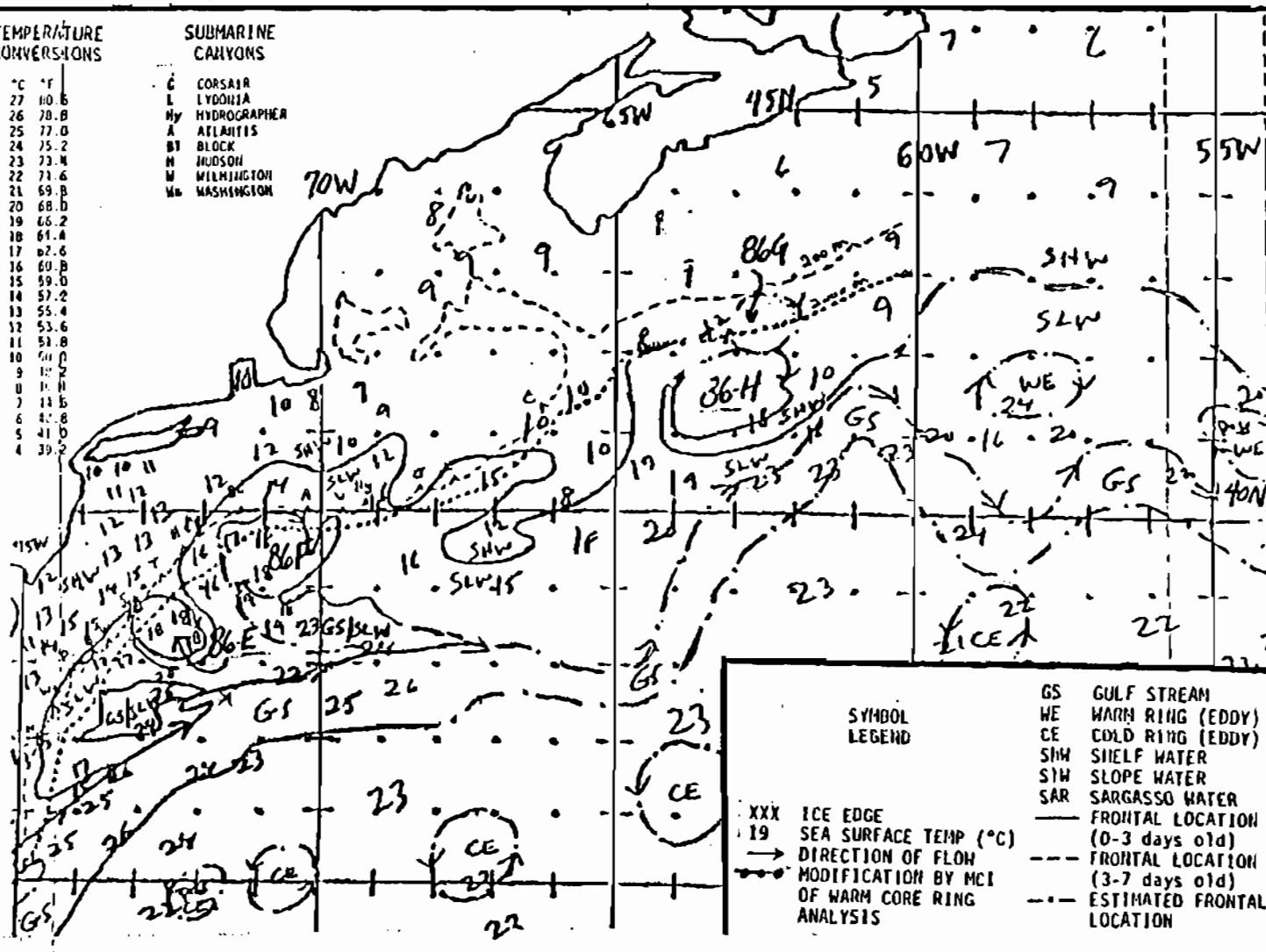


Figure 3-5d. Oceanographic Analyses of AVHRR Satellite Imagery, November 24, 1986.

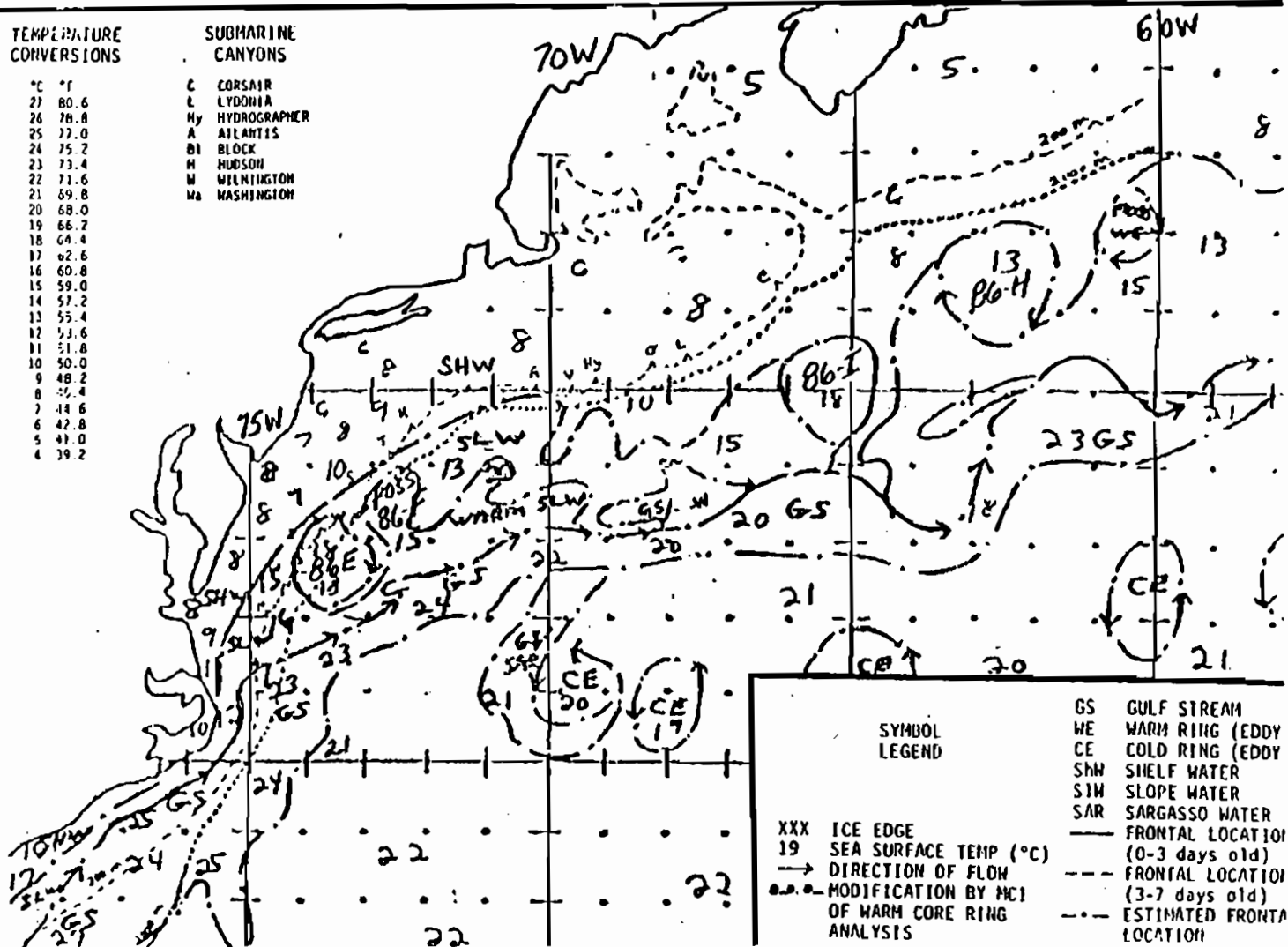
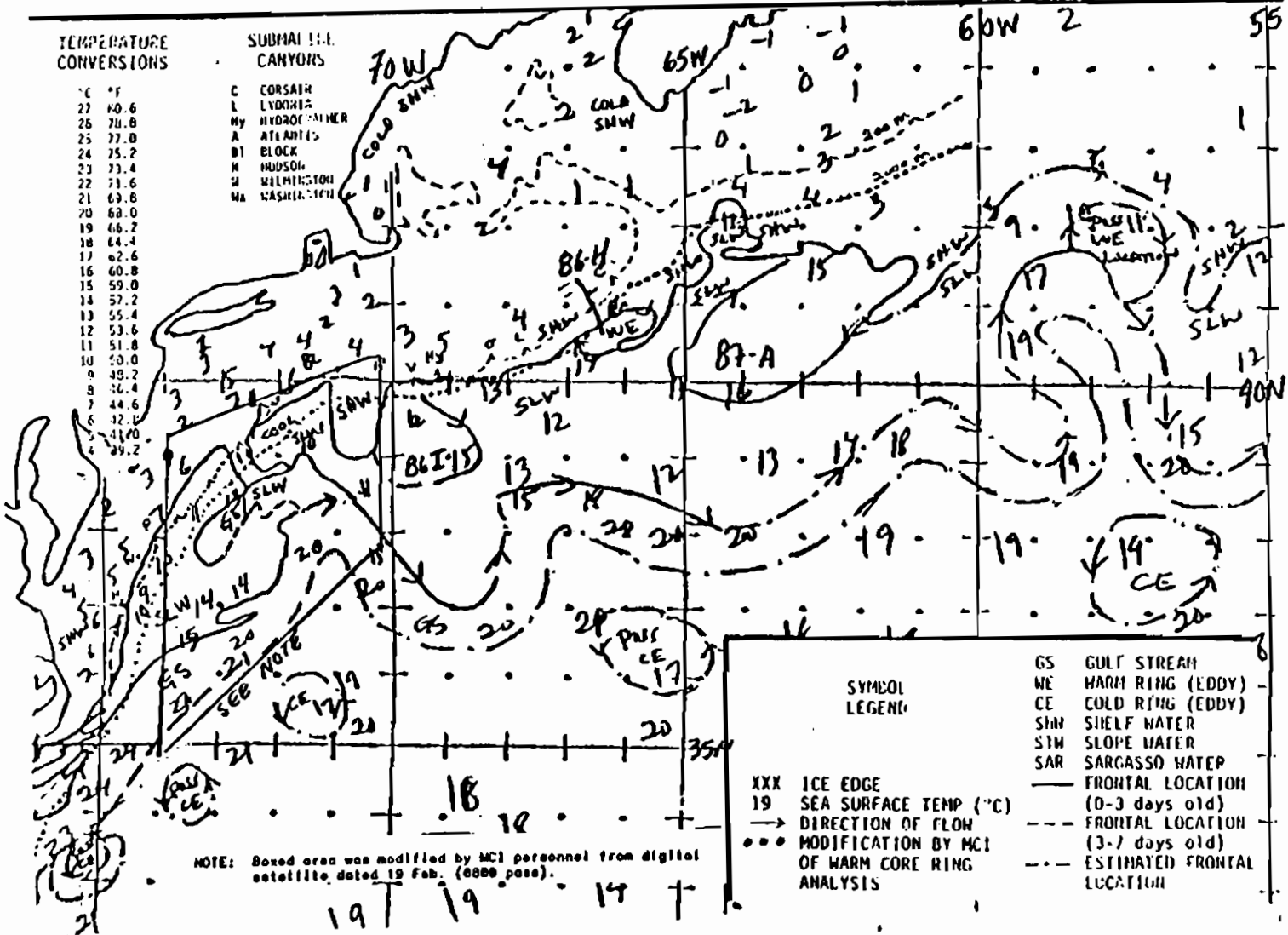


Figure 3-5e. Oceanographic Analyses of AVHRR Satellite Imagery, December 29, 1986.

18 Feb 1987
 19 Feb 1987



42

Figure 3-5f. Oceanographic Analyses of AVHRR Satellite Imagery, February 18, 1987.

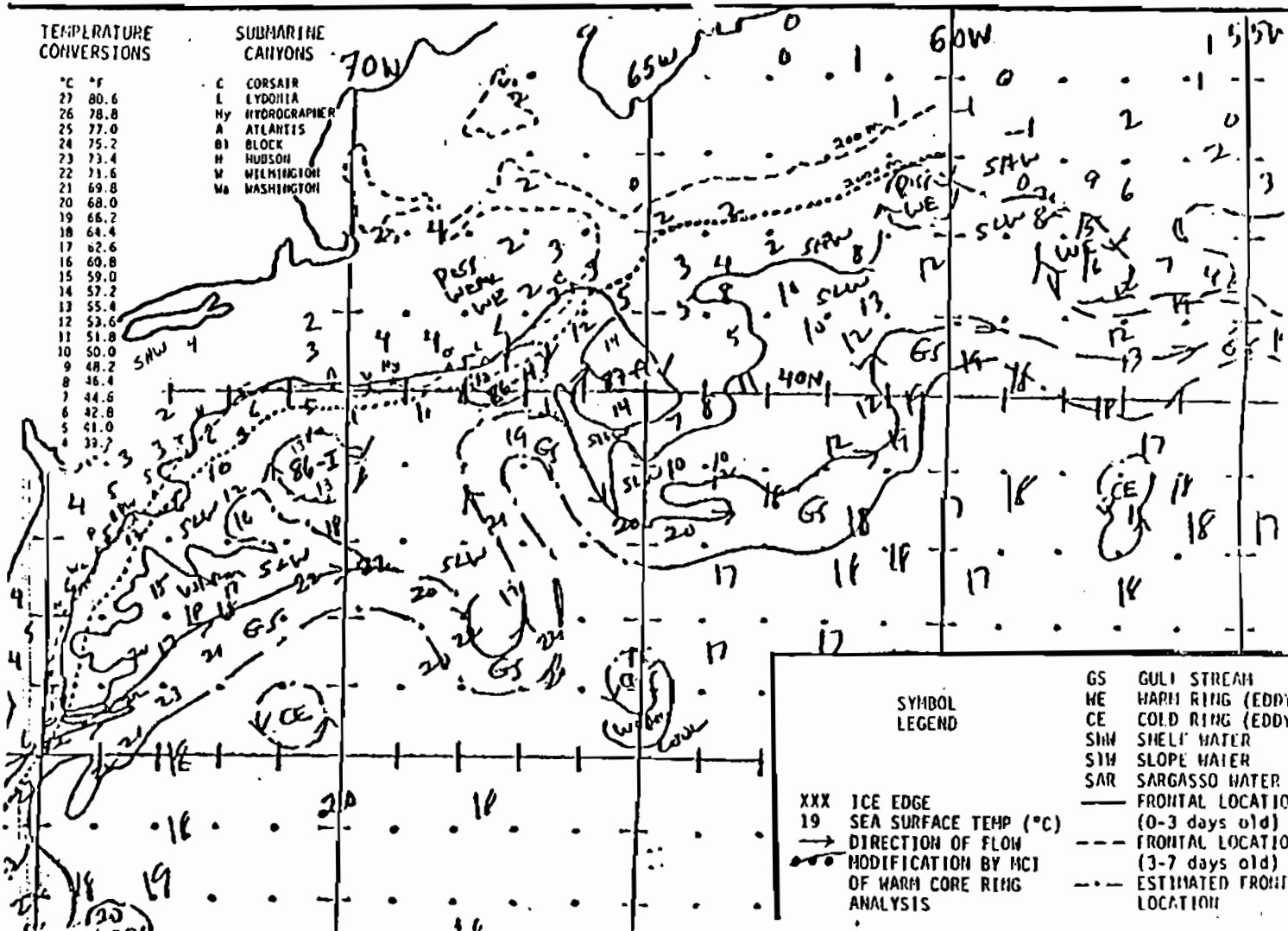
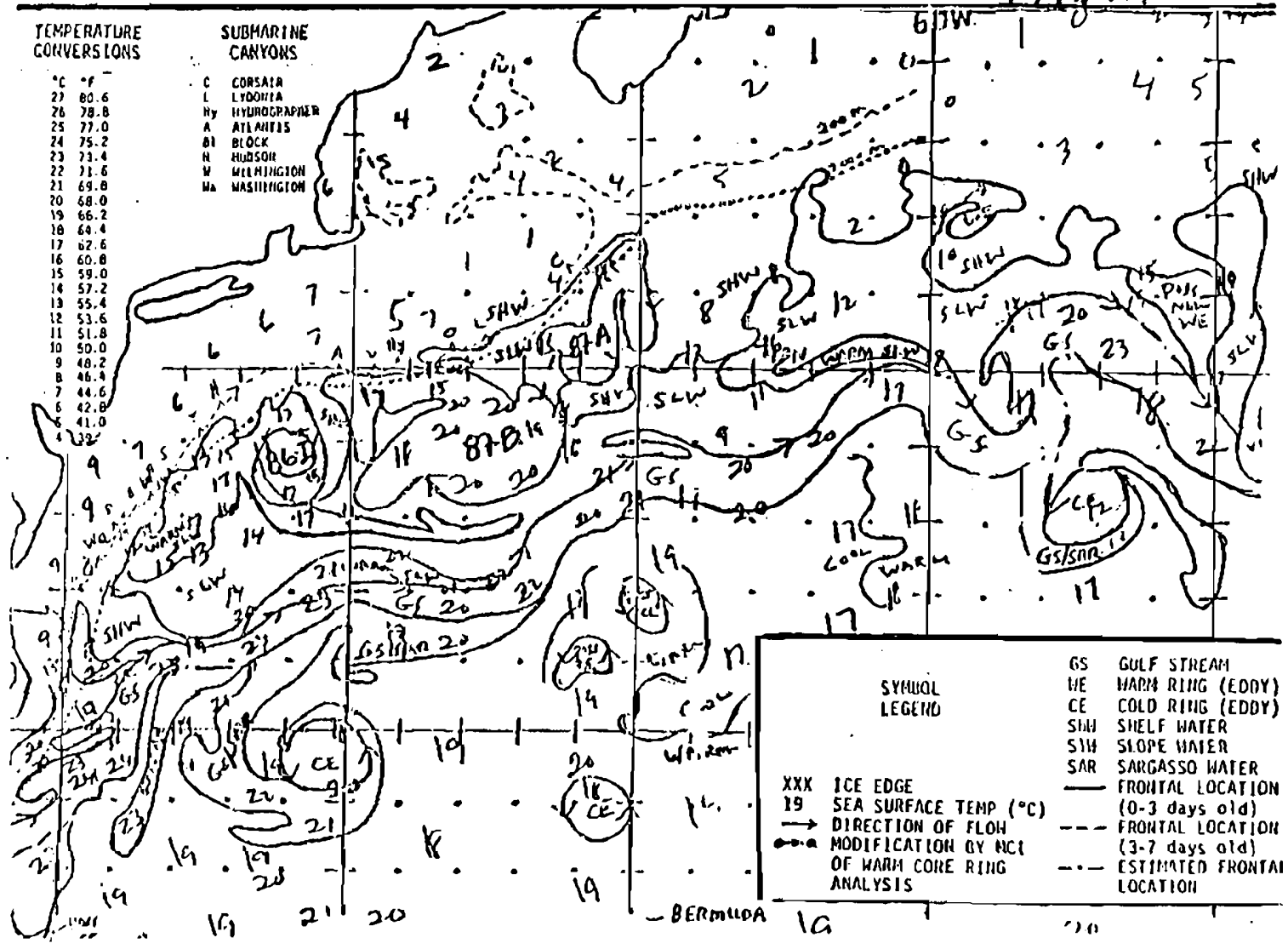


Figure 3-5g. Oceanographic Analyses of AVHRR Satellite Imagery, March 23, 1987.



44

Figure 3-5h. Oceanographic Analyses of AVHRR Satellite Imagery, April 13, 1987.

higher than average speeds of 6.5 cm s^{-1} reported by Brown et al., 1986. However, the ring seemed to slow down and move off the slope as the northern part of it passed mooring X. It took 8-10 days for the center of the trailing smaller eddy (remnant of 86-F) (JD 352-368) to pass the locations of Y and X and thus catches up with ring 86-E by the end of December. Compare the positions of 86-E and 86-F in Figures 3-5d and 3-5e.

January 1987 showed no ring activity, but February and March showed some significant warm surface-layer events generally restricted to the upper 150m of the water column. Because these events are characterized by weak currents, they are not directly ring-related. The warm outbreak occurring on February 17 to 23 is due to a large filament trailing a GS meander crest (Figure 3-5f). The large warm outbreak, affecting much of the western Slope Sea, shown in the March 23 analysis (Figure 3-5g) does not seem to have an observable cause (i.e., a GS filament or ring - GS interaction) and may be attributed to GS overrunning. The warm outbreak seen at mooring X in April seems to have been spawned by the interaction of two large rings (86-I and 87-B) off the New England and Georges Bank slopes with the Gulf Stream (Figure 3-5h). These warm outbreaks seem to affect the upper 100m of the water column and are slow moving and fairly passive. At the beginning of April, the warm-core ring (86-I) near the Hudson Canyon begins to influence the flow at mooring Y.

Another view of the temperature time series from mooring X is given by contouring isotherms with depth and time (Figure 3-6). The warm eddies and ring 86-E (JD 277, 324, and 362) are clearly shown by the dipping of the isotherms at all levels. The seasonal cooling of the surface waters through November, December and January is clear. The water column becomes homogeneous at the beginning of February when the upper and lower 12°C isotherms meet (JD40). This convergence of the 12°C isotherms illustrates the formation of the 12°C slope-water pycnostad by convective overturning in late winter, which has been documented previously in MASAR and has been surmised from earlier hydrographic work (Csanady and Hamilton, 1987).

Apart from the warm outbreaks, the water column remains homogeneous between 50m and 250m until the beginning of April, usually the time when the bottom of the pycnostad reaches its maximum depth (250m). This mooring X temperature data is the third observation of a late winter overturning made

EPA 106-MILE SITE MOORING X

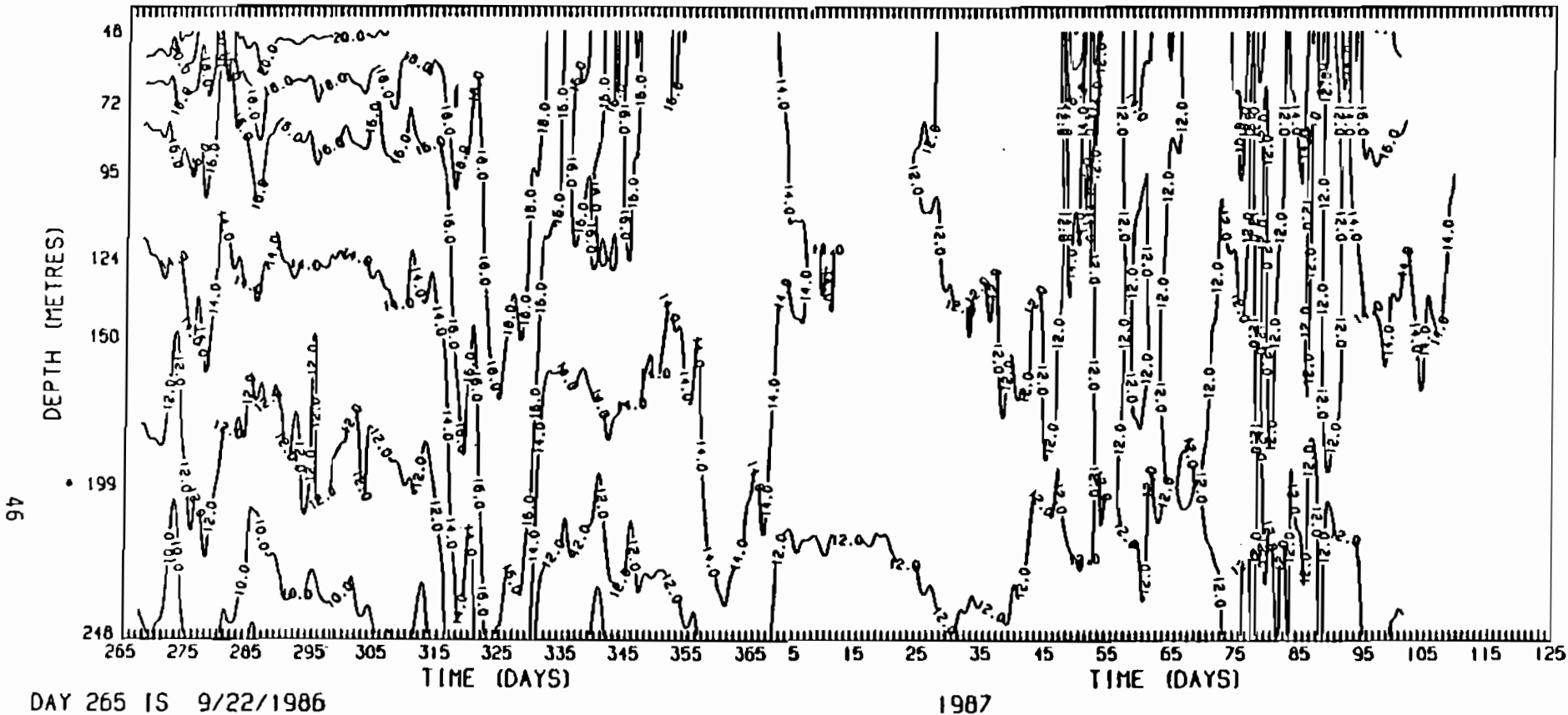


Figure 3-6. Depth-time isotherm contours from mooring X (40-HLP data).

by thermistor chains (SAIC, 1987), which helps to confirm the timing of the formation and renewal of the slope water mass as well as its characteristic temperature of about 12°C.

Perhaps the most intriguing event evident in the records is the occurrence of the sharp temperature decreases at 1000m at both Y2 and X8 between JD 56 and 65, 1987 (Figure 3-4). The temperature drop of 0.5 to 0.6°C is enormous at this depth and the narrowness of the spike implies a very small water mass being advected past the mooring. The 0.5 to 0.6°C temperature change is of order 5 times the standard deviation of the X8 temperature record. The mean long-isobath speed between Days 56 and 65, \bar{v} , at X8 is -13.5 cm s^{-1} . If the distance between moorings is 75 km, the time for a water particle to move from Y1 to X8 is 154 hours; the measured time difference, using the time of the occurrence of the lowest temperatures, is 159 hours. Thus the supposition that the anomalous, cold water mass advects along the isobath with the current is confirmed. Using the mean speed and temporal width of the spikes, the length of the anomaly is between 11 and 13 km.

The mean temperatures of the Y2 and X8 records are about 4.2°C, very close to the temperatures measured at 1000-m depth in the Slope Sea in the MASAR hydrographic sections (SAIC, 1987). Salinities for this depth and water mass range from about 34.95 to 34.98. If the anomaly has the same density as $T=4.2^\circ\text{C}$, $S=34.98 \text{ }^\circ/\text{oo}$, thus $\sigma_t = 27.75$, water, the salinity corresponding to $T=3.6^\circ\text{C}$, $\sigma_t = 27.75$, is $34.90 \text{ }^\circ/\text{oo}$. This is considerably fresher than is usually observed in hydrocasts in the western slope sea. The water mass between 1000 and 2000m, with temperatures ranging from 3.4 to 4.6°C, is characteristic of Labrador Sea Water (LSW) anomalies. Historical data suggest that LSW flows southward along the continental margin around the Ground Banks of New Foundland, and that the anomalies weaken rapidly farther southwest along the slope. The small spatial scale of low temperature spike and its inferred low salinity imply that mixing of LSW may be intermittent and patchy. The true size and depth range of this anomaly are, of course, impossible to estimate from two time series at a single depth. However, such a strong anomaly does not appear to have ever been detected by CTD casts in this region, although fresh LSW anomalies have been detected further east (McCartney et al., 1980). This implies either its

rarity or small scale patchiness or both. Normally, temperatures of 3.6°C are measured at 1600m or deeper.

The most likely explanation for the isolated LSW anomaly is that it is an example of a Submesoscale Coherent Vortex (SCV). SCVs are described and theoretically discussed in a review paper by McWilliams (1985). A subthermocline SCV was measured during the POLYMODE Local Dynamics Experiment with a radius of about 12 km, a depth scale of under 500m, and a fairly vigorous anticyclonic circulation (speeds ~ 20 cm s⁻¹). There is a suggestion of cyclonic rotation of the current vectors as the anomaly advects past X8, but the measured speeds do not markedly differ from the mean advection velocity. SCVs containing LSW anomalies are thought to be formed from the mixing of near-surface water in the Labrador Sea to its depth of neutral buoyancy (1000 to 2000m), whereby a geostrophic adjustment process, an isolated vortex, is generated preserving the density and potential vorticity of the patch. McWilliams (1985) has estimated that SCVs have lifetimes of several years.

3.3 BASIC STATISTICS

The basic statistics of all the time series from both moorings are given in Table 3-2. The mean along-isobath flow is a substantial 6.5 cm s⁻¹ to the southwest and is remarkably uniform with depth at Mooring X. The corresponding mean flow at Y1 is about 4.9 cm s⁻¹ and is directed eastward, corresponding to the 2500-m isobath direction at mooring Y (see Figure 2-1). Mean and maximum velocities were also calculated for the November warm-core ring [86-E] and the quiescent period from January 1 to March 26, 1987, when no eddies moved through the site. For the November warm-core ring, maximum speeds were the same as those given in Table 3-2, at and above 250m. Mean speeds, however, were approximately twice the record means given in Table 3-2 and mean temperatures were up to 3°C higher at 50- and 100-m levels. The mean along-isobath velocity component, v , for the November period was directed northeast at between 12 and 15 cm s⁻¹ in the upper layers (X1, X3 and X7), but the mean flow of 5 cm s⁻¹ was still southwest at 1000m (X8). The January to March period, which may be more representative of the basic Slope Sea gyre currents because no large eddies were affecting the region

Table 3-2. Basic statistics for 3-HLP and 40-HLP records from moorings X and Y.

EPA 106-MILE SITE MOORINGS
PERIOD : 86/ 9/21, 0 - 87/ 5/ 9, 0

METER ID # OF DAYS	DEPTH(M) WATER DEPTH	DIRECTION OF V-COMPONENT	VARIABLE U,V,S(CM/S) T(C).P(DB)	MAXIMUM	MINIMUM (3-HLP)	MEAN	VARIANCE (3-HLP)	<U**2>ETC. (40-HLP)	RATIO 40-HLP : 3-HLP KE	ORIENTATION OF PRINCIPAL AXES (DEGREES TRUE)
X1061	48 2500	60	U	40.9	-91.2	-1.22	291.49	219.95	.778	94.6
			V	83.8	-71.0	-6.64	314.12	250.96		
			S	91.9	.2	21.64	182.99	149.68		
			T	23.00	8.53	15.565	13.145	12.696		
X1062	72		T	20.33	9.36	14.736	6.599	6.513		
X1063	95	60	U	58.6	-104.0	.18	381.52	326.07	.861	107.6
			V	100.8	-67.8	-6.58	359.43	312.07		
			S	108.0	.9	22.81	267.09	234.24		
			T	19.19	9.56	14.006	4.731	4.708		
X1064	124		T	18.74	10.22	13.785	3.256	3.230		
X1065	150		T	18.49	10.24	13.407	2.391	2.353		
X1066 (176)	199		T	17.94	10.05	12.912	1.665	1.610		
X1067	248	60	U	47.2	-78.5	-.42	229.50	172.76	.761	102.5
			V	77.8	-55.1	-6.09	233.66	179.58		
			S	79.0	.6	18.60	168.97	141.3		
			T	16.94	7.59	11.201	2.106	2.041		
X1068	1000	60	U	19.2	-13.0	1.17	11.21	4.65	.680	47.0
			V	10.4	-29.5	-7.62	29.46	22.99		
			S	32.8	.7	8.74	23.57	18.92		
			T	4.63	3.51	4.209	.008	.007		
Y1061	249 2500	60	U	67.7	-64.1	-2.56	240.83	195.16	.772	147.8
			V	46.3	-51.6	-4.18	167.54	120.14		
			S	69.1	.2	16.61	151.18	123.82		
			T	17.01	8.15	10.991	1.947	1.886		
Y1062	1005		T	4.70	3.61	4.227	.014	.012		

Note - Variable S = Speed = $(U^2 + V^2)$

south of the Hudson Canyon, has mean along-isobath, southwest flows of about 7 to 8 m s⁻¹ at all levels on mooring X. These southwest currents are very similar to the total record means given in Table 3-2. Maximum speeds measured for this January to March period were about 50 cm s⁻¹ above 250m and 22 cm s⁻¹ at 1000m. During this period, the Gulf Stream east of Cape Hatteras was near or south of its normal position (Figures 3-5f and 3-5g).

Variability is also reasonably uniform over the upper 250m of the water column, with maximum speeds and variances of the 40-HLP fluctuations occurring at the 100-m level rather than closer to the surface. The lack of vertical shear occurs for both ring and non-ring related low frequency currents. The weak vertical shear and maximum subsurface velocity measured during the major ring event imply that mooring X was in the center part of the ring, which is usually in near solid-body rotation (Joyce, 1984). The principal axes are directed offshore of the trend of the isobaths and the near equality of the U and V 40-HLP variances above 250m may be interpreted as ring currents dominating the fluctuations, again with the center of the eddies passing close to the 2500-m isobath. The low frequency variances, excluding tides and inertial currents, are 70-85% of the total variance; thus most of the energy is contained in the low frequency fluctuations. However, during the quiescent January to March period, high frequency motions (periods > 40 hours) contained about half the total kinetic energy.

It is useful to compare the statistics in Table 3-2 with similar six-month statistics from MASAR moorings C and D, positions shown in Figure 2-1. Moorings C and D were in 2000- and 2500-m water depth, respectively and were the closest MASAR current measurements to mooring X. Moorings C and statistics for two separate six-month periods are given in Table 3-3. Discussion of the data from moorings C and D may be found in SAIC (1987). The second period (April to September, 1985) contained a large warm-core ring event (ring 84-G), which had higher maximum speeds and variances than the November 1986 ring (128 cm s⁻¹ versus 108 cm s⁻¹ at 100-m). However, the most noteworthy difference between the statistics for both of the MASAR periods in Table 3-3 and the EPA data (Table 3-2) is the strength of the southwest, along-isobath mean flows. The MASAR periods show mean southwest velocities of more than twice those measured at mooring X at both the 100m and 1000m levels. The October 1984 to October 1985 period was characterized

Table 3-3. Basic statistics for 3-HLP and 40-HLP records from MASAR moorings C and D for two six-months periods in 1984 and 1985.

MASAR MOORINGS C AND D											
PERIOD : 84/10/ 1, 0 - 85/ 4/ 1, 0											
METER ID # OF DAYS	DEPTH(M) WATER DEPTH	DIRECTION OF V-COMPONENT	VARIABLE		MAXIMUM	MINIMUM	MEAN	VARIANCE (U' ² +2)ETC.		RATIO 40-HLP ; 3-HLP KE	ORIENTATION OF PRINCIPAL AXES (DEGREES TRUE)
			U,V,S(CM/S)	T(C),P(DB)				(3-HLP)	(40-HLP)		
MC201	110 2000	52	U		50.6	-34.6	1.42	109.47	82.18	.618	74.8
			V		14.2	-55.8	-19.09	106.85	71.53		
			S		56.4	.8	22.52	77.98	44.86		
			T		17.65	10.46	13.538	1.525	1.466		
			P		125.43	109.82	113.759	6.348	5.701		
MC203	1000	52	U		13.1	-14.1	.49	11.06	2.83	.666	45.1
			V		10.8	-29.7	-10.38	47.95	36.46		
			S		29.8	.3	11.43	32.84	25.66		
			T		4.41	3.98	4.151	.003	.002		
MASAR MOORINGS C AND D											
PERIOD : 85/ 4/ 1, 0 - 85/10/ 1, 0											
METER ID # OF DAYS	DEPTH(M) WATER DEPTH	DIRECTION OF V-COMPONENT	VARIABLE		MAXIMUM	MINIMUM	MEAN	VARIANCE (U' ² +2)ETC.		RATIO 40-HLP ; 3-HLP KE	ORIENTATION OF PRINCIPAL AXES (DEGREES TRUE)
			U,V,S(CM/S)	T(C),P(DB)				(3-HLP)	(40-HLP)		
MC203	1000	52	U		18.2	-9.1	2.14	12.37	7.50	.888	43.2
			V		19.9	-34.2	-10.84	67.08	63.05		
			S		35.4	.3	12.57	44.36	39.68		
ND302	125 2500	52	U		93.	-127.2	.36	667.73	444.00	.960	123.9
			V		85.2	-69.6	-14.57	502.30	479.31		
			S		128.4	.1	31.20	421.87	394.38		
			T		15.58	8.72	12.415	1.744	1.736		
ND303	925	52	U		14.7	-18.7	-1.62	13.72	9.54	.759	59.1
			V		10.3	-32.6	-9.12	50.48	39.20		
			S		33.3	.0	10.16	48.15	36.02		
			T		4.53	3.89	4.169	.008	.007		

* - SHORT RECORD

by the Gulf Stream being displaced north of its normal path, which apparently strengthened the gyre flow over the New Jersey slope. This phenomenon is discussed in Section 1.2. The October 1984 to April 1985 period was characterized by little eddy activity south of the Hudson Canyon in the Slope Sea. The variances for mooring C (Table 3-3) are very similar to the variances calculated for the January to March 1987 quiescent period at mooring X. The 1000-m temperature records at C and D showed no cold LSW anomalies such as the one captured by moorings X and Y in February 1987. The minimum measured temperature at C and D was 3.89°C, compared with 3.51°C at Mooring X on JD65, 1987.

Tables 3-4a through 3-4e show the statistics for the 3-HLP current meter records broken into speed and direction classes. This method of presenting current data allows estimation of the percentage of time that current velocity vectors have speeds in a given speed range and the most probable compass direction. This information, in the form of frequency distributions, should be useful in determining likely plume tracks for sludge disposed at the site for the six months of the current monitoring program with its particular sequence of vents (warm-core rings, eddies, etc.) which will differ from other six-month periods, as comparison with the limited MASAR data in Table 3-3 shows.

3.4 INERTIAL AND TIDAL MOTIONS

Short-period motions (less than a day) in the deep ocean are generally due to internal waves. The astronomical tide produces very weak barotropic currents ($\sim 0.1 \text{ cm s}^{-1}$) in 2500-m water depth. The principal energy sources are (1) the wind action on the sea surface which generates inertial oscillations at a frequency close to the Coriolis parameter, f , and (2) the semi-diurnal M2 tide which generates internal waves at the shelf break. A harmonic tidal analysis of the X3 (95m) record showed that the M2 tide had an amplitude of 2.5 cm s^{-1} . Upper-level inertial current oscillations can have amplitudes of 10 to 30 cm s^{-1} and may reach 50 cm s^{-1} after major storms (Mayer et al., 1981). Inertial currents are important because they provide energy for mixing and entrainment and are the mechanism by which storm energy is propagated into deep water.

Table 3-4a. Frequency distribution of speeds and directions (expressed as a percentage of total record length) and summary statistics for the 3-HLP current records from X1061.

FREQUENCY DISTRIBUTION 1.00 HOURLY DATA												STATION: X1061		SHRLP		SPANNING 9/20/86 TO 4/9/87				4824 DATA POINTS			
DIRECTION DEGREES												PERCENT	MEAN SPEED	MIN SPEED	MAX SPEED	STD. DEV.							
0-30	.4	1.2	.7	.4	.2	.1	.0	.0	.0	.0	.0	3.0	19.51	2.59	48.24	11.49							
30-60	.6	1.2	.7	.4	.1	.1	.0	.0	.0	.0	.0	2.9	17.37	1.16	48.00	10.68							
60-90	.8	1.4	.8	1.0	.6	.4	.1	.4	.2	.1	.0	5.7	29.62	1.31	86.77	21.30							
90-120	.9	2.4	1.5	1.0	.2	.0	.1	.1	.0	.0	.0	6.3	19.91	1.03	78.87	12.18							
120-150	1.1	3.2	1.9	.6	.1	.0	.0	.0	.0	.0	.0	6.8	16.66	1.32	38.87	8.32							
150-180	1.2	3.1	2.3	.7	.1	.0	.0	.0	.0	.0	.0	7.5	17.14	1.42	41.33	8.09							
180-210	1.8	5.0	3.8	1.8	.2	.3	.1	.0	.0	.0	.0	13.0	18.98	.48	55.22	10.40							
210-240	1.5	3.6	5.3	2.5	.8	.4	.1	.2	.0	.0	.0	14.5	22.75	.59	71.70	12.03							
240-270	1.1	4.3	4.7	2.4	1.1	.3	.3	.1	.0	.0	.0	14.4	23.07	.50	66.22	11.66							
270-300	1.0	3.7	3.4	1.3	.5	.2	.0	.0	.0	.0	.0	10.1	20.16	2.80	67.02	10.51							
300-330	1.0	3.2	2.0	1.0	.5	.3	.4	.3	.3	.2	.1	9.2	27.00	.19	91.89	20.96							
330-360	1.0	2.2	1.3	.7	.6	.3	.1	.2	.0	.0	.0	6.5	23.55	.95	72.13	16.25							
SPEED	0	9	18	27	36	45	54	63	72	81	90												
CM/S	!	!	!	!	!	!	!	!	!	!	!												
PERCENT	12.4	34.3	28.4	13.9	5.1	2.4	1.3	1.3	.6	.3	.1	100.00											
MEAN DIR	198	205	214	208	221	216	242	227	212	250	321												
STD DEV	89	87	78	82	95	101	97	109	124	104	741												

SUMMARY STATISTICS

MEAN SPEED = 21.61 CM/S MAXIMUM = 91.89 CM/S MINIMUM = .19 CM/S RANGE = 91.70 CM/S
 STANDARD DEVIATION = 13.50 CM/S SKEWNESS = 1.66

IN A COORDINATE SYSTEM WHOSE Y AXIS IS POSITIONED .00 DEGREES CLOCKWISE FROM TRUE NORTH
 MEAN X COMPONENT = -5.95 CM/S STANDARD DEVIATION = 18.47 CM/S SKEWNESS = .53
 MEAN Y COMPONENT = -3.03 CM/S STANDARD DEVIATION = 16.24 CM/S SKEWNESS = .82

53

Table 3-4b. Frequency distribution of speeds and directions (expressed as a percentage of total record length) and summary statistics for the 3-HLP current records from X1063.

FREQUENCY DISTRIBUTION												STATION: X1063 3HLP				SPANNING 9/20/86 TO 4/9/87		4824 DATA POINTS	
1.00 HOURLY DATA												PERCENT		MEAN SPEED	MIN SPEED	MAX SPEED	STD. DEV.		
DIRECTION DEGREES																			
0-30	1.2	1.0	.4	.2	.1	.1	.0	.0	.0	.0	.0	3.0	16.74	1.64	57.33	13.08			
30-60	.8	1.1	.5	.1	.1	.1	.0	.0	.0	.0	.0	2.6	16.39	1.54	54.36	11.35			
60-90	1.1	1.3	.5	.4	.4	.6	.4	.5	.1	.3	.0	5.6	36.34	1.06	108.00	28.25			
90-120	1.1	2.4	1.6	.6	.2	.0	.0	.1	.1	.1	.0	6.3	22.15	1.27	104.53	16.99			
120-150	1.4	2.7	1.8	.7	.3	.0	.0	.0	.0	.0	.0	6.9	18.69	1.31	45.59	10.59			
150-180	1.2	3.2	2.5	.8	.2	.0	.0	.0	.0	.0	.0	7.7	18.73	.91	45.12	9.76			
180-210	1.7	4.6	3.9	1.0	.6	.0	.0	.0	.0	.0	.0	11.8	20.04	1.36	51.21	10.27			
210-240	2.1	6.3	6.0	1.5	.4	.4	.2	.0	.0	.0	.0	17.2	20.91	1.48	68.08	11.32			
240-270	1.6	5.7	6.2	1.7	.4	.1	.2	.0	.0	.0	.0	16.1	21.82	2.18	65.39	10.91			
270-300	1.5	3.7	2.3	1.1	.3	.0	.0	.0	.0	.0	.0	9.3	19.95	1.19	89.05	10.68			
300-330	.7	2.5	1.8	.7	.2	.2	.5	.4	.4	.5	.2	8.1	36.40	2.06	104.59	28.80			
330-360	1.0	2.2	.9	.2	.2	.4	.7	.1	.1	.1	.0	5.4	25.21	2.32	96.41	20.94			
SPEED	0	10	20	30	40	50	60	70	80	90	100								
CM/S	10	20	30	40	50	60	70	80	90	100	110								
PERCENT	15.9	36.9	28.7	8.7	3.4	1.9	1.5	1.2	.6	1.0	.2	100.00							
MEAN DIR	186	210	215	213	197	196	233	219	257	218	260								
STD DEV	93	81	70	74	65	111	97	116	106	126	1011								

SUMMARY STATISTICS

MEAN SPEED = 22.73 CM/S MAXIMUM = 108.00 CM/S MINIMUM = .91 CM/S RANGE = 107.09 CM/S
 STANDARD DEVIATION = 16.33 CM/S SKEWNESS = 2.20

IN A COORDINATE SYSTEM WHOSE Y AXIS IS POSITIONED .00 DEGREES CLOCKWISE FROM TRUE NORTH
 MEAN X COMPONENT = -5.77 CM/S STANDARD DEVIATION = 20.64 CM/S SKEWNESS = .95
 MEAN Y COMPONENT = -3.32 CM/S STANDARD DEVIATION = 17.69 CM/S SKEWNESS = 1.42

54

Table 3-4c. Frequency distribution of speeds and directions (expressed as a percentage of total record length) and summary statistics for the 3-HLP current records from X1067.

FREQUENCY DISTRIBUTION										4824 DATA POINTS				
1.00 HOURLY DATA														
STATION: X1067 3HRLP										SPANNING 9/20/86 TO 4/9/77				
DIRECTION DEGREES										PERCENT	MEAN SPEED	MIN SPEED	MAX SPEED	STD. DEV.
0-30	1.2	.8	.4	.2	.2	.1	.0	.0	.0	3.0	15.75	.98	58.86	13.17
30-60	.7	.6	.3	.1	.1	.1	.0	.1	.0	2.0	19.04	1.03	74.44	18.29
60-90	.8	.4	.4	.2	.4	.6	.5	.1	.1	3.5	32.40	1.14	78.66	22.02
90-120	1.0	1.2	1.4	.6	.5	.2	.2	.1	.0	5.2	23.36	1.01	70.29	15.43
120-150	1.3	1.4	1.4	.9	.2	.0	.0	.0	.0	5.1	17.73	1.15	42.74	10.24
150-180	1.5	2.7	1.1	.5	.1	.1	.0	.0	.0	5.8	14.79	1.00	51.67	9.35
180-210	2.2	6.2	2.8	.8	.1	.0	.0	.0	.0	12.0	15.42	1.03	51.36	7.65
210-240	2.9	8.6	5.3	.9	.7	.3	.0	.0	.0	18.6	17.13	.57	50.50	9.04
240-270	3.2	9.6	5.3	1.8	.8	.3	.0	.0	.0	21.0	17.44	1.00	55.94	9.65
270-300	2.8	5.2	2.4	.7	.4	.1	.1	.0	.0	11.6	15.64	1.19	64.98	9.93
300-330	1.9	2.0	1.3	.5	.5	.6	.4	.6	.0	7.7	25.09	.67	71.30	20.44
330-360	1.2	1.3	.6	.2	.4	.0	.3	.4	.1	4.5	24.87	1.04	78.99	22.51
SPEED	0	9	18	27	36	45	54	63	72					
CM/S	9	18	27	36	45	54	63	72	81					
PERCENT	20.5	39.9	22.6	7.4	4.1	2.3	1.5	1.3	.3	100.00				
MEAN DIR	209	225	218	207	213	188	199	272	210					
STD DEV	92	64	68	77	96	105	126	106	155					

SUMMARY STATISTICS

MEAN SPEED = 18.52 CM/S MAXIMUM = 78.99 CM/S MINIMUM = .57 CM/S RANGE = 78.42 CM/S
 STANDARD DEVIATION = 12.98 CM/S SKEWNESS = 1.72

IN A COORDINATE SYSTEM WHOSE Y AXIS IS POSITIONED .00 DEGREES CLOCKWISE FROM TRUE NORTH
 MEAN X COMPONENT = -6.26 CM/S STANDARD DEVIATION = 16.25 CM/S SKEWNESS = 1.04
 MEAN Y COMPONENT = -2.96 CM/S STANDARD DEVIATION = 14.11 CM/S SKEWNESS = 1.56

Table 3-4d. Frequency distribution of speeds and directions (expressed as a percentage of total record length) and summary statistics for the 3-HLP current records from X1068.

FREQUENCY DISTRIBUTION												4816 DATA POINTS				
1.00 HOURLY DATA																
STATION: X1068 3HALP												SPANNING 9/20/86 TO 4/ 9/87				
DIRECTION DEGREES												PERCENT	MEAN SPEED	MIN SPEED	MAX SPEED	STD. DEV.
0-30	.4	.2	.3	.1	.0	.0	.0	.0	.0	.0	.0	1.1	5.06	1.31	11.77	2.89
30-60	.3	.3	.4	.1	.0	.0	.0	.0	.0	.0	.0	1.1	6.93	1.20	10.54	2.98
60-90	.2	.2	.1	.1	.0	.0	.0	.0	.0	.0	.0	.7	5.60	1.31	11.14	3.15
90-120	.3	.2	.3	.1	.0	.0	.0	.0	.0	.0	.0	.9	5.06	1.13	11.39	2.67
120-150	.2	.6	.2	.1	.0	.0	.0	.0	.0	.0	.0	1.0	4.97	.70	10.58	2.61
150-180	.5	1.4	.7	.2	.0	.0	.0	.0	.0	.0	.0	2.8	5.10	.67	11.19	2.58
180-210	1.0	3.5	4.0	2.3	.5	.2	.1	.1	.2	.2	.0	12.4	8.16	1.01	30.50	5.30
210-240	2.0	7.0	13.0	11.6	6.4	3.5	.9	.6	.8	.5	.1	46.3	10.05	.99	32.78	5.10
240-270	1.5	5.4	8.4	5.8	2.6	1.0	.4	.1	.1	.1	.0	25.3	8.48	.87	28.59	4.27
270-300	1.0	2.0	1.6	.8	.3	.1	.0	.0	.0	.0	.0	5.7	6.26	.66	16.64	3.54
300-330	.7	.5	.3	.1	.0	.0	.0	.0	.0	.0	.0	1.6	4.11	1.23	10.59	2.74
330-360	.5	.5	.2	.0	.0	.0	.0	.0	.0	.0	.0	1.2	3.79	1.25	10.22	2.68
SPEED	0	3	6	9	12	15	18	21	24	27	30					
CM/S	3	6	9	12	15	18	21	24	27	30	33					
PERCENT	8.6	21.8	29.7	21.2	9.8	4.8	1.4	.8	1.1	.8	.1	100.00				
MEAN DIR	219	224	226	229	233	232	231	230	227	221	211					
STD DEV	83	52	44	32	23	17	17	28	48	36	641					

SUMMARY STATISTICS

MEAN SPEED = 8.66 CM/S MAXIMUM = 32.78 CM/S MINIMUM = .66 CM/S RANGE = 32.12 CM/S
 STANDARD DEVIATION = 4.85 CM/S SKEWNESS = 1.31

IN A COORDINATE SYSTEM WHOSE Y AXIS IS POSITIONED .00 DEGREES CLOCKWISE FROM TRUE NORTH
 MEAN X COMPONENT = -3.94 CM/S STANDARD DEVIATION = 4.62 CM/S SKEWNESS = -.34
 MEAN Y COMPONENT = -4.72 CM/S STANDARD DEVIATION = 4.44 CM/S SKEWNESS = -.72

56

Table 3-4e. Frequency distribution of speeds and directions (expressed as a percentage of total record length) and summary statistics for the 3-HLP current records from Y1061.

FREQUENCY DISTRIBUTION 1.00 HOURLY DATA											STATION: Y1061		3HLP		SPANNING 9/20/86 TO 4/ 9/87				4824 DATA POINTS			
DIRECTION DEGREES											PERCENT	MEAN SPEED	MIN SPFD	MAX SPFD	STD. DEV.							
0-30	1.3	1.8	1.1	.6	1.0	.8	.7	.4	.1	.0	7.9	22.73	1.24	60.80	15.60							
30-60	1.0	1.0	.6	.3	.2	.1	.0	.0	.0	.0	3.2	12.82	.99	41.10	8.77							
60-90	.8	1.7	.7	.2	.2	.0	.0	.0	.0	.0	3.6	12.31	.66	37.77	7.74							
90-120	1.2	1.7	1.0	.2	.2	.1	.0	.0	.0	.0	6.3	12.17	.15	38.21	7.63							
120-150	1.0	1.3	.6	.3	.2	.3	.4	.5	.3	.4	5.4	26.32	.16	69.15	21.15							
150-180	1.0	1.7	.8	.6	.2	.2	.6	.1	.1	.0	5.3	20.07	1.46	57.98	15.40							
180-210	1.2	2.4	1.3	.6	.3	.2	.0	.0	.0	.0	5.9	13.99	1.02	40.98	8.55							
210-240	1.9	4.4	2.3	1.3	1.7	.8	.5	.0	.0	.0	12.7	17.75	1.03	52.35	11.59							
240-270	2.3	6.5	4.8	1.6	.7	.3	.2	.0	.0	.0	16.3	14.80	.20	51.35	8.49							
270-300	2.8	5.4	3.4	1.7	.7	.2	.1	.0	.0	.0	14.3	14.03	.50	43.47	8.30							
300-330	2.0	4.2	2.1	1.1	.7	.1	.1	.0	.0	.0	10.3	14.21	.51	49.21	9.07							
330-360	1.9	2.9	1.8	1.3	1.1	.3	.3	.3	.6	.1	10.7	20.78	1.58	65.33	16.06							
SPEED	0	7	14	21	28	35	42	49	56	63												
CM/S	7	14	21	28	35	42	49	56	63	70												
PERCENT	18.4	35.0	20.5	9.8	7.1	3.2	2.9	1.5	1.0	.5	100.00											
MEAN DIR	211	223	226	235	213	174	163	161	245	199												
STD DEV	103	92	92	92	107	110	104	120	120	911												

SUMMARY STATISTICS

MEAN SPEED = 16.85 CM/S MAXIMUM = 69.15 CM/S MINIMUM = .15 CM/S RANGE = 68.99 CM/S
 STANDARD DEVIATION = 12.31 CM/S SKEWNESS = 1.50

IN A COORDINATE SYSTEM WHOSE Y AXIS IS POSITIONED .00 DEGREES CLOCKWISE FROM TRUE NORTH
 MEAN X COMPONENT = -4.87 CM/S STANDARD DEVIATION = 12.67 CM/S SKEWNESS = .55
 MEAN Y COMPONENT = .64 CM/S STANDARD DEVIATION = 15.84 CM/S SKEWNESS = .36

The 3-HLP U- and V-components of velocity are given in Figures 3-7a and 3-7b, and 3-8a and 3-8b and correspond to the 3-HLP temperature time series presented in Figures 3-3 and 3-4. The prominent oscillations superimposed on the low frequency signal are primarily inertial with a period of $2\pi/f = 19$ hours (1.26 cpd). Oscillations are ubiquitous throughout the record at all depths and highly intermittent with considerable variability in amplitude.

Two major inertial events are of particular interest. The first occurs during the passage of the major ring 86-E at mooring X on JD 322-328. A burst of inertial oscillations with 30 cm s⁻¹ amplitudes occurs as the ring currents turn from onshore to northeast. These current oscillations are possibly representations of inertial jet structures in the outer part of rings (Joyce and Stalcup, 1984) or possibly inertial internal waves trapped by the horizontal shear of the low frequency currents. The presence of inertial currents indicates that small scale structures with large shears, which could aid the dispersion of sludge, exist in rings. There is some suggestion that a similar phenomenon occurs at both moorings Y and X in the small eddy that trailed the major ring (JD 352-360).

The second period of intense inertial wave activity begins on January 22 (Figure 3-8). These waves were generated by an intense winter storm (a northeaster) that moved along the eastern seaboard on January 22 and 23, producing heavy snow in Delaware and New York. At the latitude of the moorings, the storm center was at the coast giving the strongest winds with clockwise rotating wind vectors over the ocean (i.e., at the moorings, the winds backed from easterly to southerly to westerly as the storm passes to the north). The fast moving storm generated an inertial wake with the strongest current oscillations east of the center low pressure. The strong inertial currents lasted from 10 to 20 days with highest speeds (40 cm s⁻¹) occurring at the 250-m level (X7) about 10 days after the northeaster passed. The delayed response is due to the relatively slow vertical propagation speed of inertial internal waves. Because the water column was already well mixed when the storm hit, no mixed layer deepening is seen in the temperature records (Figure 3-4) at this time.

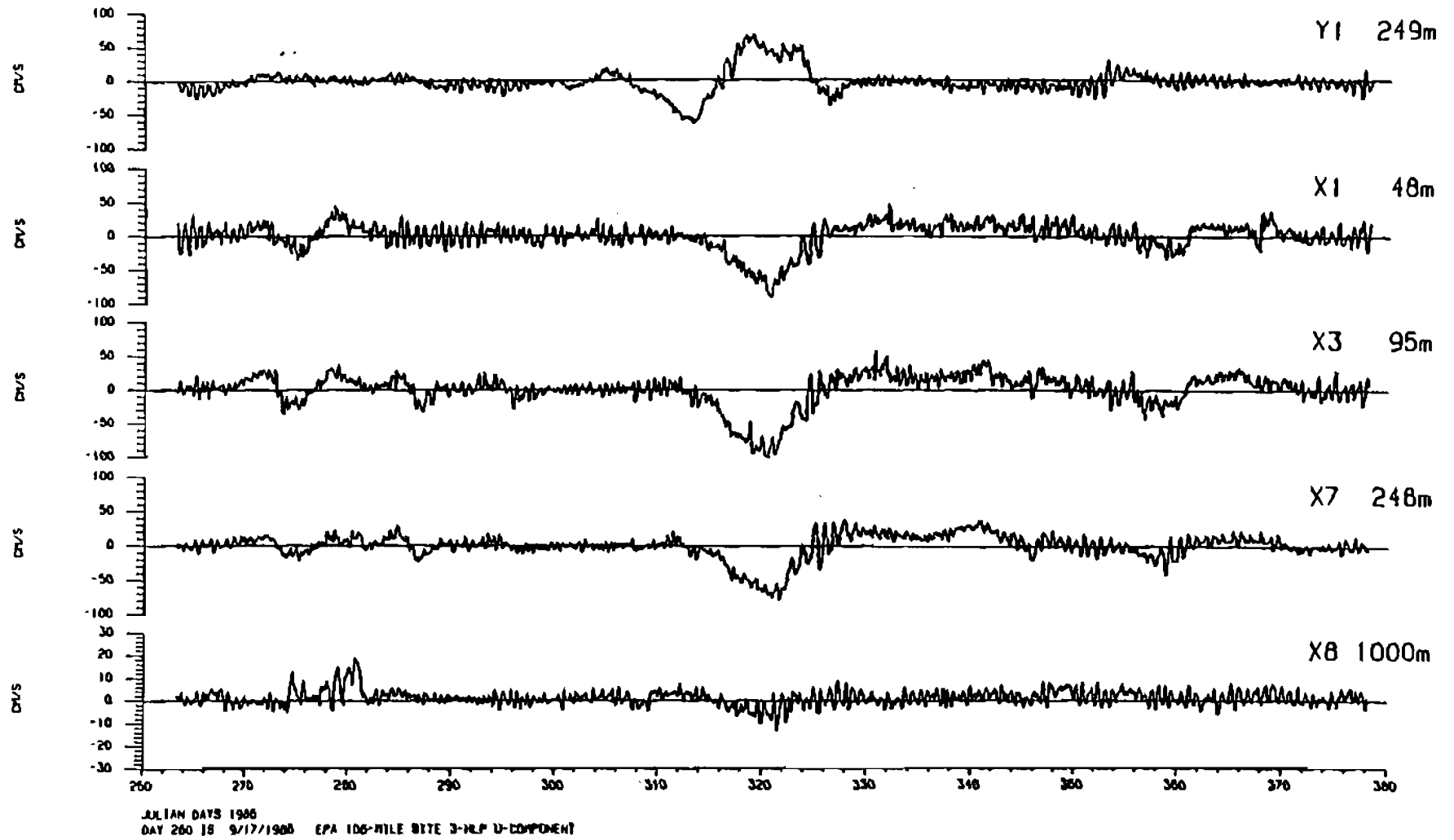


Figure 3-7a. 3-HLP velocity records of the first three months of deployment. U-component.

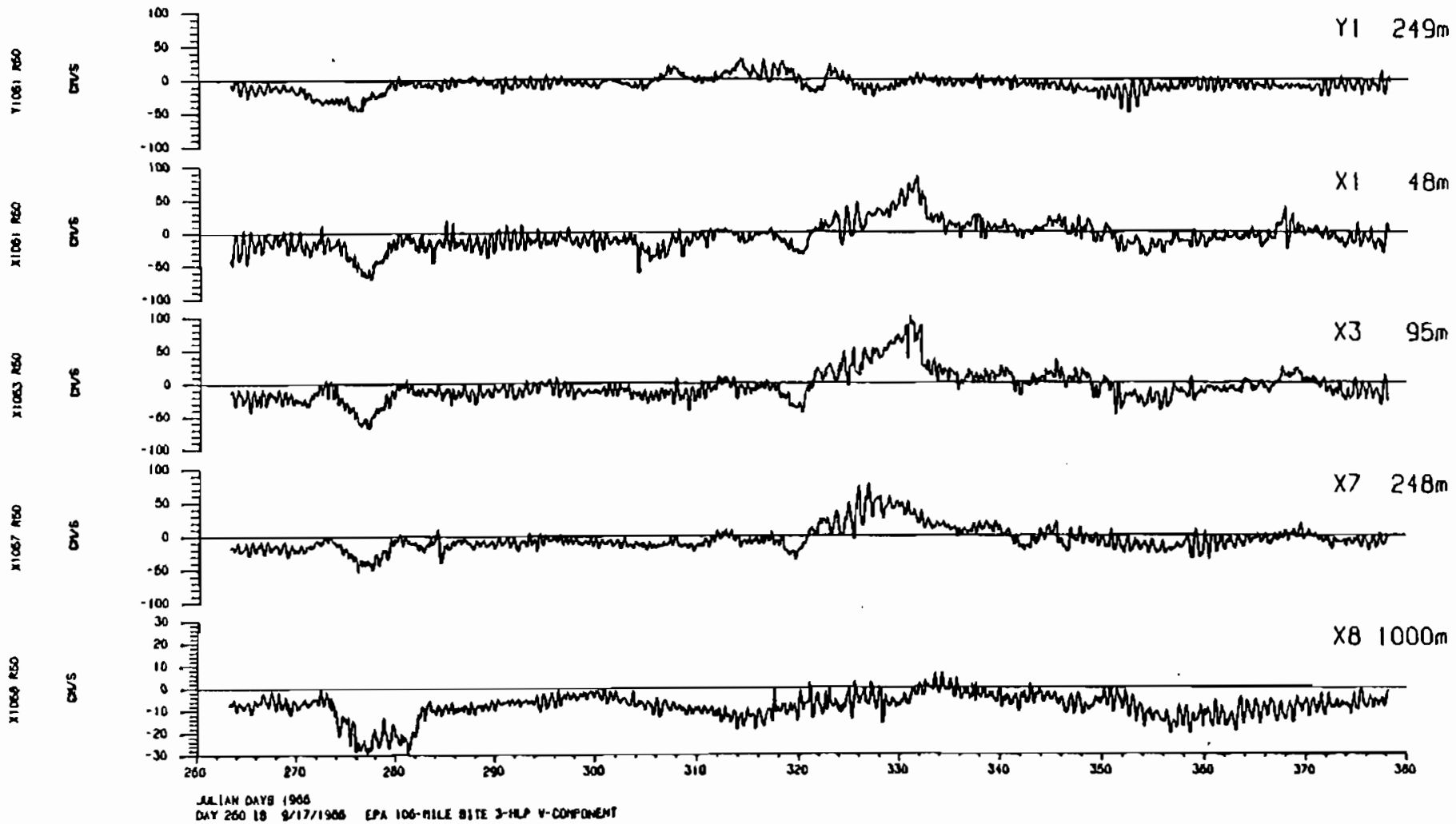


Figure 3-7b. 3-HLP velocity records of the first three months of deployment.
V-component.

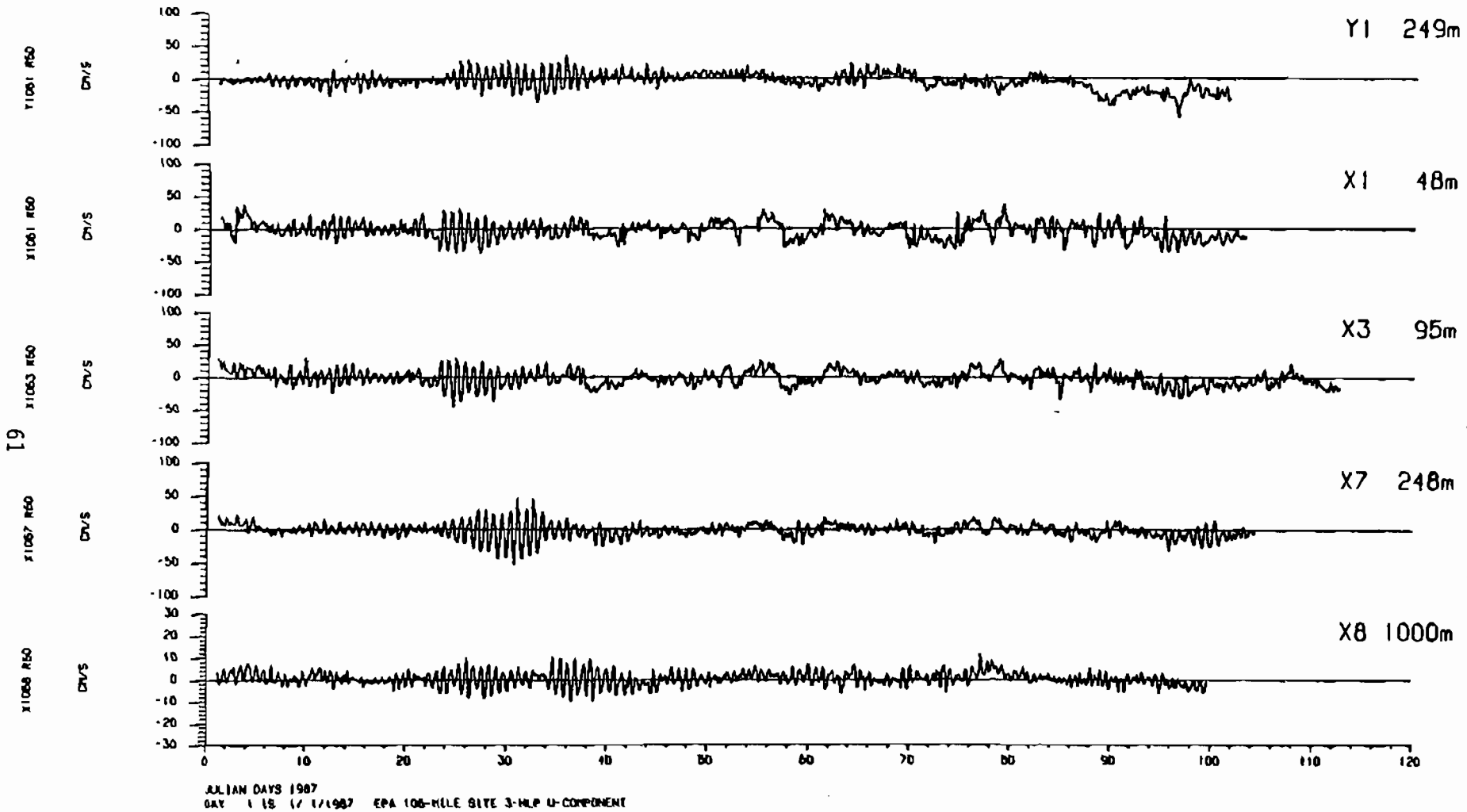


Figure 3-8a. 3-HLP velocity records of the second three months of deployment.
U-component.

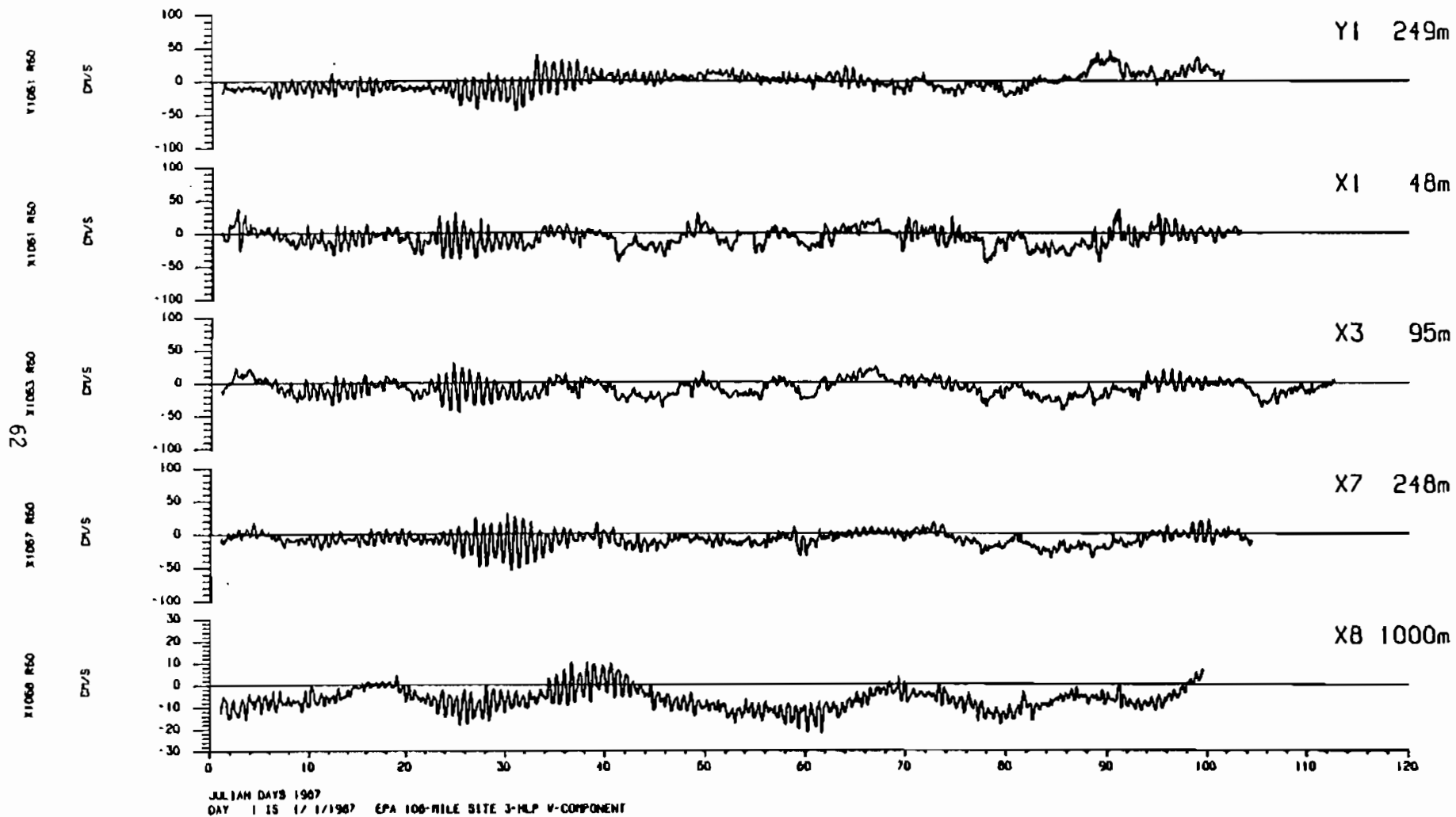


Figure 3-8b. 3-HLP velocity records of the second three months of deployment. V-component.

3.5 SPECTRA AND COHERENCE

The distribution of energy in frequency bands is illustrated by the spectra in Figures 3-9a through 3-9c. Rotary spectra are presented, where the current vector time series are decomposed into anticlockwise (+) and clockwise (-) components rotating at a given frequency (Gonella, 1971). Thus, clockwise rotating inertial currents show a strong peak in the clockwise rotary spectra in a frequency band around f . Purely rectilinear current fluctuations have equal magnitude clockwise and anticlockwise rotary spectra. The spectra are variance preserving in that equal amounts under the curve represent equal current variance. The most energetic part of the spectrum is restricted to periods longer than 10 days, which reflects the warm eddy activity in these records. The mixture of clockwise and anticlockwise components in this low frequency band varies with mooring and depth because of the relative position of the centers of the clockwise rotating warm eddies moving through the site. The predominance of clockwise currents at Mooring X indicates that the moorings were generally inshore of the large warm-core ring centers. Mooring Y shows more rectilinear fluctuations and thus is generally closer to eddy centers. The records, however, are dominated by the major ring that passed the site between JD 312 and 344. Typical of continental rise locations, there is little energy in the records between 1- and 10-day periods.

The high frequency part of the spectra is dominated by the inertial and M2 tidal peaks. The latter is weak, as indicated by the harmonic analysis discussed previously. The inertial peak is quite broad, a reflection of the intermittent nature of inertial oscillations; the peak height varies with depth. Near the surface, the inertial currents are forced by local winds, but at greater depth, the inertial signal can have contributions from non-local, higher latitude areas because inertial waves propagate energy both downward and horizontally (Hamilton, 1984; Phillips, 1977).

The stick plots (Figures 3-1 and 3-2) clearly show a high degree of visual correlation between the fluctuations over the upper 250m of the water column. This correlation is more quantitatively illustrated by the coherence squared and phase differences between X1 and X7, and X7 and X8, U and V

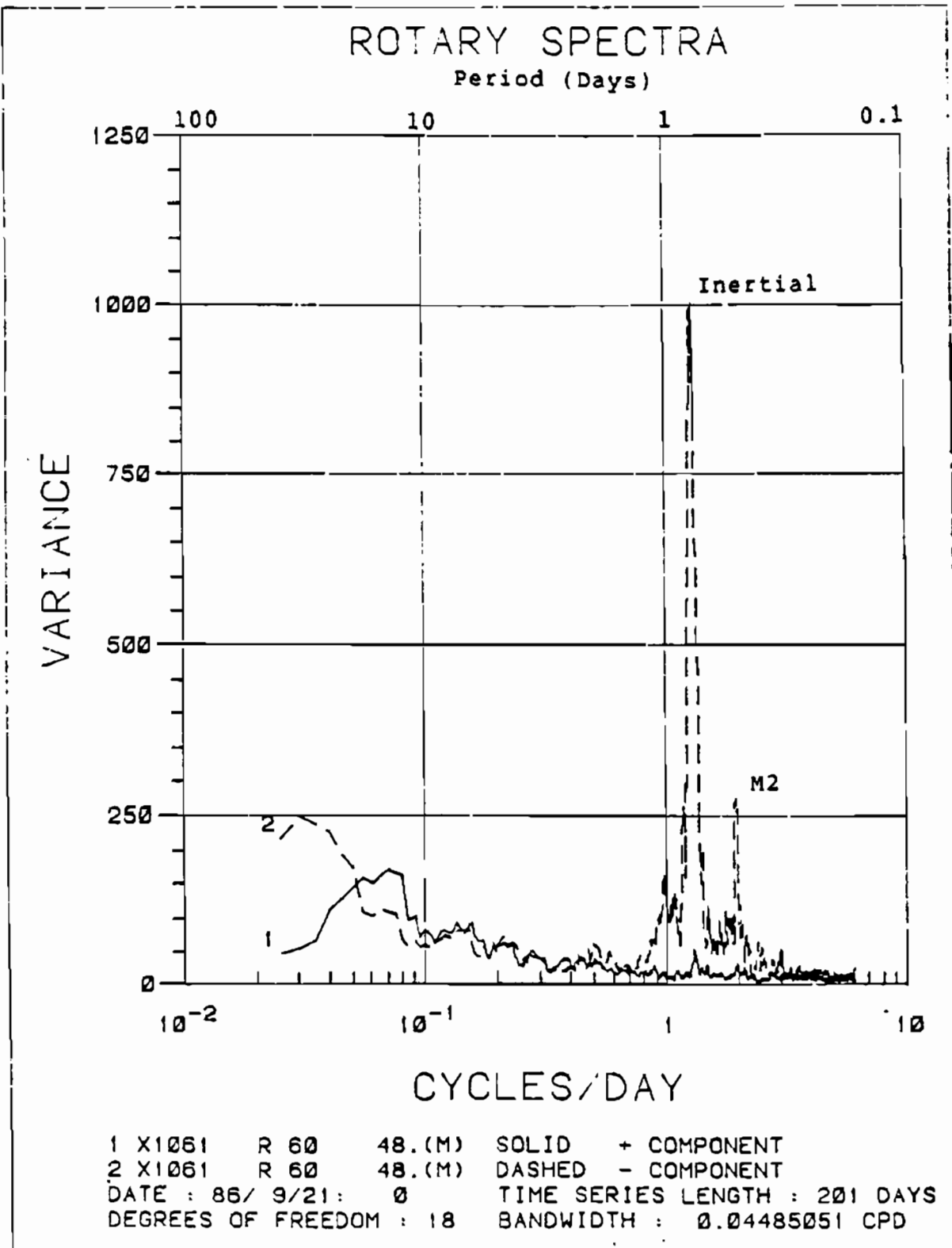


Figure 3-9a. Variance preserving rotary spectra of currents at 48m on mooring X.

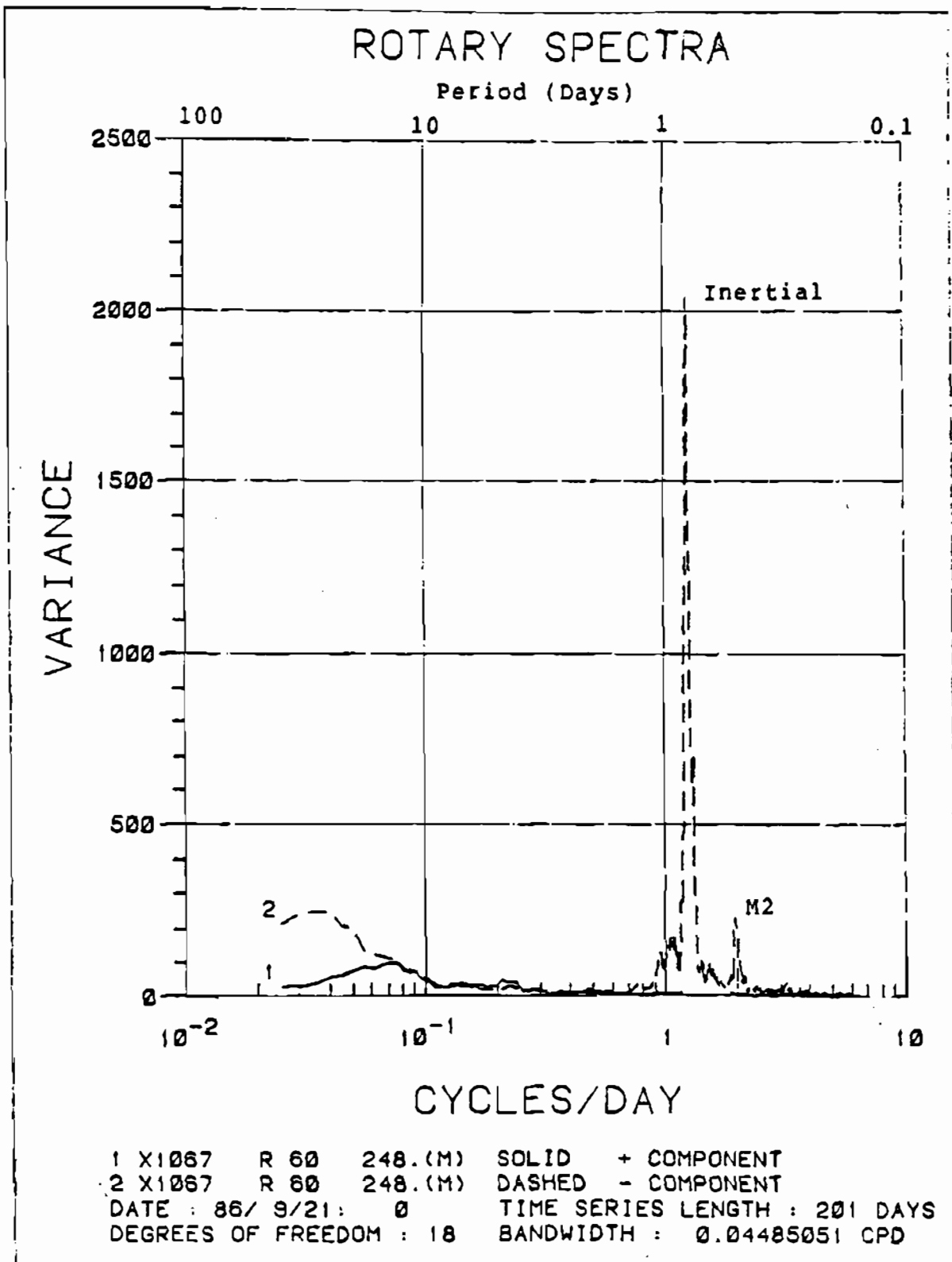


Figure 3-9b. Variance preserving rotary spectra of currents at 248m on mooring X.

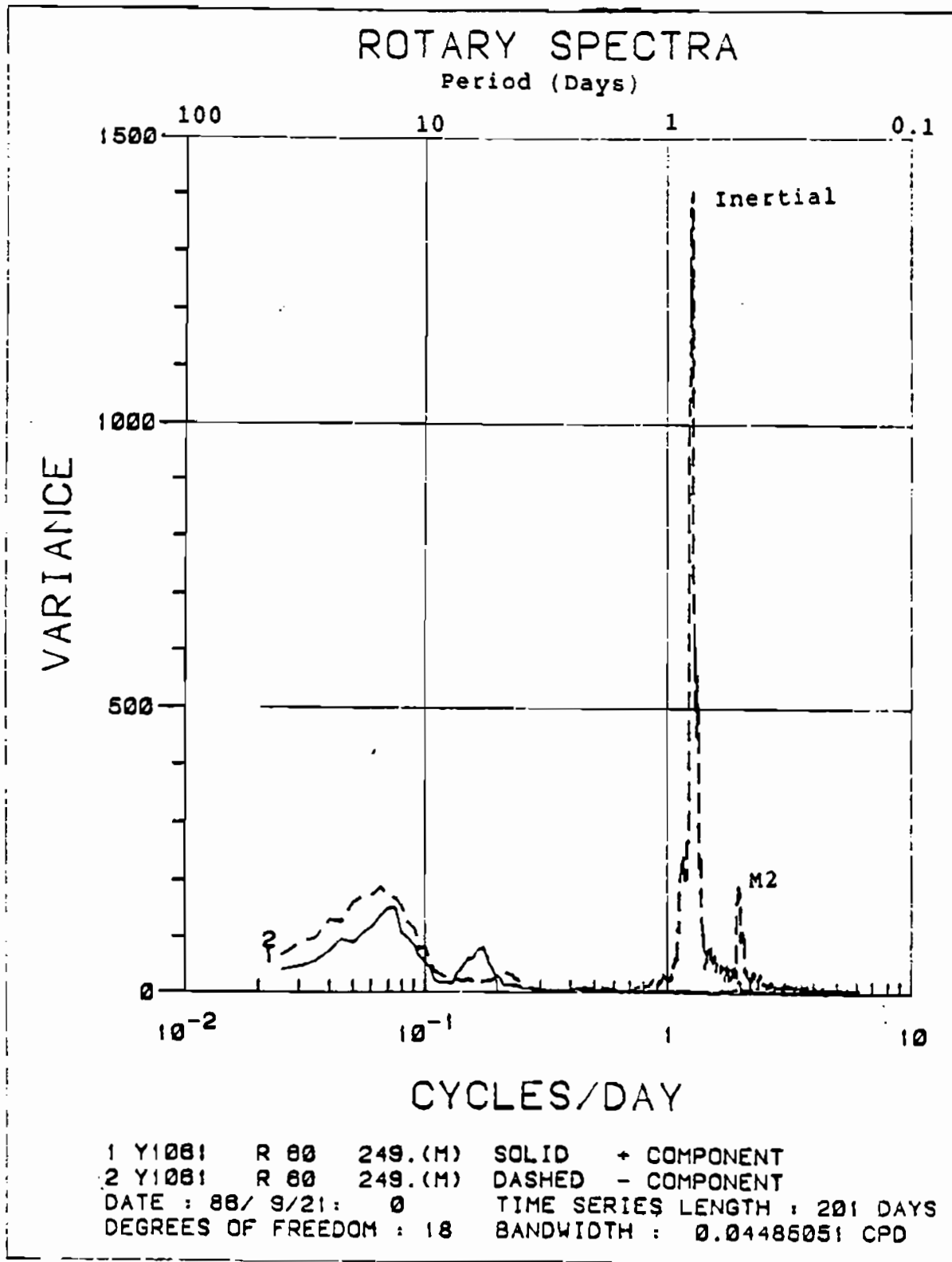


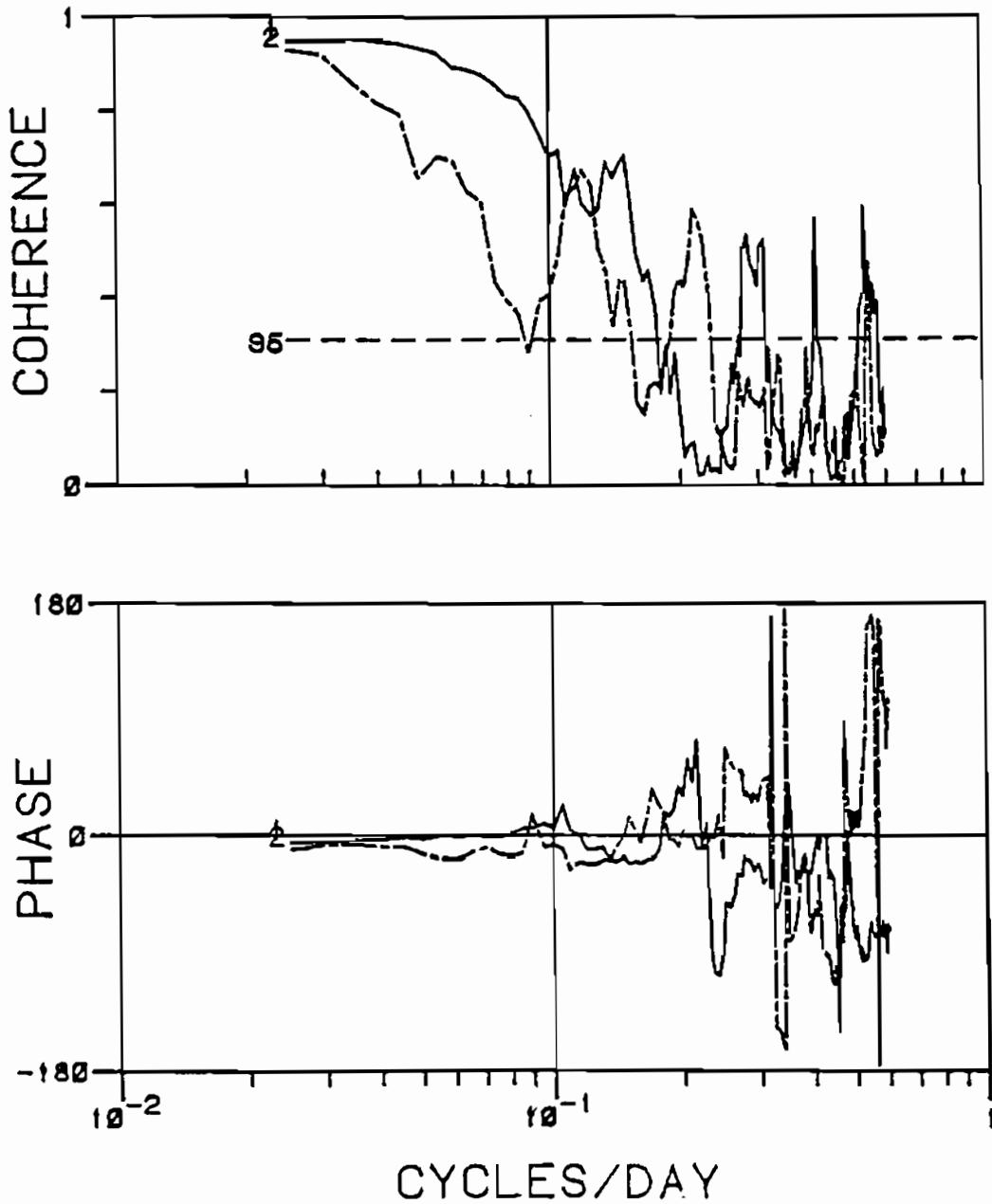
Figure 3-9c. Variance preserving rotary spectra of currents at 249m on mooring Y.

components (Figures 3-10a and 3-10b). The upper water column has highly coherent, in-phase, fluctuations at frequencies less than about 0.2 cycles/day. The offshore-onshore fluctuations (U) tend to be more coherent than the along-isobath fluctuations (V). Between 250m and 1000m, the U components are coherent between 0.05 and 0.1 cycles/day, which probably reflects the penetration of warm-core eddies to 1000m.

Coherence between the moorings (Y1 and X7) at the 250-m level (Figure 3-10c) shows high coherence between U components with about a 180° phase shift for the low frequency band, but virtually no coherence between along-isobath components. Again this coherence reflects the influence of the southwest propagating warm eddies and indicates that Stations X and Y are less than half a wave length apart. The lack of coherence in the along-isobath component probably reflects the different sizes of the eddies and the relative positions of X and Y with respect to the trajectory of their centers. The visual coherence of the Y1 and X7 stick plots when eddies are not present (i.e., January 1987, Figure 3-2) is also not very evident. At about day 30, the predominant flow at Y1 changes from southwest to northeast, but the flow at X7 remains southwest, implying a divergent flow field that could be supplied from either off- or onshore.

4. SUMMARY

The two current meter moorings deployed on the 2500-m isobath northeast and southwest of the 106-Mile Site provide further evidence of the richness of variability of both currents and density structures in this region of the Slope Sea. In the seven-month period (September 1986 to April 1987), sludge dumped at the site would have encountered several distinct environments including a large warm-core ring (86-E), two smaller warm eddies, cool filaments of shelf water extruded from the shelf by the eddies, warm Gulf Stream outbreaks, moderate southwesterly flow of the Slope Sea gyre, strong inertial currents due to a northeaster and vertical density profiles ranging from strongly stratified in September to completely homogeneous over the 250-m surface layer in late January. Some of these phenomenon have not been apparent in previous moored instrument programs because of the lack of sampling above 100m. Previous time series analyses



1	X1061	R 60	48.(M)	———	U COMPONENT	VRS
	X1067	R 60	248.(M)	———	U COMPONENT	
2	X1061	R 60	48.(M)	- - - - -	V COMPONENT	VRS
	X1067	R 60	248.(M)	- - - - -	V COMPONENT	

DATE : 86/ 9/21: 0 TIME SERIES LENGTH : 201 DAYS
 DEGREES OF FREEDOM : 18 BANDWIDTH : 0.04485051 CPD

Figure 3-10a. Coherence squared and phase differences between current records from depths of 48m and 248m on mooring X.

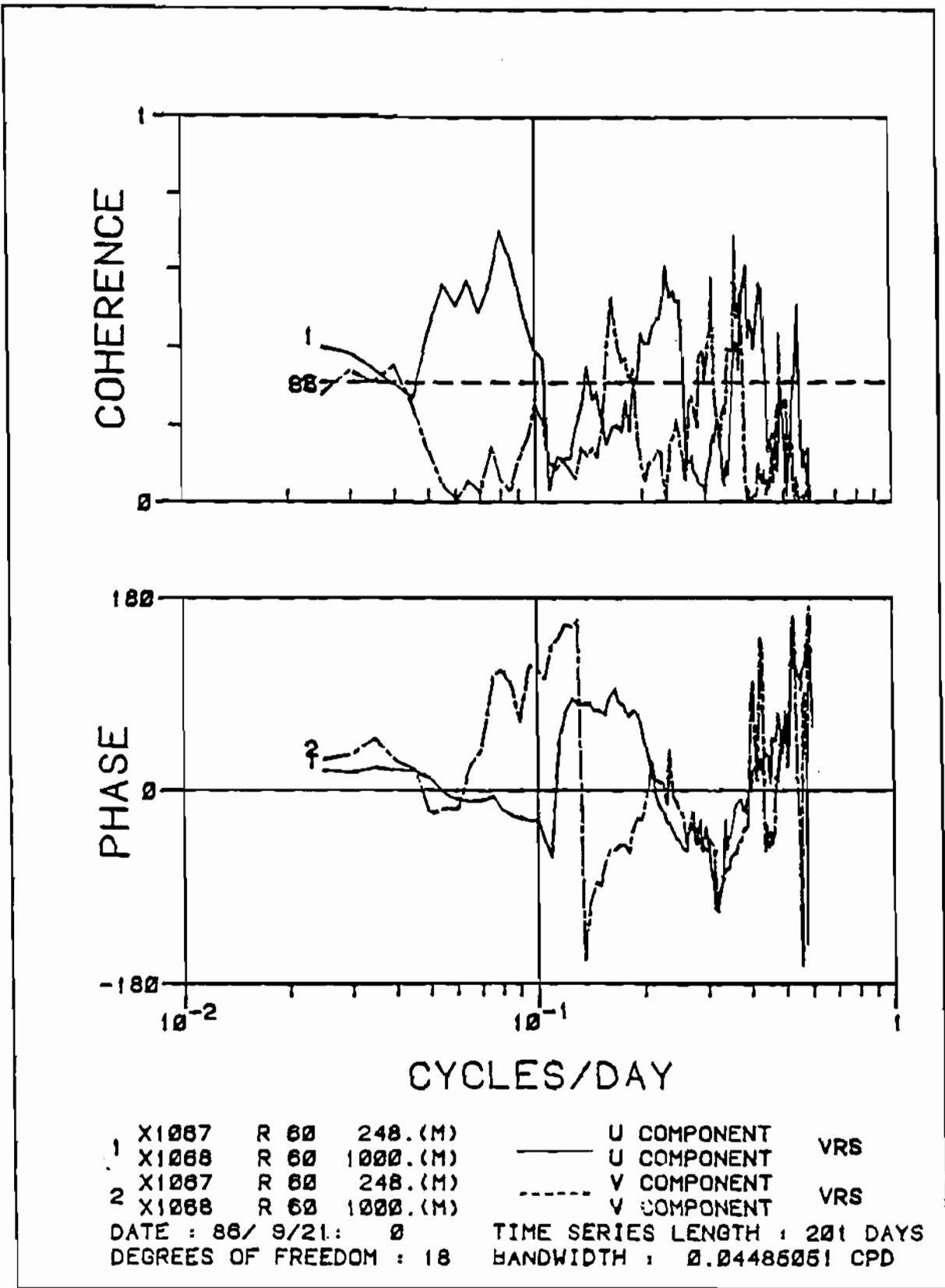


Figure 3-10b. Coherence squared and phase differences between current records from depths of 248m and 1000m on mooring X. 69

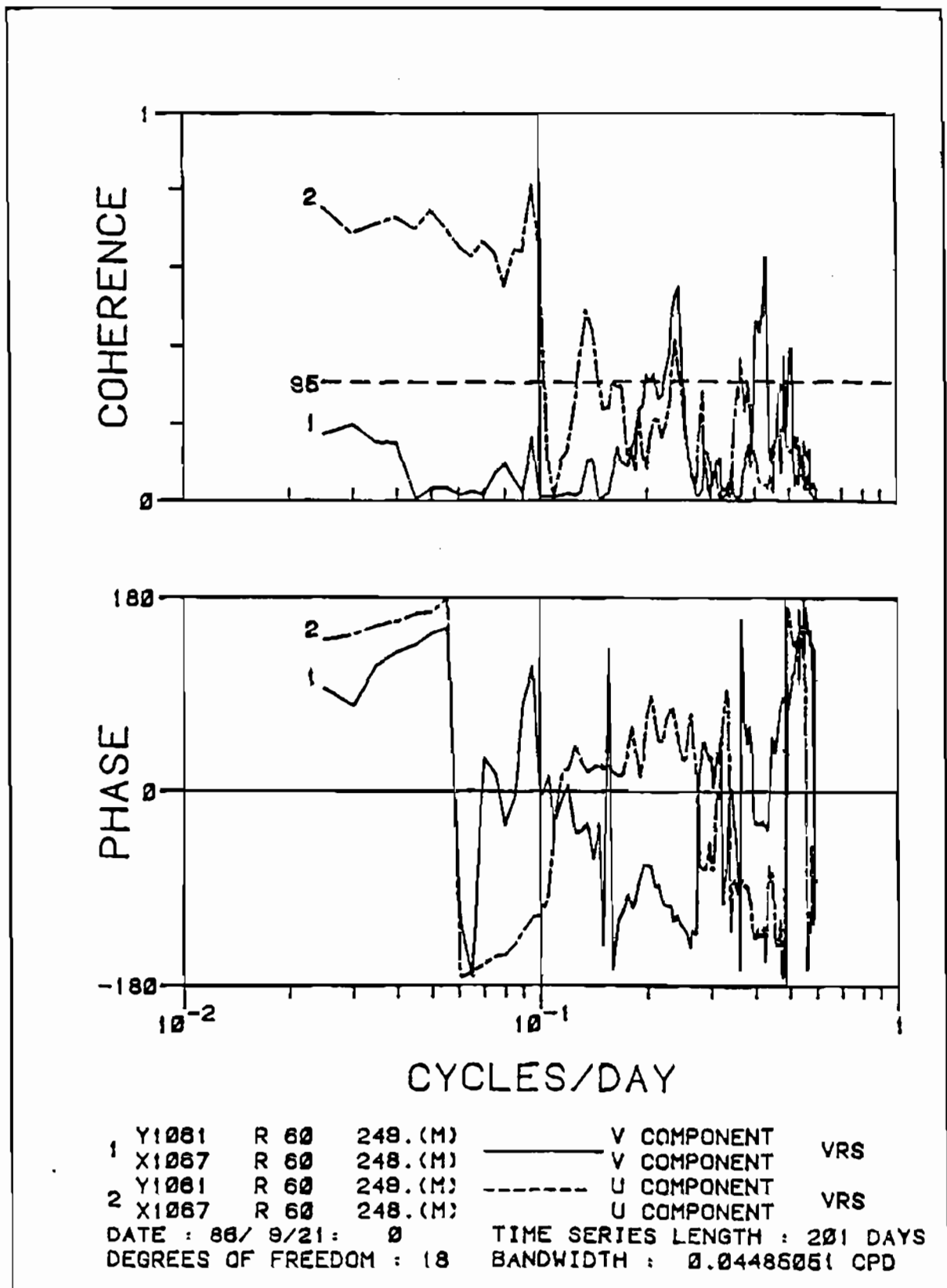


Figure 3-10c. Coherence squared and phase differences between current records from 248m on mooring X and 249m on mooring Y.

in this region have not detected cool shelf filaments, the small upper-slope warm eddies (though their presence has been suspected), and the passive warm Gulf Stream outbreaks that occurred after the winter overturning event. Similarly, the presence of a small body of anomalously cool and, by implication, fresher water advecting along the isobaths at 1000-m depth has important implications for the mixing of LSW with the surrounding deep North Atlantic water mass. This anomaly, which may be a submesoscale coherent vortex (McWilliams, 1985) being advected by the along-isobath mean flow, may not have direct impacts on the disposal of sludge at the 106-Mile Site, but may have an effect upon the oceanography of the continental margin.

The seven-month EPA current monitoring program has demonstrated a complex sequence of events, some of which are reasonably well understood (i.e., warm-core rings), and others that have been observed in satellite imagery, but have had few in situ measurements on their depth structures, and are less well understood (i.e., smaller warm eddies, shelf filaments, and warm outbreaks). The September 1986 to April 1987 period differed in type and sequence of events, and thus overall statistics, from any previous six-month period of current measurements taken by the MASAR program. The two-year MASAR current meter observations were limited in depth coverage and thus, upper ocean complex events, such as shelf water extrusions, were not captured by that program. Thus, information is particularly needed on the smaller upper slope warm eddies and their role in forcing extrusions of shelf water into the Slope Sea and intrusions of the slope water onto the shelf. The origin and formation, relationship to warm-core rings, and decay of such eddies is presently a mystery. The interannual time scales associated with the Slope Sea gyre, Gulf Stream axis shifts, and the occurrence of warm-core rings as well as the seasonal cycles associated with the shelf-slope front and the formation and erosion of the slopewater pycnoclad indicate that an adequate description of the statistics of surface layer currents in the region of the 106-Mile Site will require further monitoring.

5. REFERENCES

- Aikman, F., H-W, Ou and R. W. Houghton. 1987. Current variability across the New England continental shelf and slope. Report submitted to Continental Shelf Research.

- Bane, J.M., Jr., D. A. Brooks, and K.R. Lorenson. 1981. Synoptic observation of the three-dimensional structure and propagation of Gulf Stream meanders along the Carolina continental margin. *J. Geophys. Res.* 86(C7): 6411-6425.
- Beardsley, R.C., and W.C. Boicourt. 1981. On estuarine and continental-shelf circulation in the Middle Atlantic Bight. In: *Evolution of Physical Oceanography*, B.A. Warren and C. Wunsch eds., MIT Press, Cambridge, MA. pp 198-234.
- Bisagni, J.J. 1976. Passage of anticyclonic Gulf Stream eddies through deep water dumpsite 106 during 1974 and 1975. NOAA Dumpsite Evaluation Rep. 75-1, Dept. of Commerce, Washington, DC., 39p.
- Bisagni, J.J. 1983. Lagrangian current measurements within the eastern margin of a warm-core Gulf Stream ring, *J. Phys. Oceanogr.* 13:709-715.
- Boicourt, W.C. and P.W. and Hacker. 1976. Circulation of the Atlantic continental shelf of the United States, Cape May to Cape Hatteras. *Memoires Cociete Royale de Sciences de Liege.* 6(10):187-200.
- Brown, O.B., P.C. Cornillon, S.R. Emmerson, and H.M. Carle. 1986. Warm core rings: A statistical study of their behavior. *Deep-sea Res.* 33(11/12): 149-1474.
- Churchill, J.H., P.C. Cornillon and G.W. Milkowski. 1986. A cyclonic eddy and shelf-slopewater exchange associated with a Gulf Stream warm-core ring. *J. Geophys. Res.* 91:9615-9623.
- Cornillon, P. 1986. The effect of the New England seamounts on Gulf Stream meandering as observed from satellite IR imagery. *J. Phys. Oceanogr.* 16:386-389.
- Csanady, G.T. and P. Hamilton. In press. Circulation of slopewater. *Continental Shelf Research.*
- Fitzgerald, J.L., and J.L. Chamberlin. 1983. Anticyclonic warm-core Gulf Stream eddies off the northeastern United States in 1980. *Annal. Biol.*, 37:41-47.
- Fuglister, F.C. 1963. Gulf Stream '60. *Progr. Oceanogr.* 1:265-373.
- EPA. 1987. Final Draft Monitoring Plan for the 106-Mile Deepwater Municipal Sludge Site. Environmental Protection Agency. EPA 842-S-92-009.
- Garrett, C., and E. Horne. 1978. Frontal circulation due to caballing and double-diffusion. *J. Geophys. Res.* 83:4651-4656.

- Gonella, J. 1971. A local study of inertial oscillations in the upper layers of the ocean. *Deep-Sea Res.* 18:775-778.
- Hamilton, P. 1982. Analysis of current meter records at the northwest Atlantic 2800 meter radioactive waste dumpsite. EPA Tech. Rep. 520/1-82-002.
- Hamilton, P. 1984. Topographic and inertial waves on the continental rise of the Mid-Atlantic Bight. *J. Geophys. Res.* 89:695-710.
- Ingham, M.C., J.J. Bisagni and D. Mizenko. 1977. The general physical oceanography of deepwater dumpsite 106, in Baseline Report of Environmental Conditions in Deepwater Dumpsite 106 (Volume 1), NOAA Dumpsite Evaluation Report 77-1, Rockville, MD, pp 29-86.
- Joyce, T. 1984. Velocity and hydrographic structure of a Gulf Stream warm-core ring. *J. Phys. Oceanogr.* 14(5):936-947.
- Joyce, T.M., and M.C. Stalcup. 1984. An upper ocean current jet and internal waves in a Gulf Stream warm core ring. *J. Geophys. Res.* 89:1997-2994.
- Ketchum, B.H., and D.J. Keen. 1955. The accumulation of river water over the continental shelf between Cape Cod and Chesapeake Bay. *Deep-Sea Res. Supplement to 3:346-357.*
- Luyten, J.R. 1977. Scales of motion in the deep Gulf Stream and across the continental rise. *J. Mar. Res.* 35:49-64.
- Mayer, D.A., H.O. Mofjeld, and K.D. Leaman. 1981. Near-inertial waves observed on the outer shelf in the Middle Atlantic Bight in the wake of Hurricane Belle. *J. Phys. Oceanogr.* 11:87-106.
- McCartney, M.S., L.V. Worthington, and M.E. Raymer. 1980. Anomalous water mass distributions at 55°W in the North Atlantic in 1977. *J. Mar. Res.* 38: 147-172.
- McLellan, H.J., L. Lauzier, and W.B. Bailey. 1953. The slopewater off the Scotia Shelf. *J. Fish. Res. Bd. Can.* 10(4):155-176.
- McLellan, H.J. 1956. On the sharpness of oceanographic boundaries south of Nova Scotia. *J. Fish. Res. Bd. Can.* 12(3):297-301.
- McLellan, H.J. 1957. On the distinctness and origin of the slopewater off the Scotian Shelf and its easterly flow south of the Grand Banks. *J. Fish. Res. Bd. Can.* 14:213-239.
- McWilliams, J.C. 1985. Submesoscale, coherent vortices in the ocean. *Rev. Geophys.* 23:165-182.
- Phillips, O.M. 1977. *The dynamics of the upper ocean* (2nd edition). Cambridge University Press, London, 336 p.

- Rhines, P.B. 1971. A note on long-period motions at Site D. *Deep-Sea Res.*, 18:21-26.
- Rossby, C.G. 1936. Dynamics of steady ocean currents in the light of experimental fluid mechanics. *Papers in Physical Oceanography and Meteorology*, 5, Woods Hole Oceanographic Institution, pp 1-43.
- Science Applications International Corporation (SAIC). 1987. Study of physical process on the U.S. Mid-Atlantic slope and rise. Final Report, Volume II Technical. Minerals Management Service, OCS Study MMS 87-0024, Atlantic OCS Region, Vienna, VA.
- Thompson, R. 1977. Observations of Rossby waves near Site D. *Prog. Oceanogr.* 7:1-18.
- Tracey, K.L., and D.R. Watts. 1986. On Gulf Stream meander characteristics near Cape Hatteras. *J. Geophys. Res.* 91:7587-7602.
- Walker, H.A., J.F. Paul and V.J. Bierman, Jr. 1987. Methods for waste load allocation of municipal sewage sludge at the 106-Mile Ocean Disposal Site. *Environ. Tox. Chem.* 6:475-489.